Design, Implementation and Solar Energy Efficiency Comparison between a Dual Axis and a Single Axis Solar Panel Tracker in Sea Vehicles

Ibrahim Karahuseyin

Submitted to the
Institute of Graduate Studies and Research
in partial fulfillment of the requirements for the degree of

Master of Science
in
Electrical and Electronic Engineering

Eastern Mediterranean University
September 2023
Gazimağusa, North Cyprus

Approval of the Institute of Graduate Studies and Research

Prof. Dr. Ali Hakan Ulusoy
Director

I certify that this thesis satisfies all the requirements as a thesis for the degree of Master of Science in Electrical and Electronic Engineering.

Assoc. Prof. Dr. Rasime Uyguroglu
Chair, Department of Electrical and Electronic Engineering

We certify that we have read this thesis and that in our opinion it is fully adequate in scope and quality as a thesis for the degree of Master of Science in Electrical and Electronic Engineering.

Prof. Dr. Sener Uysal
Supervisor

Examining Committee

1. Prof. Dr. Sener Uysal

2. Assoc. Prof. Dr. Davut Solyalı

3. Asst. Prof. Dr. Moein Jazayeri

ABSTRACT

Sea vehicles such as cruise ships require so much electrical energy. They have multiple diesel generators to meet those requirements. Usage of fossil fuels to power those generators is creating economic problems which leads to a search for an alternative energy source to produce electricity. Producing electrical energy by using solar photovoltaic cells is one of the popular green energy production methods. However, solar energy applications are facing efficiency problems. In order to get the maximum efficiency from the panel, the sunlight has to be normal to the surface of the panel. The intensity and angle of radiation of the sunlight changes from earth`s season to season thus making the fixed solar panels less effective. There are several ways of improving the performance of solar panels. Improving the material of panels is one way of increasing efficiency and the other way is to use electromechanical solar trackers. In this thesis, a simple model of dual axis sun tracking system is designed and implemented on a sea vehicle to make a performance analysis of three different modes of the designed system which are; Azimuth-Axis Tracking Mode, Altitude-Axis Tracking Mode and Dual-Axis Tracking Mode. A 3D model of the system is designed in the NX ® platform. A voltage sensor and current sensor is used to record the data. The recorded data is then copied from the serial monitor of Arduino and transferred to Microsoft Excel table. The results showed that the use of the Dual-Axis Tracking mode produced more charge and energy output when compared with Zenithal Axis Solar Tracking mode Azimuth Axis Solar Tracking mode.

Keywords: Solar Tracking, Dual Axis, Sea Vehicles.

ÖZ

Yolcu gemileri gibi deniz araçları çok fazla elektrik enerjisi gerektirir. Bu gereksinimleri karşılamak için birden fazla dizel jeneratörleri vardır. Bu jeneratörlere güç sağlamak için fosil yakıtların kullanılması ekonomik sorunlar yaratmaktadır. Bu tür sorunlar alternatif bir elektrik enerjisi kaynağı arayışına yol açmıştır. Güneş fotovoltaik hücreleri kullanarak elektrik enerjisi üretmek, popüler olan yenilenebilir enerji üretim yöntemlerinden biridir. Ancak, güneş enerjisi uygulamaları verimlilik sorunlarıyla karşı karşıyadır. Panelden maksimum verim alabilmek için güneş ışığının panel yüzeyine dik olması gerekmektedir. Güneş ışığının radyasyon yoğunluğu ve açısının mevsimden mevsime değişmesi sabit güneş panellerini daha az etkili hale getirir. Güneş panellerinin performansını artırmanın birkaç yolu vardır. Verimliliği artırmanın bir yolu panel malzemesinin iyileştirilmesi, diğer yolu ise elektromekanik güneş takip cihazlarının kullanılmasıdır. Bu tezde, basit bir çift eksenli güneş takip sistem modeli tasarlanmış ve bir deniz aracı üzerinde uygulanmıştır. Sistem 3 boyutlu modeli NX ® platformunda tasarlanmıştır. Verileri kaydetmek için bir voltaj sensörü ve akım sensörü kullanılmıştır. Kaydedilen veriler daha sonra Arduino'nun seri monitöründen kopyalanıp Microsoft Excel tablosuna aktarılmıştır.

Sonuçlar, Çift Eksenli Takip modunun kullanımının, Zenithal Eksenli Güneş Takip modu ve Azimut Eksen Güneş Takip modu ile karşılaştırıldığında daha fazla şarj ve enerji çıkışı ürettiğini gösterdi.

Anahtar Kelimeler: Güneş Takibi, Çift Eksen, Deniz Araçları.

ACKNOWLEDGMENTS

Acknowledgement to the sponsors;

Thanks to my major professor, Prof. Dr. Şener Uysal, whose guidance and encouragement helped me with the thesis. Thanks to all committee members whose technical advice and support for making this accomplishment possible.

My appreciation also goes to Mr. Volkan Alper Kıvrak and Mr. Arda Denizer for their steady assistance throughout the whole project.

Last but not least, my profound gratitude goes to my parents, who inspired me to study and to pursue the master degree. Their encouragement has made it possible for me to complete this portion of my education in life.

TABLE OF CONTENTS

LIST OF TABLES

LIST OF FIGURES

LIST OF SYMBOLS AND ABBREVIATIONS

°C	Degrees Celsius
3d	Three Dimensional
A	Analog Pin Of Arduino
Aast	Azimuth Axis Solar Tracker
Acw	Anti-Clockwise
Adc	Analog To Digital Converter
Ah	Ampere Hours
Aref	Analog Reference
Av	Average
Bl-Ldr	Bottom Left Ldr
Br-Ldr	Bottom Right Ldr
Cw	Clockwise
Dast	Dual Axis Solar Tracker
Dc	Direct Current
Dip	Dual In-Line Package
Gnd	Ground
Hr	Hour
I	Current
Ic	Integrated Circuit
Impp	Maximum Power Point Current
Isc	Short Circuit Current
K	Kilo
Ks-H	Horizontal Motion Kill Switch

Ks-V	Vertical Motion Kill Switch
KΩ	Kilo Ohm
Ldr	Light Dependent Resistor
Ma/H	Milliampere Per Hour
Millisec	Milliseconds
Min	Minute
Min/S	Minute Over Second
Mpp	Maximum Power Point
Mppt	Maximum Power Point Tracker
Ø	Diameter
P-N	Positive- Negative
Pld	Party Lighting Device
Pv	Photovoltaic
R	Resistance
Sec	Seconds
Spst	Single Pole Single Throw
Tl-Ldr	Top Left Ldr
Tr-Ldr	Top Right Ldr
Vcc	The Regulated Dc Supply Voltage Needed To Operate The Ic Of Arduino
Vmpp	Maximum Power Point Voltage
Voc	Open Circuit Voltage
Vs	Versus
W/H	Watt Per Hour
Zast	Zenith Axis Solar Tracker

Ω	Ohm

Chapter 1

INTRODUCTION TO THESIS RESEARCH

1.1 Introduction

Relying on fossil fuels to produce energy has become harmful for the environment. Rapid rise in climate change, and toxic pollution is not a secret anymore. Also the descending level of oil resources is an increasing concern for a lot of industries. Cruise ships are using fossil fuels to generate electricity with the help of big generators and by using this energy they provide both motion and also electricity to the appliances that are used in those ships. Solar energy is an alternative energy source that can be used as a backup to the cruise ships.

1.2 Problem Description

Efficiency of solar panels however, is very low. Cloudy weather, dusty weather and even if the panel has a clean surface but especially in summer, the hot weather affects the performance of solar photovoltaic panels a lot and drops the efficiency drastically. In order to minimize this loss, either the material of the PV panel has to be changed with a better one or a solar tracker mechanism should be used in order to follow the sunlight constantly with a perfect position.

There are different types of solar tracker mechanisms. There is a system that moves only in a unidirectional way. In this method the position of the sun is recorded from a specific time with respect to regional and seasonal properties of the area. Later on with the help of a database of the microcontroller and motors, the direction of the

solar panel is being controlled with respect to the information that is stored in the database. Each system is applied to a specific region and it will not function properly if the device is transferred to another place.

However, dual axis solar trackers follow the direct solar radiations with the help of the feedback signals coming from the LDR`s. With respect to those signals, an algorithm is developed to make sure that the PV panel is always tracking the sun with a right angle for getting the maximum solar insolation.

1.3 Aims and Objectives

In this work, the dual axis solar tracker concept has been designed and implemented on a sea vehicle by using four LDR`s and two stepper motors with pulley and belt arrangements. The DAST`s control algorithm has been implemented via Funduino (Arduino) microcontroller.

The primary aim of a dual-axis solar tracker is to increase the energy output of the solar panels by maintaining a more direct and intense angle of incidence with the sun's rays. This can help to power the vessel's electrical systems and reduce the need for other forms of energy.

By adjusting the angle of the solar panels in response to the movement of the sun, a dual-axis solar tracker can help to improve the overall efficiency of the solar energy system. This can help to minimize energy losses and maximize the amount of energy that is produced by the solar panels.

By using solar energy to power the vessel's systems, a dual-axis solar tracker can help to reduce the dependence of the vehicle on fossil fuels. This can lead to cost

savings in terms of fuel consumption and reduce the environmental impact of the vessel.

A dual-axis solar tracker can enhance the energy independence of a sea vehicle, by providing a reliable source of energy that is not dependent on external sources such as fossil fuels or shore power. This can improve the overall sustainability of the vessel.

The dual-axis solar tracker should be designed and implemented in a way that it meets the power and load requirements of the sea vehicle, and that it can adapt to different solar radiation conditions of the area of operation.

Overall, the main objective of a dual-axis solar tracker implemented on a sea vehicle would be to increase the energy output of the solar panels, improve the overall efficiency of the system, reduce dependence on fossil fuels, enhance energy independence, and improve the overall sustainability of the vessel.

1.4 Contribution of Thesis

This thesis introduces substantial advancements in the realm of integrating renewable energy and marine engineering. It accomplishes this by devising, executing, and conducting a thorough comparison of the efficiency of solar energy utilization between dual-axis and single-axis solar panel tracking systems on maritime vehicles. An essential focal point of this thesis involves creating and executing optimized dual-axis and single-axis solar panel tracking mechanisms tailored for deployment on sea-faring vehicles. Formulating these custom systems directly tackles the distinctive obstacles presented by the maritime setting, encompassing factors like fluctuating

sea conditions, vessel dynamics, and spatial constraints. The process of designing these systems encompasses factors like structural soundness, resilience against weather elements, and the efficiency of energy generation. The innovative tracking systems thus conceived lay a cornerstone for propelling subsequent progress in harnessing renewable energy within maritime contexts.

In this thesis, a thorough and all-encompassing comparative evaluation of solar energy efficiency is presented, focusing on dual-axis and single-axis solar panel tracking systems when integrated into sea-faring vehicles. Through rigorous experimentation and meticulous data gathering, the performance of each tracking system across diverse scenarios, encompassing differing sea conditions, angles of sunlight, and tracking algorithms were scrutinized. This efficiency analysis encompasses a range of metrics, spanning energy generation yield, stability in power delivery, and adaptability in the face of shifting environmental circumstances. The outcomes yield invaluable insights into the trade-offs and merits inherent in each tracking approach, thereby contributing to well-informed decision-making for the implementation of marine-based renewable energy systems.

Through a meticulous examination of the amassed data, this study provides valuable revelations concerning the most advantageous tracking approach for solar panel setups on maritime vessels. These discoveries shed light on the contexts wherein dual-axis tracking demonstrates superiority over its single-axis counterpart, and conversely. Furthermore, the precise circumstances in which each tracking system

excels, granting marine engineers and proponents of renewable energy was pinpointed the ability to make well-informed decisions aligned with their vessel's operational characteristics and geographic placement.

This thesis serves as a pivotal link in the realm of research concerning marine renewable energy by directly addressing the unique obstacles associated with incorporating solar energy systems onto maritime vehicles. The contributions put forth within this investigation carry the potential to propel the uptake of renewable energy solutions within maritime transport, thereby diminishing reliance on fossil fuels and playing a role in fostering a more sustainable and eco-friendly maritime industry.

In summary, this thesis introduces fresh insights and tangible contributions pertaining to the design, execution, and comparative analysis of solar energy efficiency in the context of dual-axis and single-axis solar panel tracking systems integrated into sea-faring vehicles. The outcomes presented herein align with the broader objectives of bolstering the utilization of renewable energy within the maritime sector and deepening comprehension of renewable energy technology's performance within the demanding conditions of the marine environment.

Chapter 2

LITERATURE REVIEW

This section of the thesis contains a review of literature related to P-N Junction, Photovoltaic Effect, History of Solar Panels, History of Solar Panels in Sea Vehicles, Voltage and Current Characteristics of Solar Cells, Efficiency of Solar Panels and Dual Axis Solar Tracking Systems.

2.1 P –N Junction

A P-N junction is a boundary between two types of semiconductors, one of which is doped with impurities that create a surplus of positive charge carriers (holes) called P-type semiconductor, and the other doped with impurities that create a surplus of negative charge carriers (electrons) called N-type semiconductor. When these two types of semiconductors are brought into contact, a P-N junction is formed. [25] [26]

As shown in **Figure 1** the P-N junction acts as a barrier for the flow of electrons. However, this barrier is not completely impenetrable, and a small number of electrons will cross over from the N-type side to the P-type side. This creates a depletion region, a region in which there are very few mobile charge carriers. [25] [26]

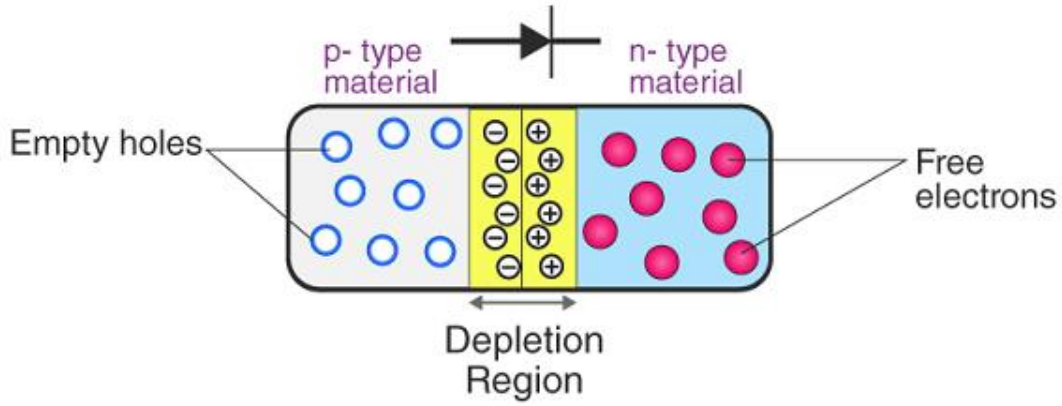

Figure 1: P-N junction structure definition [25]

P-N junctions are widely used in electronic devices such as diodes, transistors and solar cells. They are also the basic building blocks of many other electronic components such as optoelectronics devices, such as light-emitting diodes (LEDs) and laser diodes, and integrated circuits, such as microprocessors and memory chips. [25]

2.2 Photovoltaic Effect

The photovoltaic effect is the process by which certain materials, when exposed to light, produce an electric current. This phenomenon was first discovered by French physicist Edmond Becquerel in 1839. [20]

When light shines on certain materials, such as semiconductors, it can knock electrons into a higher energy state. These excited electrons can then be harnessed to generate an electric current. [22]

The most common type of solar cell used today is the silicon solar cell. A silicon solar cell is made up of two layers of silicon, one layer is doped with a small amount

of impurities such as boron, which creates a positive charge, and the other layer is doped with impurities such as phosphorus, which creates a negative charge. This creates a P-N junction. [24]

The efficiency of a solar cell, which is a measure of how well it converts sunlight into electricity, depends on the material used, the quality of the cell, and the conditions under which it is used. [22] [23]

Today, the efficiency of commercial solar cells are around 20-24% for single-crystalline silicon and around 12-16% for multi-crystalline silicon. [22] [23

2.3 History of Solar Panels

The history of solar panels used in sea vehicles can be traced back to the early 20th century, when the first commercial solar cells were developed by inventors and engineers such as Charles Fritts, William Grylls Adams, Richard Evans Day, Alexandre Edmond Becquerel, and Edward Weston. [30]

The history of solar panels can be traced back to the late 19th century when French scientist Edmond Becquerel discovered the photovoltaic effect, which is the process by which solar cells convert sunlight into electricity. [30] [31]

In **1839**, Becquerel discovered that when certain materials, such as silver chloride, were exposed to light, they generated an electric current. He called this phenomenon "photovoltaic effect" and it was the first scientific explanation of the phenomenon of solar energy conversion. This discovery marked an important step forward in the development of solar energy technology and provided the foundation for the

development of modern solar cells. [30] [31]

William Grylls Adams and Richard Evans Day developed the first solar cell with a conversion efficiency of around 6% in **1876**. William Grylls Adams was an English physicist and chemist who, along with his colleague Richard Evans Day, made important contributions to the development of solar cells in the late 19th century. In 1876, they discovered that a solid material, selenium, could convert light into electricity. They built a device that was able to generate a small current when exposed to sunlight. This was the first demonstration of the principle of solar energy conversion. [30]

Their research showed that the efficiency of the device was around 6%, which was relatively low compared to modern solar cells, but it was the first time anyone had successfully converted light into electricity. The discovery of the photoelectric effect in selenium provided the first scientific explanation of the phenomenon and marked an important step forward in the development of solar energy technology. [30]

Adams' work also inspired other researchers to pursue the development of solar cells, including Charles Fritts, who created the first solar cell in **1883** as shown in **Figure 2**. He created the first solar cell by coating selenium with a thin layer of gold. This invention is considered to be the first step in the development of modern solar cells. [32] [20]

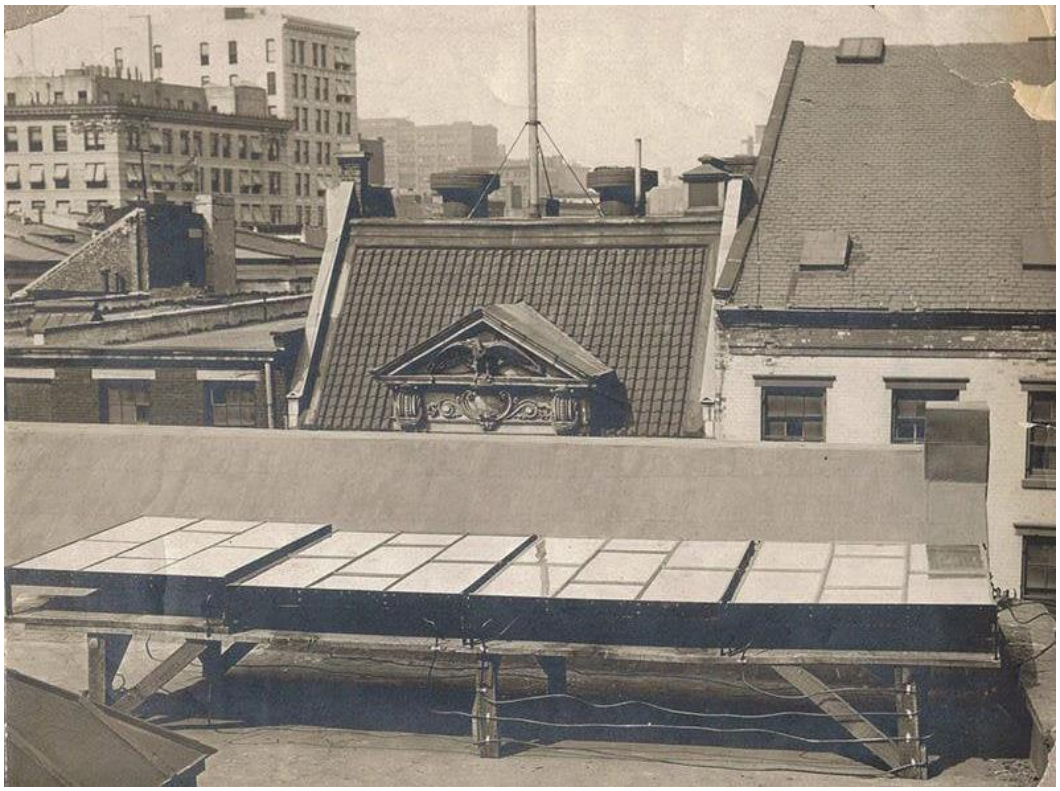

Figure 2: The first solar panel that is installed on the New York City rooftop in 1884 by Charles Fritts.[20]

Fritts was an American inventor and physicist who worked on the development of early electrical devices. He began experimenting with solar cells in the late 1800s, and in 1883, he created a solar cell that was capable of converting sunlight into electricity with an efficiency of around 1%. While this efficiency was relatively low compared to modern solar cells, it was the first demonstration of the principle of solar energy conversion. Fritts' invention was not widely adopted at the time, due to the high cost of the materials he used and the limited understanding of the underlying science.

Edward Weston was an American inventor and electrical engineer who made important contributions to the field of photovoltaics in the early 20th century. He was known for his work on the development of the first commercial solar cell and is

considered one of the key figures in the history of solar energy technology. [20] [32]

As shown in **Figure 3** Edward Weston managed to receive two patents for solar cells in **1888**. He managed to transform radiant energy that is coming from the sun into electrical energy or through this electrical energy into mechanical energy.[20]

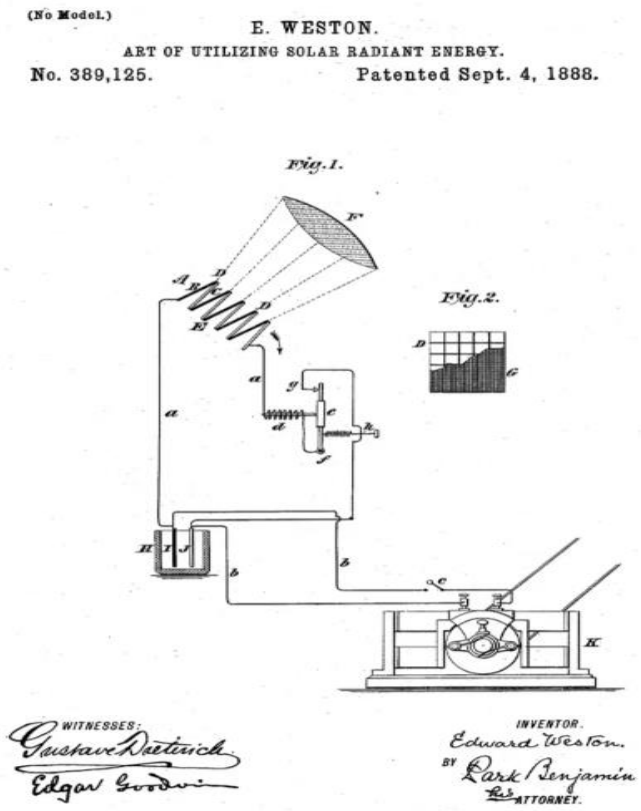
(No Model.)

E. WESTON.

ART OF UTILIZING SOLAR RADIANT ENERGY.

No. 389,125. Patented Sept. 4, 1888.

Fig. 1.

Fig. 2.

WITNESSES:

Gustave Daetwich

Edgar Goodwin

INVENTOR.

Edward Weston.

BY Park Benjamin

ATTORNEY.

Figure 3: Edward Weston`s design, used for Solar Radiant Energy utilization.[20]

In the early days, solar cells were primarily used for telegraphy and other remote applications, such as powering communication devices in remote locations. However, it wasn't until the **1950`s** that the first practical solar cells were developed, primarily for use in space satellites. In the following decades, improvements in technology and manufacturing led to a decrease in the cost of solar cells, making

them increasingly accessible for use in residential and commercial applications as well as powering a sea vehicle.

2.4 History of Solar Panels in Sea Vehicles

The history of solar-powered boats dates back to the late 19th century, with the first recorded solar-powered boat being built in 1881 by Augustin Mouchot, a French inventor. [33]

However, it wasn't until the 1970s that solar-powered boats began to be developed more seriously, as advancements in solar cell technology made it possible to generate more electricity from the sun. In the decades that followed, solar-powered boats were used for a variety of purposes, including research, transportation, and recreation. Some notable examples include the **Solar Navigator**, a solar-powered catamaran that was powered by a combination of solar panels, wind turbines, and a backup generator. It was built in the UK and soon completed a transatlantic crossing in 2005. [33] [34]

The world's largest catamaran, **PlanetSolar** (as shown in **Figure 4**) was designed by Craig Loomes, a naval architect from New Zealand, and funded by German entrepreneur Immo Ströher. Construction began in 2008 at the Knierim Yachtbau shipyard in Kiel, Germany. Over time, the project took shape and resulted in the creation of a massive catamaran. [39] MS Tûranor Planet Solar is a 31 meter long and 15 meter wide catamaran built in 2010 and it is equipped with over 600 square meters of solar panels. It can sail at a speed of 5 knots. This solar-powered catamaran completed a circumnavigation of the globe in 2012. It set a world record for the

longest journey ever made by a solar electric vehicle. [35]

Figure 4: MS Turanor Planet Solar catamaran. [36]

Sun 21 (as shown in **Figure 5**) is a solar-powered trimaran that set a world record for crossing the Atlantic Ocean in a solar-powered boat in 2014.

A Swiss company constructed a 14-meter (46-foot) boat, registered in Basel that can travel at a steady speed of 10 km/h. The boat has 48 solar panels installed on its roof, which accumulate energy from the sun during the day. The collected energy is stored in batteries, enabling the boat to continue sailing through the night. The catamaran is powered by a motor and comprises two polyester hulls, with dimensions of 46 feet (14 meters) by 21 feet (6.5 meters). Its roof, which spans an area of 700 square feet (65 square meters), is fitted with solar panels. [37]

Figure 5: Sun 21 solar-powered trimaran.[37]

Solar Impact (as shown in **Figure 6**) is a solar-powered yacht that was built in Germany in 2016. It is equipped with more than 3,000 square feet of solar panels and can reach speeds of up to 20 knots. It is a 24m electric yacht with a solar surface that features the SWATH technology. Roland Friedberger has designed a stylish solar yacht concept, which is being developed by the German boatbuilder, Schaaf Yachtbau. The electric technology for this SWATH yacht is provided by Kreisel, who is famous for developing special electric vehicles, including an electric Hummer H1 for Arnold Schwarzenegger. Additionally, they supplied the technology for the SAY 29 Carbon with e-propulsion, which has proven successful. [38]

Figure 6: Solar Impact electric yacht with a solar surface.[38]

The Solar Impact has 280 square meters of solar cells by Sun power that can store the generated energy in 800 kWh batteries. In optimal conditions, the solar cells can produce 300 kWh per day. The yacht can travel up to 170 nautical miles in eco mode at 5 knots. With twin engines that each have a power of 500 kW, the vessel can reach a top speed of 20 knots. There are also two 65 kW generators as backup and/or hybrid mode, allowing for a range of 2,500 nautical miles.

Solar Voyager (as shown in **Figure 7**) is a solar-powered boat built by a team of high school students from Massachusetts, USA. It completed a journey from Cape Cod to Bermuda in 2019 using only solar power. The Solar Voyager is a drone boat and it embarked on a mission to traverse the Atlantic Ocean. If successful, it will be the first drone and the first vessel powered entirely by solar energy to cross the ocean. [40]

Figure 7: Solar Voyager.[40]

Over a span of four years, the Solar Voyager underwent significant improvements, transitioning from a plastic kayak to a bespoke aluminum-hulled vessel outfitted with a reliable engine and electronics, a 280-watt solar panel, and two antifouling propellers that allow it to reach speeds of up to 5 miles per hour. The hull is also protected from potential damage by a special coating.

The Solar Voyager's solar panels are independent of each other, ensuring that if one fails, the other can continue to generate power. Additionally, two sets of screws and rudder pens were installed to ensure that the boat can move even if one pair becomes entangled or covered in debris. To avoid collisions with other vessels, the hull was painted for better visibility and the boat's course was charted away from heavily trafficked sea routes. [40]

Energy Observer (as shown in **Figure 8**) is a solar-powered catamaran that completed a six-year journey around the world in 2022, it is equipped with over 20 KW of solar panels and can sail at a speed of 5 knots. [41]

Figure 8: Energy Observer.[41]

Energy Observer demonstrates a fully sustainable energy solution by harnessing solar, wind, and hydro power in combination with a hydrogen storage system that employs lithium-ion batteries and a complete hydrogen system. This impressive achievement in technology is the outcome of two decades of research and development at CEA-LITEN (Laboratory for Innovation in New Energy Technologies and Nanomaterials). The intention of CEA-LITEN is to demonstrate the readiness of the integrated technologies and the possibilities that renewable energy mixes offer for a sustainable, efficient, and forward-thinking future. [42]

Energy Observer utilizes two different solar panel technologies to generate energy. The custom-made, curved panels on the deck hug the round hull, while bifacial panels with heterojunctions are installed aft and along the entire length of the hull. These panels are designed to capture both direct sunlight and light reflected by the water to produce 120 square meters of solar power. [42]

The catamaran uses lithium-ion batteries for short-term storage to supply two separate power systems, one at 400 V and the other at 24 V. The former manages power demands, propulsion, electrolysis, and hydrogen compression, while the latter is for life on board and instrumentation, control, and safety equipment. For long-term storage, Energy Observer has a complete hydrogen system comprising a desalination system, an electrolyser, tanks, and a fuel cell. This system will produce hydrogen from seawater, store it on board, and use it to power the fuel cell, with excess electrical energy from the fuel cell fed back into the circuit, and the reaction heat used to heat domestic water on board. [42]

Complete system management - CEA-LITEN, Energy Observer's R&D team, has developed a system to manage and monitor the entire energy system onboard. The goal is to ensure optimal operation according to resources, which vary depending on the time of day, weather conditions, and the vessel's itinerary. Engineers analyze all the navigation data in real-time to propose suitable scenarios. [42]

Photovoltaics is a rapidly growing industry, with solar power being seen as a key component in the transition to a sustainable energy future. Advances in technology continue to improve the efficiency and reduce the cost of solar cells, making it an increasingly viable source of electricity for both residential and commercial applications. [20] [21]

Solar panels are increasingly being used in sea vehicles as a way to reduce the vehicle's dependence on fossil fuels and to reduce their environmental impact. Solar panels can be used to generate electricity for the vehicle's lights, air conditioning,

and other systems. They can also be used to charge the vehicle's batteries, which can then be used to power the systems when the sun is not shining or when the vehicle is in port. [51]

The type of solar panels used on sea vehicles can vary depending on the design and the specific application. Generally, the most efficient solar panels are those made of monocrystalline silicon, which have an efficiency of around 20%. Thin-film solar panels, which are made of materials like amorphous silicon or cadmium telluride, can also be used. They have lower efficiencies, around 10-15%, but they are more flexible and lightweight, which makes them more suitable for marine environments. [51]

2.5 Voltage and Current Characteristics of Solar Cells

Solar panels have certain voltage and current characteristics that are important to understand when designing and installing a solar power system.

Voltage, measured in volts (V), is the electrical force that pushes electrons through a circuit. Solar panels typically have an open-circuit voltage (Voc) and a maximum power point voltage (Vmpp). The open-circuit voltage (Voc) is the voltage that the panel produces when there is no load connected to it. The maximum power point voltage (Vmpp) is the voltage at which the panel produces the most power.

Current, measured in amperes (A), is the flow of electrons through a circuit. Solar panels typically have a short-circuit current (Isc) and a maximum power point current (Impp). The short-circuit current (Isc) is the current that the panel produces when a

short circuit is applied to it. The maximum power point current (Impp) is the current at which the panel produces the most power.

The combination of voltage and current is what produces power, measured in watts (W). The maximum power point of a solar panel is the point at which the panel produces the most power. It is important to ensure that the solar panel is operating at this point in order to maximize the power output of the solar system. Solar panels have a characteristic curve that shows the relationship between the voltage, current and power of the panel. It is important to match the voltage and current of the solar panel to the voltage and current of the load, to ensure efficient and safe operation of the solar system. Also, the operating temperature of the solar panel has a significant impact on the performance of the solar panel. The temperature coefficient is used to adjust the power output of the solar panel based on the operating temperature. [27]

2.6 Efficiency of Solar Panels

The efficiency of solar panels refers to the percentage of sunlight that is converted into usable electricity. The efficiency of a solar panel depends on several factors, including the type of solar cell, the quality of materials and manufacturing methods, environmental conditions, cell temperature and spectral mismatch. [44]

As shown in **Figure 9** solar cells can be categorized into three main types: crystalline silicon-based, thin-film solar cells, and a hybrid of the two. [45]

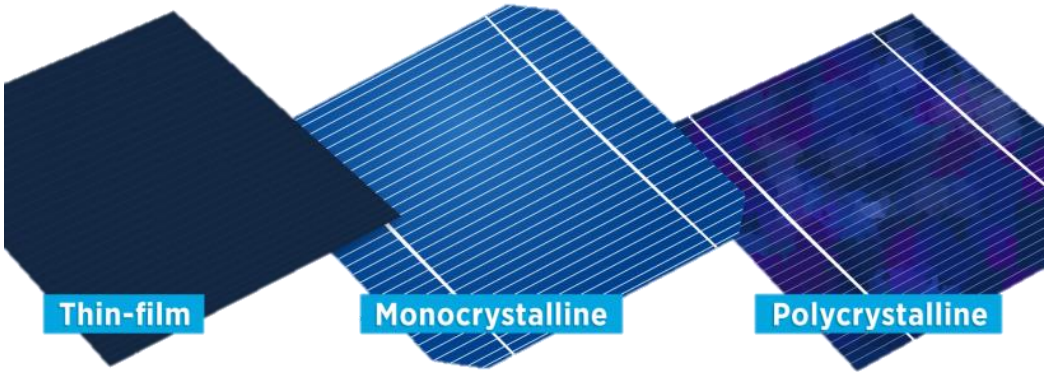

Figure 9: shows the images of three different silicon solar cell materials.[46]

Crystalline Silicon Cells are the most common, with around 90% of solar cells being made from sliced wafers of crystalline silicon ingots. These ingots, which can take up to a month to grow, can be single or multiple crystals. Single crystals are used to create monocrystalline solar panels and cells (mono-Si), while multiple crystals are used for polycrystalline panels and cells (multi-Si or poly c-Si). [45]

Monocrystalline cells have a cylindrical shape and a distinct appearance due to their high efficiency, but they are wasteful as they must be cut into shape. Polycrystalline cells, on the other hand, are melted and poured into square molds and are considered a mid-range option in terms of price and efficiency. [45]

Thin Film Solar Cells, on the other hand, are around 100 times thinner than crystalline silicon cells and are made from amorphous silicon or other materials like cadmium-telluride (Cd-Te), copper indium gallium diselenide (CIGS), or organic PV materials. These cells are created by layering photovoltaics to make a module and are the cheapest option for producing solar panels. They can be laminated onto various substrates, but they are less efficient than crystalline silicon cells, with only

7-12% efficiency. [45]

Third Generation Solar Cells are the newest type, combining the best features of crystalline silicon and thin-film solar cells to achieve high efficiency and practicality. They are made from materials like amorphous silicon, organic polymers, or perovskite crystals and have multiple junctions made of different semiconducting materials. They are cheaper, more efficient, and more practical than other types of cells, with the potential to achieve up to 30% efficiency with a perovskite-silicon tandem solar cell. [45] [46]

High-quality materials and manufacturing processes can lead to more efficient solar panels. The efficiency of a solar panel refers to its ability to convert sunlight into electricity. The quality of materials and manufacturing methods used in solar panel production can have a significant effect on its efficiency. [49]

High-quality materials, such as silicon wafers with fewer impurities, can generate more electricity per unit area than lower-quality ones. Similarly, using high-quality glass and other components can help minimize energy losses due to reflection, absorption, and other factors. [49]

Manufacturing methods, such as the deposition of metal contacts or the application of anti-reflective coatings, can also affect the efficiency of solar panels. Poor manufacturing methods can lead to defects or inconsistencies that can reduce the panel's overall performance. In summary, using high-quality materials and manufacturing methods can help improve the efficiency of solar panels, resulting in

more electricity generation per unit area and higher overall performance. The efficiency of solar panels can be affected by **environmental conditions** such as irradiance, temperature, dust allocation, soiling, wind, shading, humidity and orientation. [47] [49]. **Irradiance** pertains to the quantity of energy received on a flat surface within a specific range of wavelengths, per unit of time. The performance of a PV panel relies greatly on solar power or solar irradiance, a factor that can vary significantly due to weather, seasonal changes, geographical location, time of day, and sun position in the sky. The degree of variability depends on the time resolution, and this variability increases as the time resolution becomes finer. As shown in **Figure 10** the primary factor affecting the variability of irradiance is cloudy conditions. [47] [56]

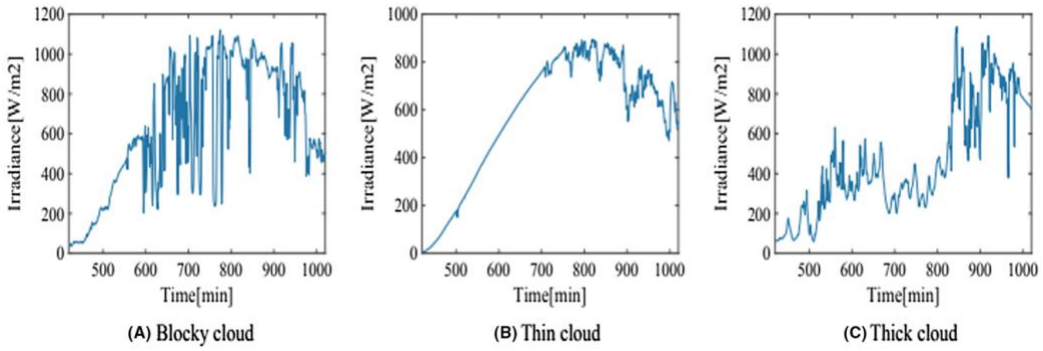

Figure 10: shows the change in irradiance value with respect to different cloudy conditions. [47]

Photovoltaic modules receive both direct and scattered light, but direct solar irradiation contributes significantly more to the panel's output. Estimating incident irradiance becomes complicated when nearby objects cast shadows or reflect sunlight onto the PV modules. To receive the maximum amount of irradiance, the solar panel should be tilted to face the sun at an optimum angle, which varies with the latitude

angle of the location. The ideal tilt angle is determined by the latitude angle (ϕ) of the specific location. During summer, the tilt angle diverges −15° from the latitude angle and during winter, it deviates by approximately +15° from the latitude angle. Various solar tracking mechanisms are used to orient PV panels towards the direct portion of solar irradiance, and even a minor departure from southern azimuth orientation can lead to a reduction in irradiance. In the azimuth orientation, each degree of deviation from the south causes a 0.08% irradiance loss. The performance of a PV module improves with rising irradiance levels. The impact of solar irradiance on the PV panel`s operation is not quantifiable by a specific percentage due to the linear correlation between module current and irradiance, as demonstrated by the G-P (sun radiation-output maximum power) curve. [56]

The production of electricity from a PV panel is highly dependent on its module temperature. When the temperature of the module rises, its electrical efficiency decreases due to the fact that PV panels convert only 20% of solar energy into electricity and the rest is converted into heat. The correlation between the temperature of the module and the bandgap energy of the PV cell material holds notable importance. At higher operating temperatures, the bandgap energy generally decreases, which causes the cell to capture photons with longer wavelengths, often prolonging the lifespan of minority carriers. [56]

Such factors increase the current generated by light (Isc) very less, which results in a decrease in the open-circuit voltage (Voc) and a reduction in the cell fill factor (FF). The quantity of series and shunt resistance contained within a solar cell and its circuit

is measured by the fill factor. The generation of electricity in the module of PV depends on the *Isc* (which provides information about the maximum current capacity of the PV module under standard test conditions) and the *Voc* (which provides information about the maximum voltage the PV module can produce when exposed to sunlight under standard test conditions), which creates power at maximum and are given by ***Equation (2.1)*** shown below. [56]

$$\boldsymbol{P = Vm\ X\ Im = (FF)\ X\ Voc\ X\ Isc} \qquad (2.1)$$

According to existing studies, the PV panel module temperature is caused by various environmental factors, including solar irradiance, wind speed, and temperature of environment, also factors such as materials and glass transmittance. The formula to calculate the temperature of the module is given by ***Equation (2.2)*** shown below. [56]

$$\boldsymbol{Tmod = Tamb + Irradiance\ X\ exp\ (-a\ -b\ X\ WS\ ) + \Delta T\ X\ \frac{Irradiance}{1000}} \qquad (2.2)$$

The constants in Equation (2) are represented by a, b, and ΔT, with values of 3.56, 0.0750, and 3 respectively for glass/cell/polymer sheet. Wind speed (WS) is denoted by the variable. According to the literature, the solar cell performance slightly rises up to 12% when the cell temperature is 36°C. [56]

However, further this temperature, the performance starts to decrease with increasing temperature, as depicted in **Figure 11** shown below. [56]

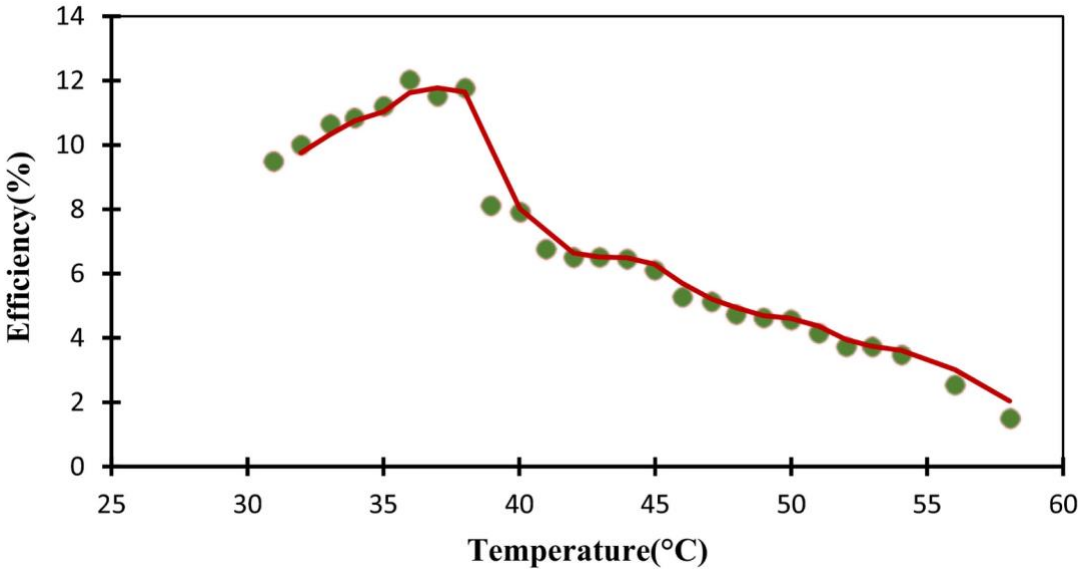

Figure 11: Module temperature effect on efficiency [56]

The efficiency of single crystal silicon solar cells is significantly impacted by the temperature at which they operate. When operating at 56 °C and 1000 W / m2 irradiance without cooling, the solar cell performance decreases by 3.13 % (the cell temperature was 32.1 °C at the beginning of the operation). [56] [57]

Research has shown that at 64 °C, the performance goes down to 69 % and down to 5 % when the temperature of the module rises from 43 to 47°C because of the wind speed effect on temperature increase level. It has been observed that without cooling, the electrical efficiency of the solar cell reduces by 0.03 % - 0.05 % with each 1 °C temperature rise. [56] [57]

The properties such as absorption and thermal dissipation of the cover materials have an effect on the photovoltaic (PV) systems performance. To improve the power extraction from PV, research is ongoing to enhance cooling techniques. However, usage of phase change material (PCM) and water cooling through microchannels in

conjunction can improve heat transfer and overall efficiency. [56]

The performance of photovoltaic (PV) modules is negatively impacted by various atmospheric pollutants such as **dust, water vapor,** and air molecules that obstruct the sun's rays from reaching the PV panel. Dust particles in the air can scatter sunlight, which reduces solar irradiation due to their larger size than the incoming solar beam wavelength. Moreover, dust can accumulate on the surface of the PV module, forming a thick layer that changes its optical properties, resulting in reduced surface transmissibility, absorption, and reflection of light thereby affecting the PV module output. The amount of dust accumulation is influenced by external elements like wind speed, humidity, precipitation, dust origin, PV module type, and surface protection play a role. This issue becomes more pronounced in arid regions with dense dust and little rainfall. Research conducted in Saudi Arabia has shown that the performance decreasing rate averages 6-7% per month, which could rise up to 13 % in six weeks without the need of cleaning. [56]

Moreover, failure to clean PV modules can lead to a significant reduction in power generation, with output dropping to half of its maximum value (50%), as indicated in research. According to research the output power in Egypt decreased by approximately 17.4% per month. [56]

The situation becomes even more challenging in areas with high levels of atmospheric pollutants, harmful gasses, airborne particles and particulate matter, where the reduction in PV energy output can exceed 60%. Dust particles accumulate on the module surface under the influence of gravity, and in humid air environments,

these particles can absorb water vapor, forming an adhesive and sticky mud on the surface. [56]

In fact, studies showed that dust accumulation for 45 days reduced overall glass cover transmittance by 20%. Rainfall can have a significant impact on dust deposition, with areas receiving low annual rainfall experiencing more severe reductions in PV power output. For instance, in Egypt, where the yearly precipitation is 18-50 mm, PV power output decreases to 60 - 70 %. [56]

Nonetheless, studies conducted in areas like the UAE and Qatar, with the annual rainfall levels of 80 - 90 mm and 70 - 75 mm respectively, have indicated a comparatively lesser decline in PV power generation (10%) compared to that observed in Egypt. [56]

The performance conversion of PV modules also reduces with risingsing dust particles, as illustrated in **Figure 12**. Although the density of dust particles may drop in some regions because of environmental factors such as rainfall and wind, an appropriate cleaning cycle is essential to maximize the PV module output throughout the year. [56]

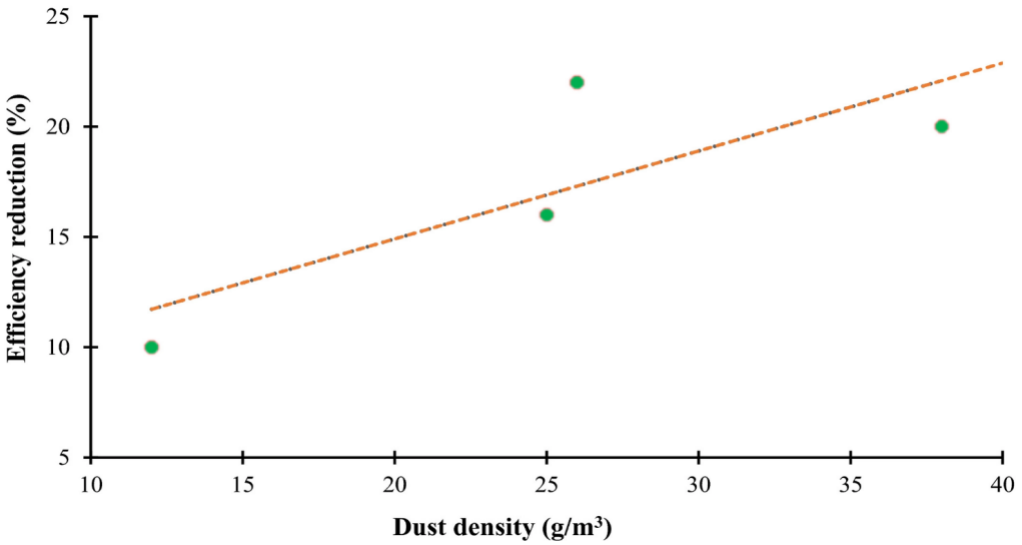

Figure 12: The correlation between module efficiency and dust density.[56]

Accumulation of dust can lead to the soiling of PV modules, particularly in humid environments where the dust particles can combine with water in the air to form mud. The extent of dust accumulation is highly dependent on atmospheric humidity, with higher humidity levels leading to greater accumulation. Additionally, when there is condensation on the PV surface, it can create capillary bridges that increase the adhesion between dust particles and the surface, further exacerbating the issue of dust build-up. Soiling on the PV panel can cause both soft and hard shading, which can reduce power output. Soft shading is caused by smog in the atmosphere, while hard shading is due to the accumulation of soil or mud on the panel surface. While solid shading can lead to a reduction in module voltage, the current remains consistent as unshaded cells continue to receive solar irradiance. [56]

The power loss due to soiling can vary depending on the location, as different types of dust can have different effects on light transmission. There is extensive research in the literature on the relationship between soiling mass and PV power loss. [56]

In certain scenarios, the reduction in PV power output is directly proportional to the amount of soiling present. When additional dust settles on an already heavily soiled surface, it does not have a significant impact on light obstruction. Studies have demonstrated that after 40 days of exposure in Saudi Arabia, coated glass experiences a 30% reduction in transmittance, while uncoated glass experiences a 37% reduction. [56]

The extent of transmission reduction varies depending on the type of glass material used, with multilayer, self-cleaning, and anti-reflection glass demonstrating less reduction in transmission than regular glass. [47] [56]

Soiling has a more significant impact on panels that have a lower tilt angle, as demonstrated in **Figure 13**. Alternating the surface texture and energy can enhance hydrophobic properties, thereby reducing the settling of dust and enhancing transmittance. The soiling issue can be addressed through natural cleaning by rainfall or mechanical cleaning through the application of fluids or water. [56]

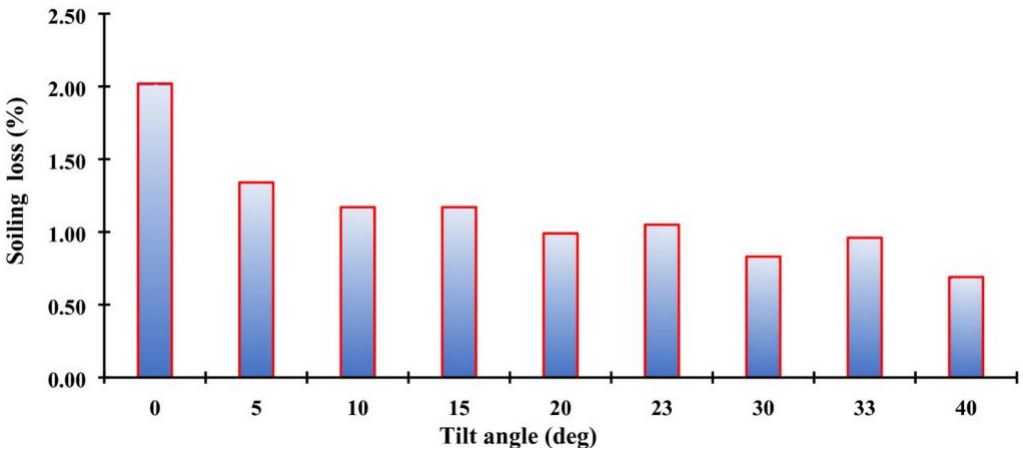

Figure 13: Soiling effect on energy loss in various tilt angles. [56]

The energy generated by a photovoltaic module is controlled by wind conditions, which include wind speed and direction. The module`s performance in windy conditions can be influenced by several factors, including temperature of the module, structure of surface and accumulation of dust deposition. The most economical option for cooling a PV module, is to maximize the use of heat transfer through convection aided by natural wind movement. Wind speed has a greater impact on the temperature of PV cells than wind direction. The surface structure and shape also affect the cooling effect of a PV panel through convection. Surfaces with grooves and structures can operate at lower temperatures at higher wind speeds. However, flat surfaces have a greater cooling effect at low wind speeds. Research in the USA has revealed that using grooved glass covers can lower the operating temperature by 3.5°C for speed of 10 m / s of wind. [56]

Moreover, the working temperature of a PV module can be reduced by as much as 10°C for wind speeds of 2.8-5.3 m/s in the USA, and by half at 12 m / s in Slovenia. In addition, wind can wipe dust away from the PV module surface, resulting in reduced dust accumulation. For instance, a study conducted in Egypt showed a drop in dust accumulation on the module surface at a given angle of tilt due to wind blowing. In desert regions, wind transports a notable quantity of dust and sand particles, causing negative impacts. In Libya, dust accumulates rapidly on the surface of PV panels at a rapid pace due to atmospheric wind movement. [56]

Shading refers to any blockage in the sunlight`s trajectory hitting on a PV panel, which can result in reduced power output. Shading can take various forms, including

hard shading caused by accumulations and obstructions that create a clear and recognizable shadow. In contrast, atmospheric factors such as dust, fog, and smoke create a soft shading effect by reducing the intensity of irradiance on the PV module. [56]

Self-shading is caused by the PV modules in the row ahead (as shown in **Figure 14**). Certain research endeavors have devised methods to mitigate the impact of self-shading, such as Brecl's empirical formula that uses a 30° angle of incline to find out the relative annual energy losses (RAEL) caused by self shading. ***Equation (2.3)*** estimates RAEL using an energy loss parameter ***A***, and a spacing factor ***F = d/b*** (where 1.5 < F < 5). [56]

$$\boldsymbol{RAEL = A\ X\ e^{-2.3F} - 0.001\ X\ F + 0.01} \qquad (2.3)$$

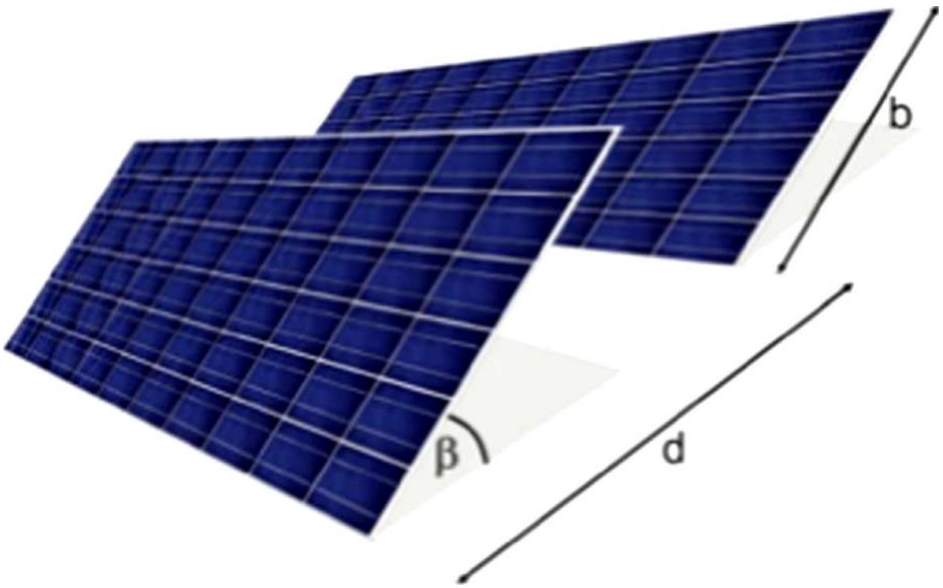

Figure 14: Effect of self-shading caused by preceding row of PV modules.[56]

The degree of shading, whether partial or complete, depends on the position of the module, layout arrangement, shading conditions, and configuration of the array, leading to a substantial decline in the PV module's output. [56]

Partial shading takes place when certain cells within a PV module become obstructed, leading to a substantial impact on module output. This is because the shaded cells are unable to generate any current, causing the current from unshaded cells to pass through the shaded ones. Consequently, the shaded cells operate in a voltage region with negative values, resulting in power dissipation rather than generation. Moreover, shading can cause the maximum power point tracker (MPPT) to deviate from the overall maximum power point (MPP), leading to a reduction in energy production. [56]

The buildup of water drops and water vapor onto solar panels from the surrounding environment can be attributed to the relative humidity, which is a determining factor. The presence of these water droplets can cause sunlight to move away from solar cells, resulting in reduction of the amount of electricity they can produce. Furthermore, the intensity of radiation is affected by humidity in a non-linear manner because of increased angles of scattering caused by water vapor particles. When exposed to a humid atmosphere for an extended period of time, corrosion happens to PV modules due to moisture infiltration into the solar cell. Furthermore, the accumulation of moisture within the module enclosure elevates the electrical conductivity of the material, potentially leading to the occurrence of leakage currents. [56]

Furthermore, there is a risk of increased corrosion rates and encapsulated delamination because of the condensation of water at the boundary between the encapsulating material and the solar cell components. This degradation in module performance can be addressed through the application of either a hermetic seal or an encapsulating material containing desiccant with low diffusivity. Additionally, high relative humidity can lead to the accumulation of adhesive and cohesive layers of dust on the surfaces of PV panels, resulting in soiling and reduced power output. In fact, the efficiency of solar cells can increase by up to 2.34 % when the relative humidity drops from 60 % to 48 %, there is a reduction in power generation. Conversely, increasing the relative humidity by 20 % can lead to a decrease in power generation by 3.16 W. Research indicates a decline in PV power output as well significantly in rainy or cloudy conditions with high relative humidity, with reductions of 40% at 76.3% relative humidity and 45% at 60.5% relative humidity. Although moisture-related losses in irradiance are natural, proper cleaning methods can help recover the power output lost due to dust adhesion on the module surface. [56]

The solar spectrum changes throughout the day and year, and some solar cells are better suited for specific portions of the spectrum than others. Solar cell spectral mismatch refers to the difference between the solar spectrum and the spectral response of a solar cell. The sun emits radiation across a wide range of wavelengths, but solar cells can only effectively convert a portion of this radiation into electrical energy based on their spectral response. The spectral response of a solar cell refers to the efficiency with which it can convert light at different wavelengths into

electricity. If the solar spectrum and the spectral response of the solar cell do not match, then the efficiency of the solar cell will be reduced. This can lead to lower power output and lower energy conversion efficiency. Spectral mismatch can be caused by a variety of factors, such as variations in the solar spectrum at different times of day or in different weather conditions, as well as differences in the spectral response of different types of solar cells. [48] The efficiency of most commercially available solar panels ranges from about 15% to 20%, meaning that for every 100 watts of sunlight that hits the panel, it generates between 15 and 20 watts of electricity. However, some advanced solar panels can have efficiencies above 20%. [44]

2.7 Dual Axis Solar Tracking Systems

Dual-axis solar tracking systems (as shown in ***Figure 15***) are used to optimize the amount of sunlight that a solar panel receives, by adjusting the panel's angle to match the position of the sun in the sky. [28] [29]

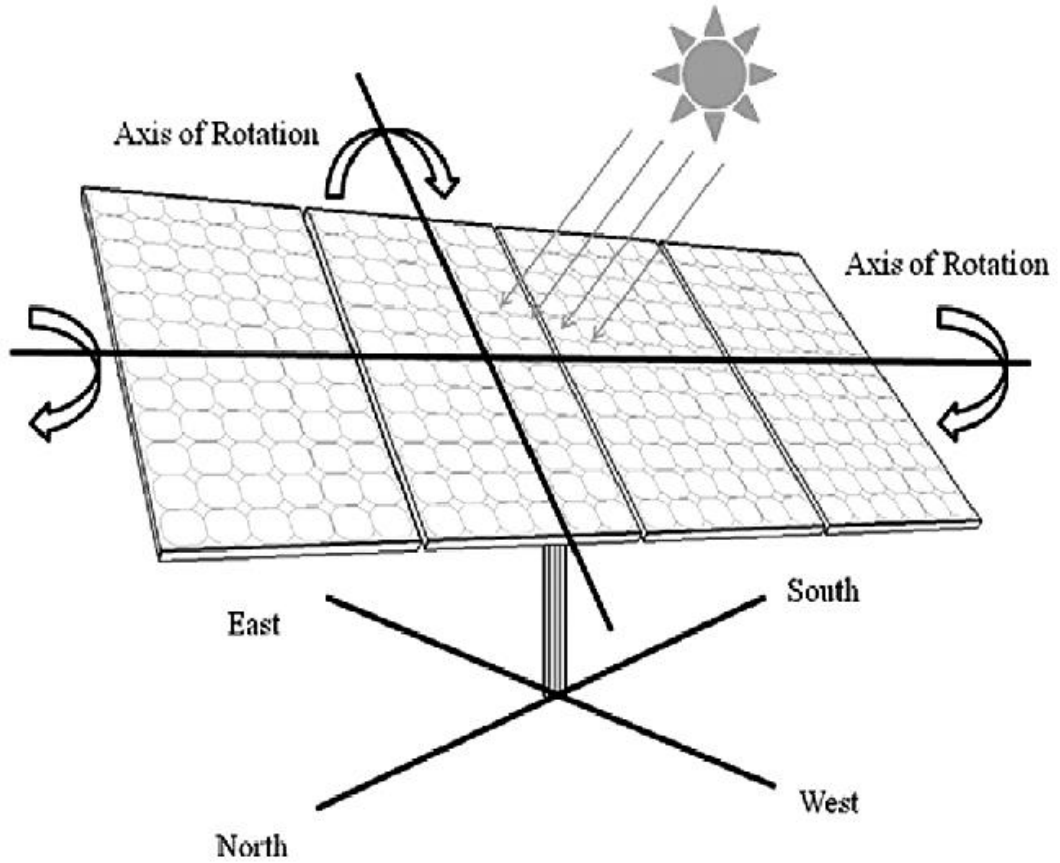

Figure 15: Dual Axis Solar Tracker model example.[43]

There are different models of DASTs around the world. Some of the models use linear actuators. Linear actuator dual-axis type of tracking system uses linear actuators to move the solar panels, which rotate about both the horizontal and vertical axes, allowing them to follow the sun's movement throughout the day.

Another type of DAST system is Dual-rotor dual-axis. This type of tracking system uses two rotors to rotate the solar panel array about both the horizontal and vertical axes, allowing them to follow the sun's movement throughout the day.

There is also a mixture of those two models defined above. Such models use rotors to trace the sun in vertical direction and linear actuators to trace the sun in horizontal

direction. All Earth Renewables is one of many companies in the world that offers dual-axis solar trackers (shown in **Figure 16** below) for residential and commercial applications. Their trackers use a patented GPS and wireless technology that allows the panels to track the sun's movement throughout the day, optimizing energy production. [50]

Figure 16: All Earth Renewables company dual axis solar tracker model.[50]

All of these types of dual-axis solar tracking systems have the ability to optimize the energy production of the solar panel. However, the choice of the system depends on the specific requirements of the project, such as location, terrain, budget, and the size of the solar panel array.

Chapter 3

METHODOLOGY

In this chapter, the design process and building process of the Dual Axis Solar Tracker (DAST) panel concept are discussed.

3.1 Design Process of the DAST Concept

In this section, the designing process of the DAST concept is going to be explained in detail. Designing process involves the Block Diagram Designing, Three Dimensional (3D) Designing and Software Designing of the concept.

3.1.1 Block Diagram Design

In this section, a graphical representation of the DAST concept is going to be discussed by showing and also explaining the working principle of the components with each other.

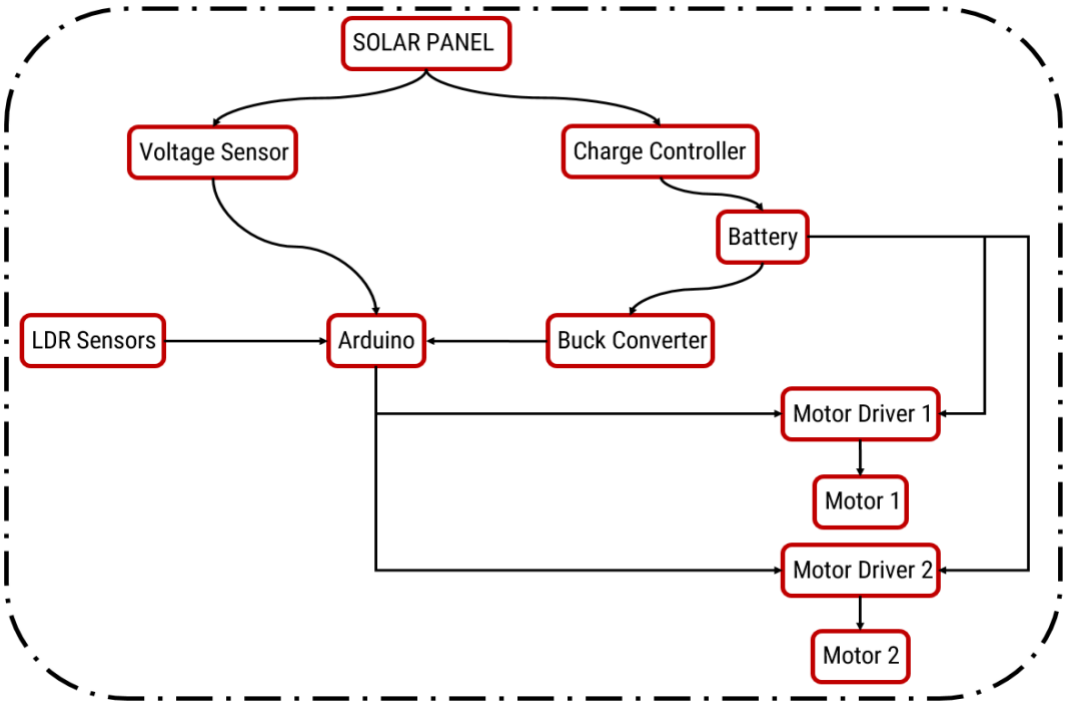

Figure 17: The graphical representation of the DAST concept design.

As shown in the **Figure 17** voltage sensor and charge controller are connected to the solar panel. Two 12 V batteries are connected in series to the solar charge controller in order to get charged properly from the electrical energy that comes from the solar panel.

Then a buck converter (step down chopper) is connected to the battery where it is adjusted to drop the battery voltage into 5V for the Arduino power supply. Other end of the voltage sensor is connected to one of the analog pins of the Arduino where the Arduino will detect the voltage that is going to be produced by the solar panel. Later on, the LDR sensor positive ends are connected to 4 of the analog pins of the Arduino.

After finishing the connections between solar panel, voltage sensor, charge controller, 24V (two 12V connected in series) battery, buck converter, LDR`s and Arduino, the

stepper motor drivers are connected to the 24V battery and also to Arduino where they are going to be used to control the stepper motor movements.

3.1.2 Three Dimensional Design

In this section, the 3D modelling of the DAST concept is going to be discussed. **Siemens NX** is the program that is used for the 3D modelling. There are components that are taken from **Grabcad** as well to make a better understanding. [3] This section consists of two parts which are, the Azimuthal Motion Design and Zenithal Motion Design of the DAST concept.

3.1.2.1 Azimuthal Motion Design

In this section, the 3D modelling of the mechanism that is providing the Azimuthal Motion of the DAST concept is going to be discussed.

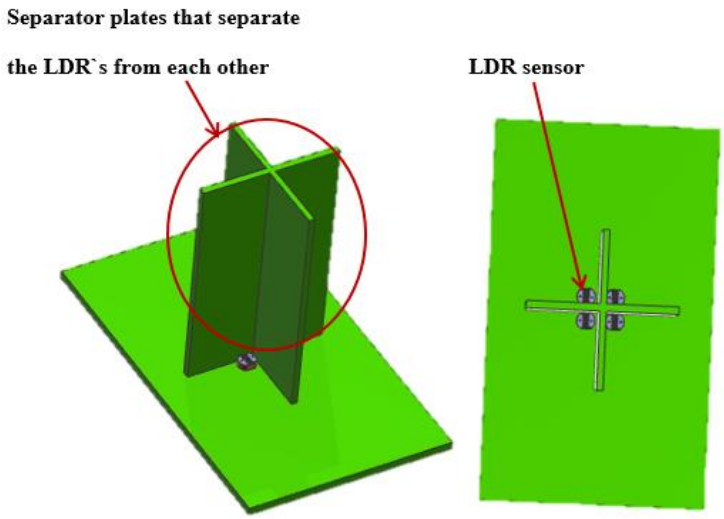

Figure 18: LDR Plate design.

As shown in **Figure 18** the LDR sensors are placed side by side and they are separated from each other with separator plates that have reasonable height. The reason for that

is to create shadow in case of change of an angle of the sun light, which is the main logic of solar tracking.

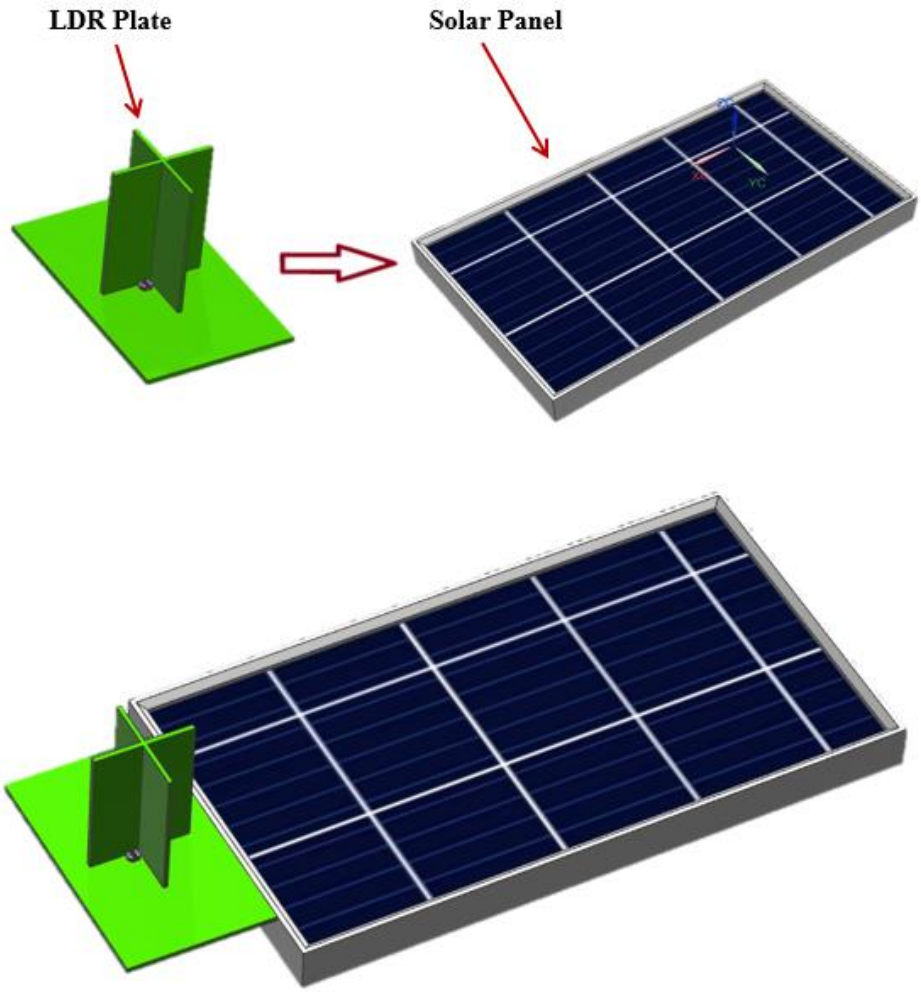

Figure 19: The mounting place of the LDR plate to the solar panel is shown

The LDR plate is going to be attached on the tip of the solar panel as shown in **Figure 19.** The reason for this is to make the LDR plate at the same position with the solar panel all the time. The LDR plate and the solar panel has to be like a rigid part because the stepper motors will rotate according to the feedback from the LDR sensors.

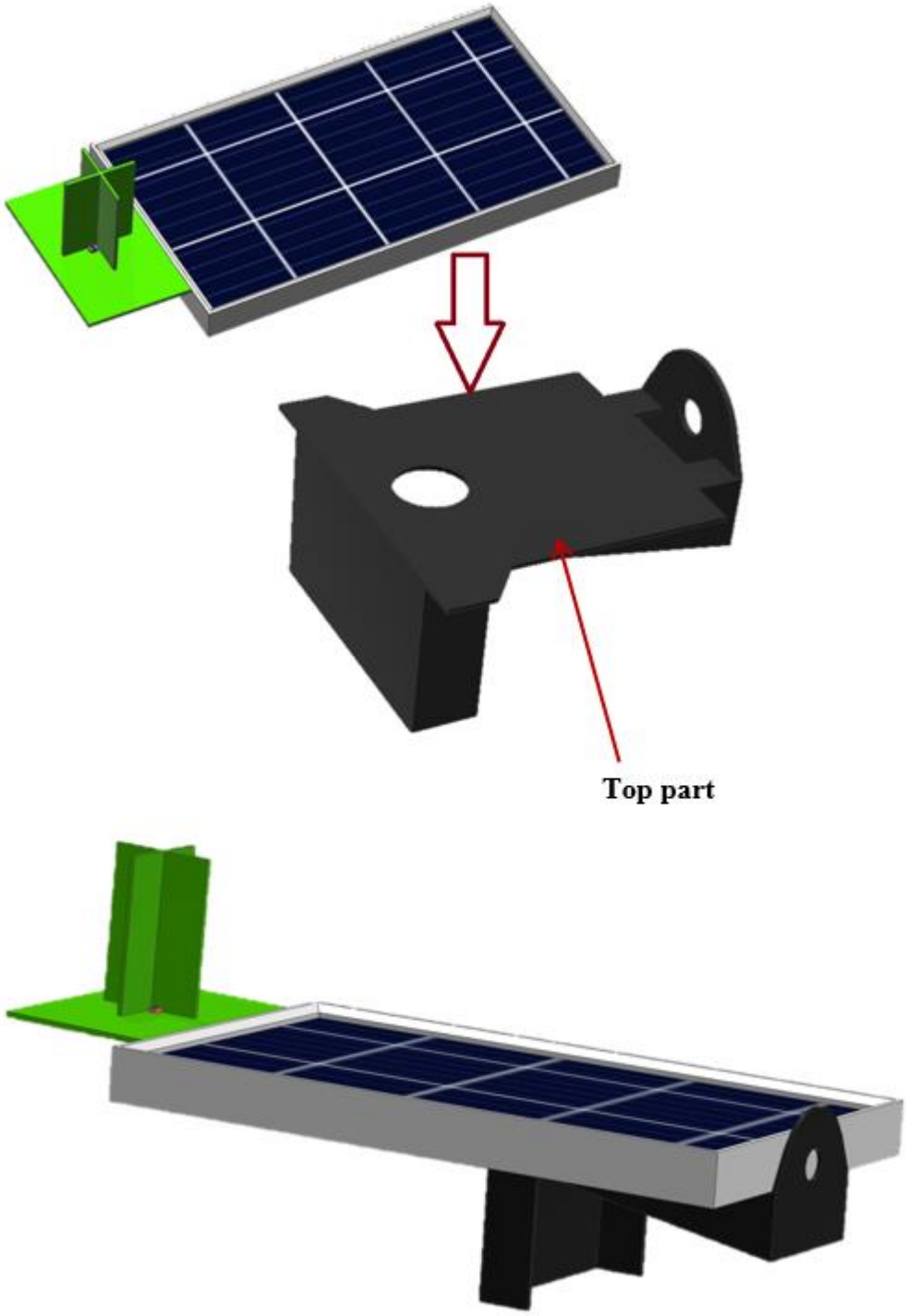

Figure 20: The attachment procedure of the top part and solar panel is shown.

The solar panel and LDR plate is going to be attached on top of the Top part of the assembly just like it is shown in **Figure 20**.

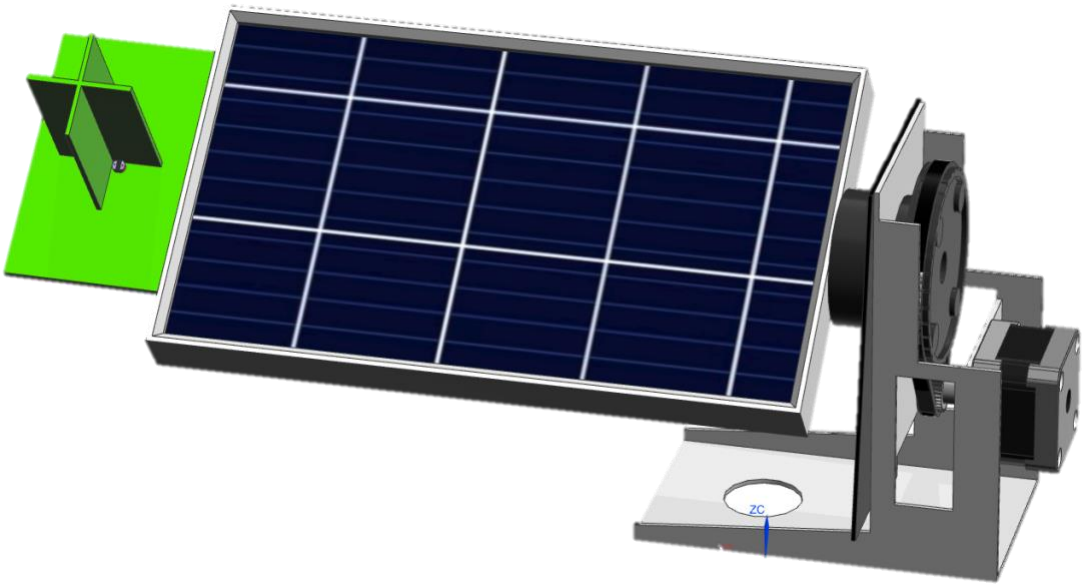

Figure 21: The horizontal rotation mechanism.

As shown in **Figure 21**, a stepper motor is giving the horizontal rotation to the mechanism and a belt is used for connecting the stepper motor with the big pulley which is attached to the mechanism. The big pulley has a diameter of approximately 75 mm and the small pulley that is attached to the stepper motor has a diameter of 20 mm.

From here it can be calculated that there is nearly a torque increase of (75 / 20) ***3.75*** times the output of the stepper motor. This will help to rotate the horizontal rotation mechanism easier or to rotate even much heavier masses placed on it. The belt connection can be seen from **Figure C.1** clearer.

3.1.2.2 Zenithal Motion Design

In this section, the 3D modeling of the mechanism that is providing the Zenithal Motion of the DAST concept is going to be discussed.

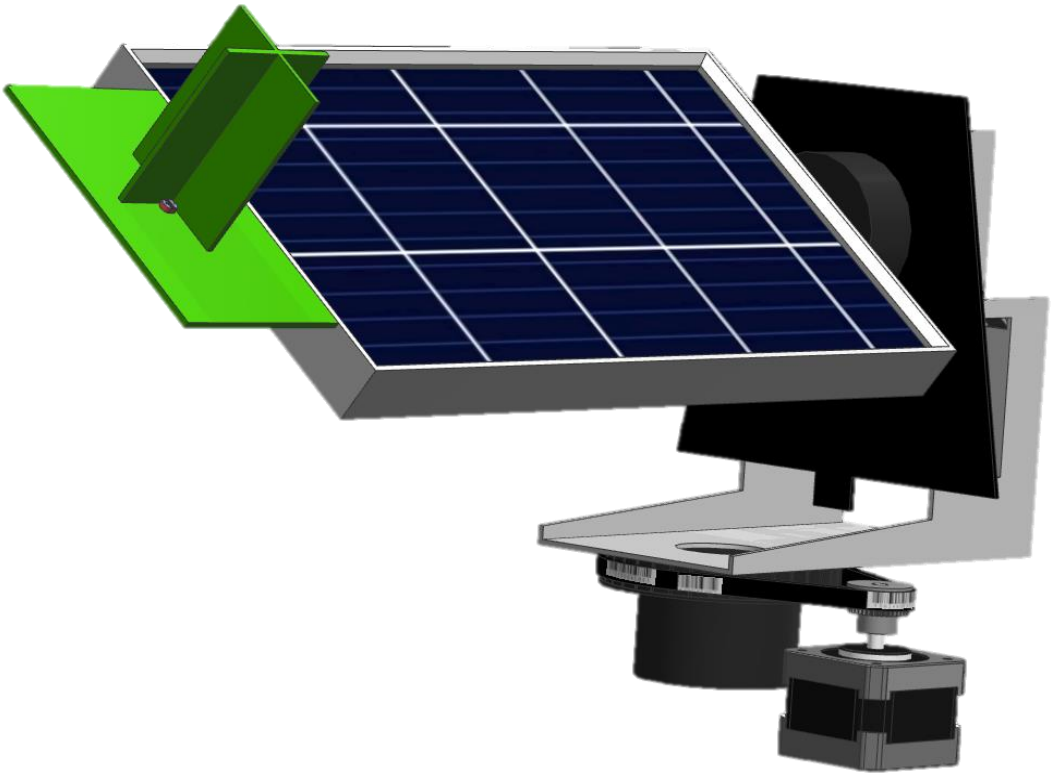

Figure 22: The solar PV panel is placed on top of the mechanism as shown above.

A stepper motor is giving the vertical rotation of the mechanism and a belt is used for connecting the stepper motor and a big pulley that is attached to the mechanism (as shown in **Figure 22**). The big pulley has a diameter of approximately 75 mm and the small pulley that is attached to the stepper motor has a diameter of 20 mm. From here it can be calculated that there is nearly a torque increase of (75 / 20) ***3.75*** times the output of the stepper motor. This will help to rotate the vertical rotation mechanism easier. The belt connection can be seen from **Figure C.2** clearer.

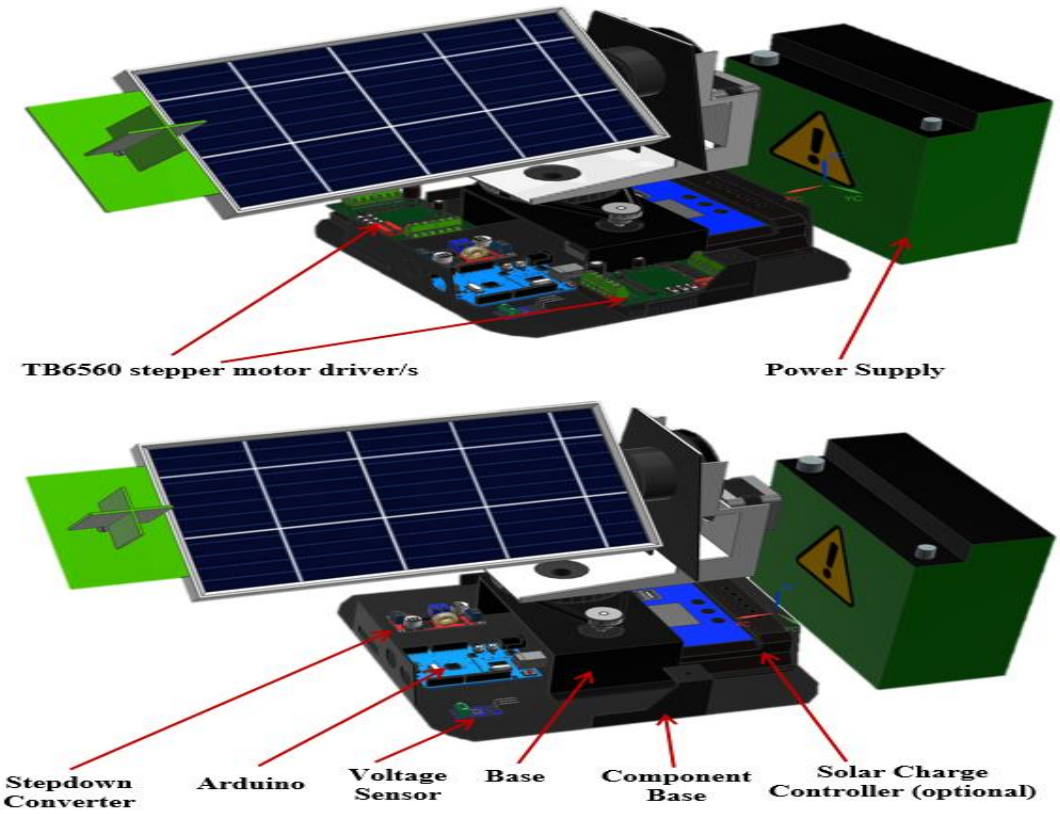

Figure 23: Electrical and mechanical components of the DAST concept design.

The whole mechanism shown in **Figure 22** has been placed on a sheet metal called the Base of the design as shown in **Figure 23**. The base is then connected to a sheet metal with bolts called Component Base. All the electronics components such as Step-down Converter, Arduino, Solar Charge Controller (optional), two TB6560 stepper motor drivers and Voltage Sensor, shown in **Figure C.2** are placed on the Component Base. Later on the Component Cover that is shown in **Figure 24** is used to prevent all the electronic components from harsh environment conditions. All the system is designed to run with direct current so a 24V Power Supply is placed next to the DAST mechanism as shown in **Figure 24** and **Figure 23.**

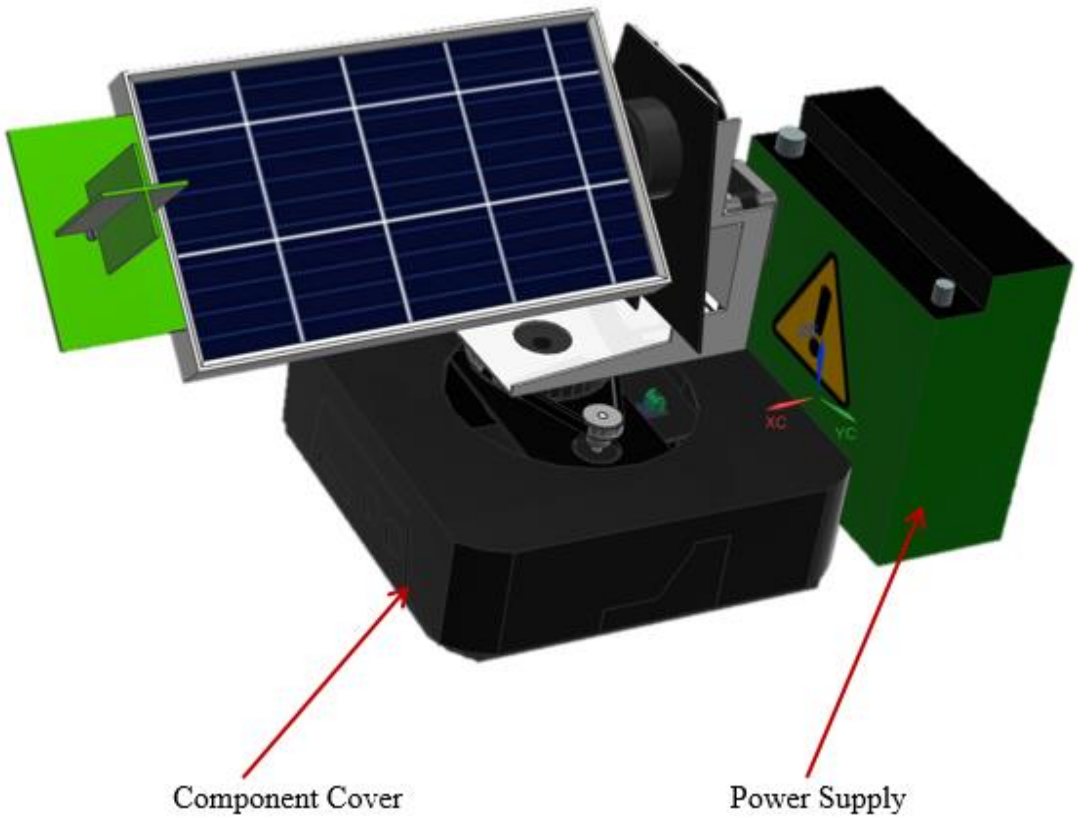

Figure 24: Final assembled version of the DAST concept design.

3.1.3 Software Design

In this section, the steps that are followed for the designing of the software to operate the DAST concept is going to be explained. This section consists of four main parts which are; the Solar Panel Voltage Value Reading, Load Current Value Reading, the LDR Value Reading and the Solar Tracking in both horizontal and vertical directions.

3.1.3.1 Solar Panel Voltage Value Reading

In this section, the software that is used to get the voltage values of the solar panel, the schematic of the connections and the logic of the software is going to be explained.

Arduino has the ability to convert Analog data to Digital data. Analog to Digital Converters (ADC) gets an analog input and converts a digital output. [1] [6]

Number of Bits of the ADC affects the accuracy of the result. This number determines how many times the converter can divide the input into. The higher the number is the better the output. [1] [6]

ADC is only as precise as the reference voltage applied to it which also determines the maximum voltage the ADC can take as an input. [1] [6]

Arduino Uno is equipped with built-in ADCs and it has six 10-bit ADCs, which means they can resolve the input down to 2 to the power of 10 which is equal to 1024 discrete steps. [1] [6]

The maximum input voltage that an Arduino Uno ADC can take is 5-volts. A voltage divider that has two separate resistors is used to measure very high voltages. Arduino can measure lower voltages that are less than 26 volts and this is all possible with the help of VCC Voltage Sensor device (Shown in **Figure B.1**) which uses precision resistors to give an accurate reading. It consists of a 7.5 kΩ resistor and a 30 kΩ resistor. [1] [6]

The reference voltage of ADC can affect its accuracy. The power supply voltage of Arduino Uno is around 5 V and it uses this as a reference voltage. This voltage supply is connected to Arduino either from its USB port or from its barrel connector which has an internal linear voltage regulator. As long as the voltage is between 4.75 and 5.25 V that would be acceptable for the Arduino. [1] [6]

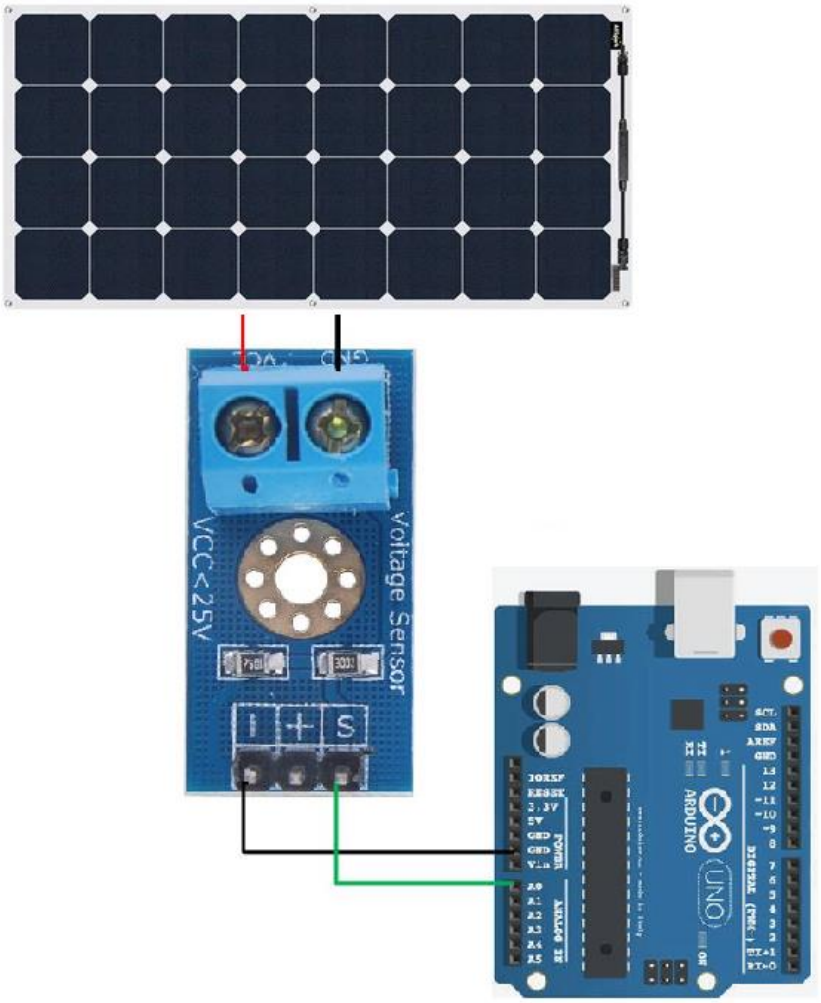

Figure 25: The connection of Arduino, voltage sensor and solar panel.[4] [6][1]

As shown in **Figure 25**, the solar panel is connected to the voltage sensor using wires. The positive terminal of the solar panel is connected to the positive terminal of the voltage sensor and the negative terminal of the solar panel to the negative terminal of the voltage sensor. [1] [6]

The voltage sensor is connected to the Arduino using jumper wires. The VCC pin of the voltage sensor is connected to the 5V pin of the Arduino and the GND pin of the voltage sensor to the GND pin of the Arduino. The OUT pin of the voltage sensor is connected to one of the analog input pins of the Arduino (in this case A0 is chosen).

The steps shown below are the logic behind the code that is uploaded to the Arduino in order to read the voltage from the voltage sensor and print it to the serial monitor;

Step 1: An analog input pin of A0 has been defined inside the code.

Step 2: As a power supply, Arduino`s 5V pin is used so a float number is defined as a reference voltage inside the code.

Step 3: Float numbers have been defined inside the code for ADC voltage and for the voltage on the input of the divider.

Step 4: Float numbers for the resistors values of the voltage sensor have been defined inside the code.

Step 5: The value produced by the ADC is an integer that can range from 0 to 1023 and that value is also defined inside the code.

Step 6: In the Setup part, a Serial Monitor named "DC Voltage Test "has been set up.

Step 7: In Loop part, an analog input read command has been made.

Step 8: Then Voltage determining at the ADC input command has been made.

Step 9: Calculating voltage at divider input command has been made.

Step 10: Code of printing results to Serial monitor has been made.

3.1.3.2 Load Current Value Reading

In this section, the software that is used to get the current consumption of the load that is applied to the solar panel, the schematic of the connections and the logic of the software is going to be explained.

The ACS712 Hall-effect current sensor (shown in **Figure B.10** in the Appendix B) is compatible with both DC and AC current, although for the purposes of this thesis, it is exclusively utilized for measuring Direct Current (DC). [1]

This device functions effectively with a 5-volt power supply, generating an output voltage that corresponds proportionally to the current under measurement. Notably, the input connection is electrically isolated from the output, ensuring its safety for deployment in high-voltage applications. [1]

It's important to note that there exist three distinct variants of this sensor, offering current measurement capabilities at 5A, 20A, and 30A. In the context of this thesis, the 20A version is used. Due to the availability of three chip versions, it is imperative to apply a 'scale factor' for precise current measurement, as illustrated in **Figure 26** shown below. [1]

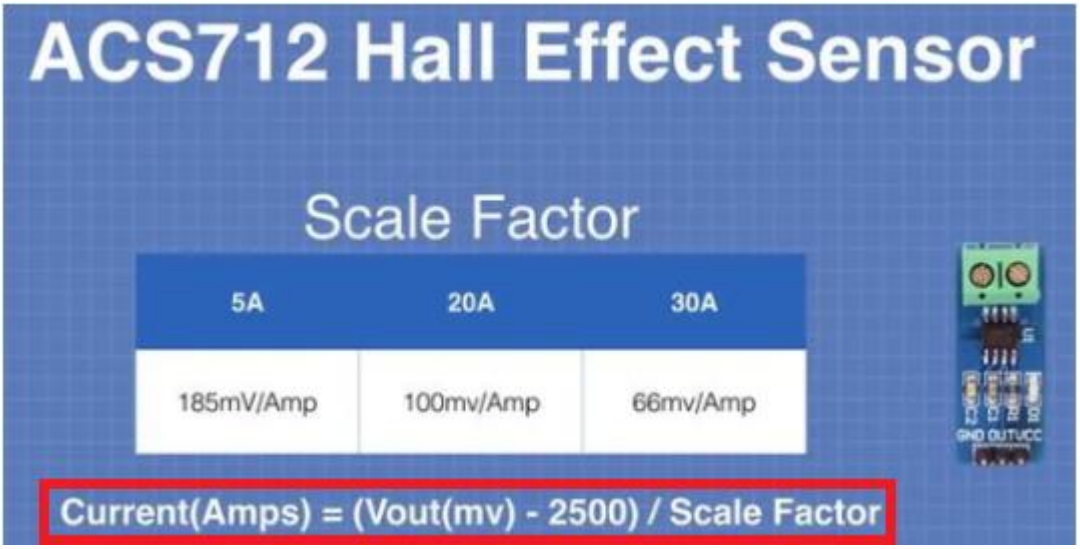

Figure 26: The formula for measuring current for different models of ACS712 hall effect sensor is shown [1]

The ACS712 sensor can effectively measure both positive and negative currents as there is no polarity. Under normal conditions, the ACS712 yields a voltage output of

2.5 volts when no current is detected. Any voltage reading above this 2.5-volt baseline indicates a positive current flow, whereas readings below 2.5 volts denote a negative current. [1]

Figure 27: shows a LED light that is connected to a solar panel as a load.

In order to measure current, a load has to be connected to the solar panel so that efficiency comparison amongst different modes of solar tracking systems can be done. As shown in **Figure 27**, a LED light that is capable of operating nominally at 4.5V is added as a load to the system.

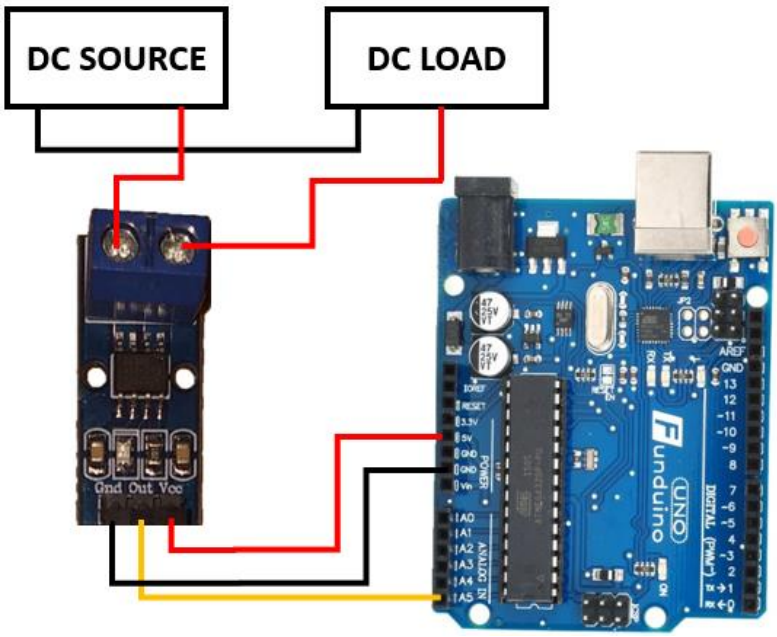

Figure 28: The connection of ACS712 hall effect sensor, Arduino, DC Source and DC Load is shown.[17]

The ACS712 has 3 pins which are GND, OUT and VCC pins. As shown in **Figure 28**, GND pin is connected to GND of Arduino, VCC pin is connected to 5V of Arduino (as the sensor is working with 5V) and OUT pin of the sensor is connected to analog pin A5 of Arduino. [1]

The steps shown below are the logic behind the code that is uploaded to the Arduino in order to read the voltage and current from the current sensor and print it to the serial monitor;

Step 1: An analog input pin of A5 has been defined inside the code.

Step 2: The measured load voltage and current is defined inside the code.

Step 3: The scale factor of the ACS712 is defined inside the code.

Step 4: As a power supply, Arduino`s 5V pin is used so a float number is defined as a reference voltage inside the code.

Step 5: The value produced by the ADC is an integer that can range from 0 to 1023

and that value is also defined inside the code.

Step 6: The output of the ACS712 sensor that represents 0 Volts is defined inside the code.

Step 7: In the Setup part, a Serial Monitor named “Load Voltage and Load Current “ has been set up.

Step 8: In the Loop part, the code for finding the equation for the calculation of Load Voltage is defined and converted in millivolts.

Step 9: Then Load Voltage is converted into Load Current inside the code.

Step 10: Code of printing results of Load Voltage and Load Current to Serial monitor has been made.

3.1.3.3 LDR Value Reading

In this section, the software that is used to get the LDR values of the DAST concept, the schematic of the LDR connections and the logic of the software is going to be explained.

LDRs also known as light dependent resistors (as shown from **Figure B.2**) are used to detect the level of light. As the light intensity increases the resistance of LDR decreases proportionally. As it gets darker or at low light levels, the resistance of the LDR is getting higher.

From Ohm's Law (V=I.R) if R is increasing the current flowing through the LDR is decreasing to balance the equation.

In bright light, the resistance of an LDR is low which means more current is flowing through it. [11]

Down below in **Figure 29**, the symbol of LDR is given and the symbol of resistor is given in **Figure 30** where later on they are going to be used in schematic design of Arduino and LDR connection.

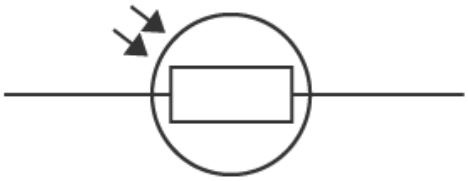

Figure 29: LDR symbol. [9]

Figure 30: Resistor Symbol. [9]

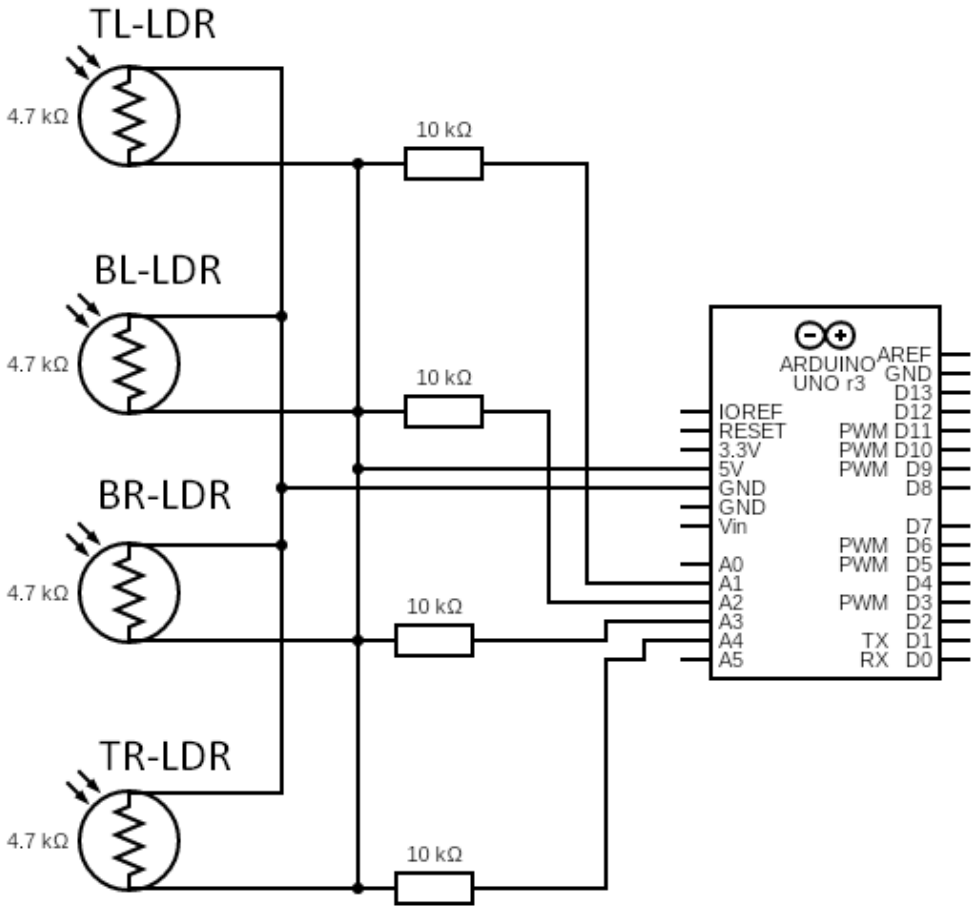

Figure 31: Schematic design of connection of LDR with Arduino [9]

In this project, four LDR is used as a sensor for tracking the sun. The connections can be seen from the schematic design shown in **Figure 31**. Each LDR is connected to a 10 k**Ω** resistor which is used as a pulldown resistor. Pull-down resistors make sure that the voltage between VCC and a microcontroller pin is actively controlled when the switch is open. Pull-down resistors pull the pin to a low value instead. [12]

If the LDR is only connected between 5V and GND without using a resistor and if the analog input pin is connected to the lower GND, despite the LDR resistance changing, the only thing that is going to be measured is going to be the potential difference between the AREF (5V) and GND. [10]

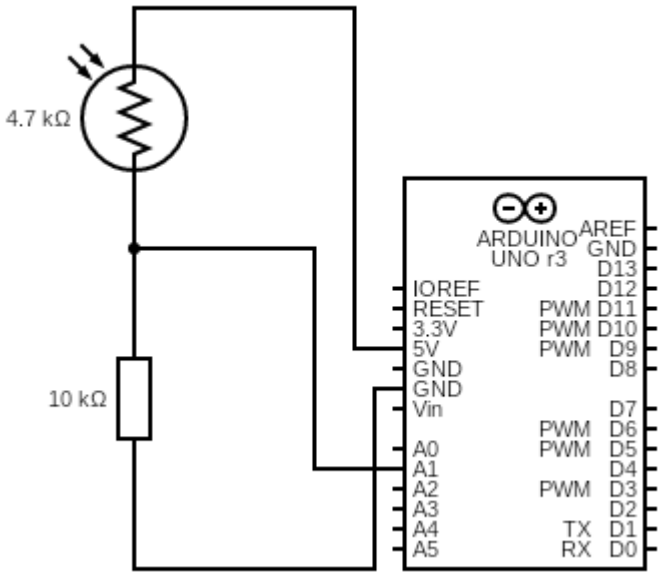

Figure 32: Voltage divider relation between LDR and Arduino [9]

In order to be able to read the resistance of an LDR, a voltage divider logic should be applied as shown in **Figure 32**. The voltage difference across the resistor should be measured thus a series connection with LDR and 10 kΩ resistor were made.

Then the analog input has been connected in between the LDR and resistor so that the voltage drop between AREF (5V) and the 10 kΩ resistor input can be measured. The resistance value of the resistor that is going to be selected should be reasonably high so that the current drawn is insignificant if the LDR is 0 ohms.

LDR`s are placed side by side as shown in **Figure 33.** The LDR`s are named Top Left LDR, Top Right LDR, Bottom Left LDR, Bottom Right LDR and they are connected to cables with different colors as shown in **Table 1.**

Table 1: Connection of LDRs to cables with different colors. [13]

LDR Cable Connections	
LDR	Color
Top Left	Yellow
Top Right	Blue
Bottom Left	Green
Bottom Right	White

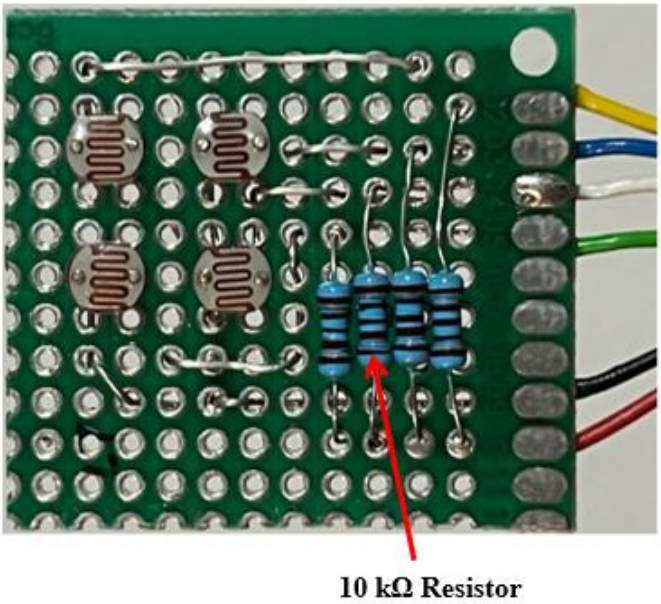

Figure 33: The placement of LDR sensors and resistors.

The steps shown below are the logic behind the code that is uploaded to the Arduino in order to read the values of all four of the LDR sensors and print them to the serial monitor;

Step 1: Top Left LDR value has been defined inside the code as an integer to analog pin A1.

Step 2: Top Right LDR value has been defined inside the code as an integer to analog

pin A4.

Step 3: Bottom Left LDR value has been defined inside the code as an integer to analog pin A2.

Step 4: Bottom Right LDR value has been defined inside the code as an integer to analog pin A3.

Step 5: In the Setup part, a serial monitor has been set up and LDR`s have been defined as input.

Step 6: In Loop part, the LDR analog value reading command has been given.

Step 7: Serial monitor to show LDR values has been given.

3.1.3.4 Solar Tracking In Both Horizontal And Vertical Directions

In this section, the software that is going to be used to operate the stepper motors of the DAST concept and give them rotation with respect to the LDR values is going to be explained.

The highest energy can be stored by a solar panel is when the sunlight is perpendicular to the panels surface. A cross-shaped part called a separator plate is used to separate those four LDR`s as shown in **Figure 34**.

The logic behind this is to create shadows and with the change in position of the sun those shadows will have different effects on each one of the LDR`s which means each one of the LDR`s will give different readings.

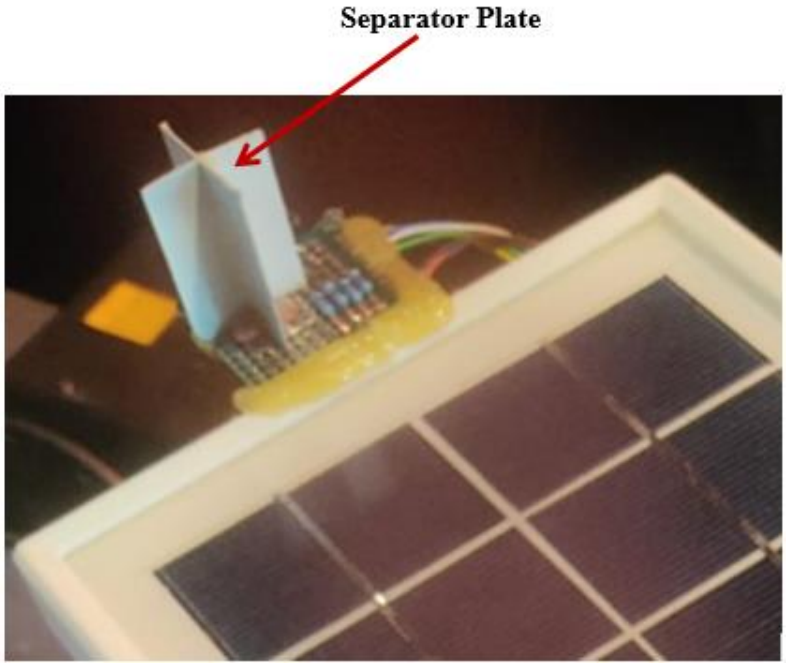

Figure 34: The separator plate that has been made is shown.

As discussed in Solar Panel Voltage Reading part, the analog pins of Arduino reads values between 0 and 1023, so it converts the analog signals to a digital representation called Analog Digital Converter (ADC), which is already built into the Arduino. [8]

According to those readings, the stepper motors will try to make the panel perpendicular to the sunlight by rotating the panel in both horizontal and vertical direction. [7]

The resistance of LDR decreases as light increases so more power will pass through it through the Analog pins, which results in the Arduino reading a higher value.

The logic behind the horizontal rotation is; if the sun is assumed to be on the right side of the panel, the TL-LDR and the BL-LDR readings will be lower than the TR-LDR and the BR-LDR readings thus the stepper motor will rotate towards CW direction.

Same logic works if the situation is vice versa which means this time the rotation of the stepper motor will be on ACW direction as shown in **Figure 35**. [8] [7]

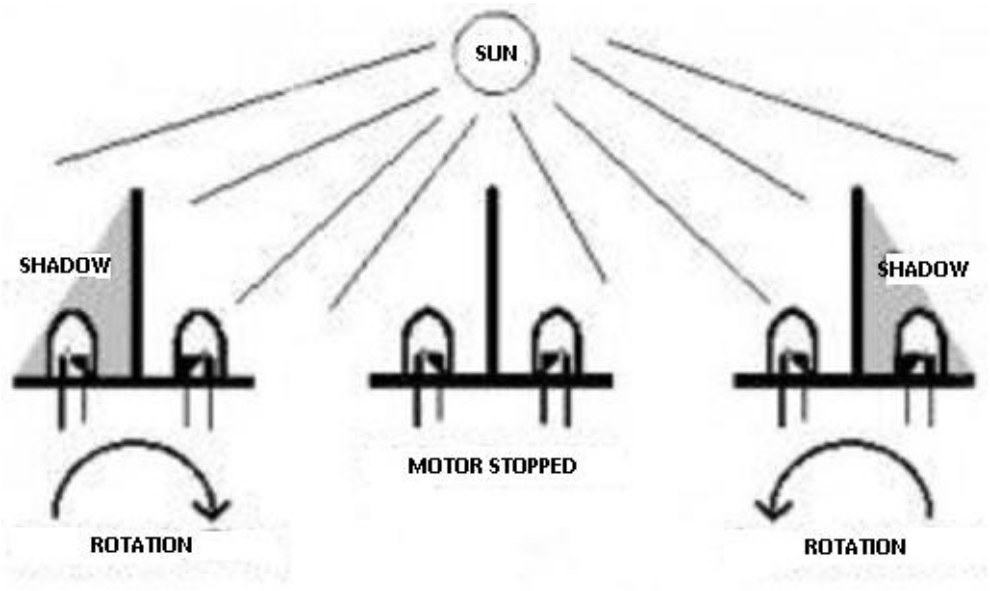

Figure 35: The logic of rotations of solar tracking[7]

KH42HM2B017 is a stepper motor that is manufactured by Japan Servo Co. which has now changed its name and is known as NIDEC SERVO CORPORATION. It is a high-torque, two-phase, hybrid stepper motor with a step angle of 1.8 degrees (200 steps per revolution). The KH42HM2B017 stepper motor is commonly used in a wide range of applications such as robotics, CNC machines, 3D printers, and automation equipment, where precise positioning and high torque are required. [53] [54]

KH42HM2B017 is a two phase, 6 wire unipolar stepper motor however in this project, it is going to be controlled by using only 4 wires. As 4 wires of the stepper motor is going to be used, a bi-polar connection is going to be made to the stepper motor as shown in **Figure 36** and **Figure 37** below.[53]

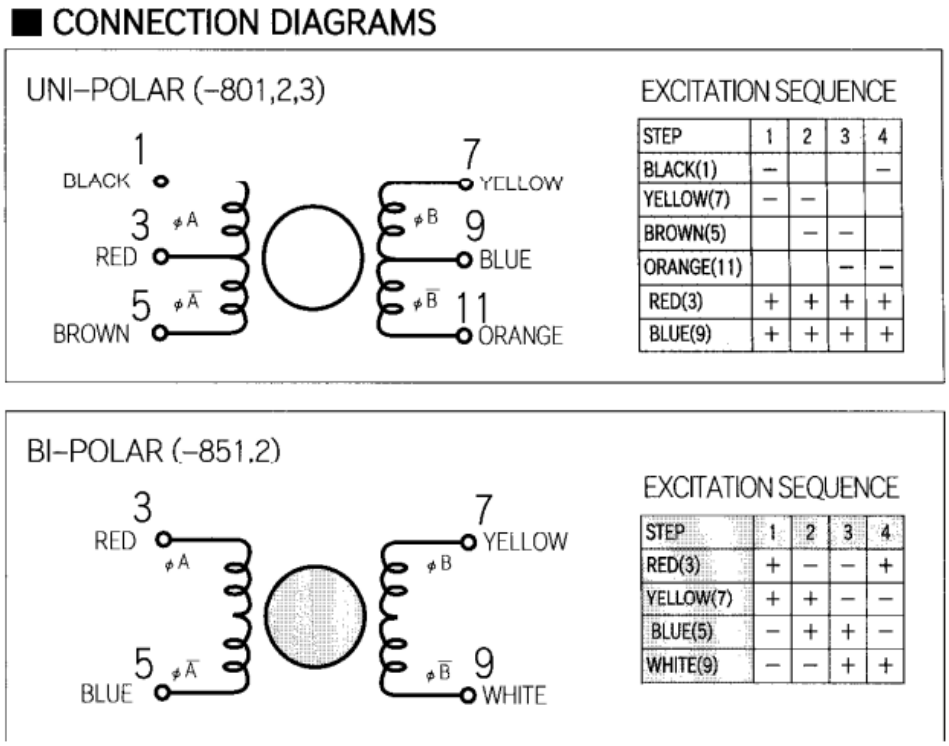

Figure 36: Unipolar and bi-polar connection diagram of KH42HM2B017 stepper motor. [53]

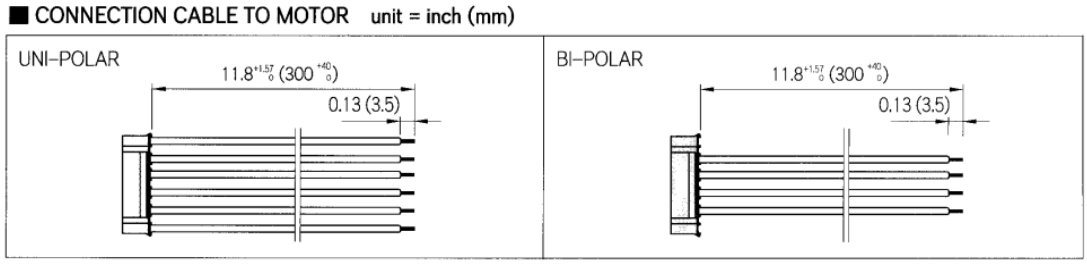

Figure 37: Unipolar and bi-polar connection cable to motor diagram of KH42HM2B017 stepper motor. [53]

The TB-6560 stepper motor driver as shown in **Figure B.3**, is based on Toshiba TB-6560-AHQ stepper motor IC with a 6N137 high-speed Optocoupler integrated on it. [13]

The operating voltage of TB-6560 is in the range of 10 – 35V DC but the recommended supply voltage is 24V DC (where in this project 24V is going to be used as well). The

rated maximum output current of TB-6560 driver is ± 3A with 3.5A peak. [13]

TB-6560 is capable of driving 2 – 4 phase or 4 - 6 wire stepper motors by using a maximum load current of 3A. In this project, for giving both horizontal and vertical rotation motion, the same model of stepper motor is used. TB-6560 is capable of giving a smooth forward and reverse driving of two-phase bipolar stepping motors by using only a clock signal. [13]

The TB6560 has three SPST (Single Pole Single Throw) switches SW1, SW2, SW3 and DIP (Dual In-line Package) switches of S1, S2, S3, S4, S5 and S6. These switches are used to adjust the output current, excitation mode and percentage of decay. The TB6560 driver module can be adjusted by setting the switches to get the required settings for controlling the stepper motor. [13]

Table 2: Running Current settings.[13]

Running Current														
A	**0.3**	**0.5**	**0.8**	**1**	**1.1**	**1.2**	**1.4**	**1.5**	**1.6**	**1.9**	**2**	**2.2**	**2.6**	**3**
SW1	OFF	OFF	OFF	OFF	OFF	ON	OFF	ON	ON	ON	ON	ON	ON	ON
SW2	OFF	OFF	ON	ON	ON	OFF	ON	OFF	OFF	ON	OFF	ON	ON	ON
SW3	ON	ON	OFF	OFF	ON	OFF	ON	ON	OFF	OFF	ON	ON	OFF	ON
S1	ON	OFF	ON	OFF	ON	ON	OFF	ON	OFF	ON	OFF	ON	OFF	OFF

As shown in **Table 2** all of the SPST switches (SW1, SW2 and SW3) and the DIP

switch S1 are used to adjust the output current. This setting is done according to the current input of the stepper motor. In this project 3A is selected as the running current of both of the stepper motors which is done by setting both of the TB6560 driver switches of SW1, SW2, SW3 to ON and S1 to OFF.

Table 3: Stop Current settings. [13]

Stop Current	
	S2
20%	ON
50%	OFF

Stop current is the current that is used to hold the motor shaft at a stopped position. This setting is necessary in order to prevent the unnecessary heating of the motor. This value should be increased if the motor struggles to hold its position. The S2 is the DIP switch that defines the stop current and there are two settings for it which is 20% when ON or 50% when OFF as shown in **Table 3**.

The Solar panel that is used is not so heavy in mass thus the horizontal rotation stepper motor will not require more holding torque so the Stop Current mode is selected as 20% which means the DIP switch S2 is set to ON.

However for the vertical rotation, the holding torque required will be higher than the horizontal rotation thus the Stop Current mode of the second TB6560 driver is selected as 50% which means the DIP switch S2 is set to OFF.

Table 4: Excitation Mode settings. [13]

Excitation Mode		
Step	S3	S4
Whole	OFF	OFF
Half	ON	OFF
1/8	ON	ON
1/16	OFF	ON

The excitation mode allows microstep settings for the TB6560 driver. In full step mode, the KH42HM2B017 stepper motors make 200 steps per revolution which is a step size of 1.8°.

Drivers like TB6560 are microstepping drivers which provide higher resolutions. They can drive stepper motors in other step modes like half (½) step mode which will give 400 microsteps per revolution. They can go up to 1/16 step mode which gives 3200 steps per revolution. Smaller microstep settings result in smoother and quieter operation however this limits the top speed of the stepper motor when controlling it with a microcontroller like Arduino.

The DIP switches S3 and S4 are for setting the excitation mode. They need to be set to correct mode in order to achieve the desired movement. Both of the TB6560 drivers in this project are set to " Whole " step mode by setting S3 and S4 switches to OFF as shown in **Table 4**.

Table 5: Decay Mode settings. [13]

Decay Mode		
Step	S5	S6
0%	OFF	OFF
25%	ON	OFF
50%	OFF	ON
100%	ON	ON

The decay setting controls how the driver chip handles the back EMF from the motor. It can be adjusted by changing these settings and by observing the performance of the motor, a suitable setting can be found. S5 and S6 are for setting decay percentage.

In this project the motor driver that is used for controlling both of the horizontal and vertical rotation motion of the panel is set to 0% decay mode where both of the switches S5 and S6 are set to OFF as shown in **Table 5**.

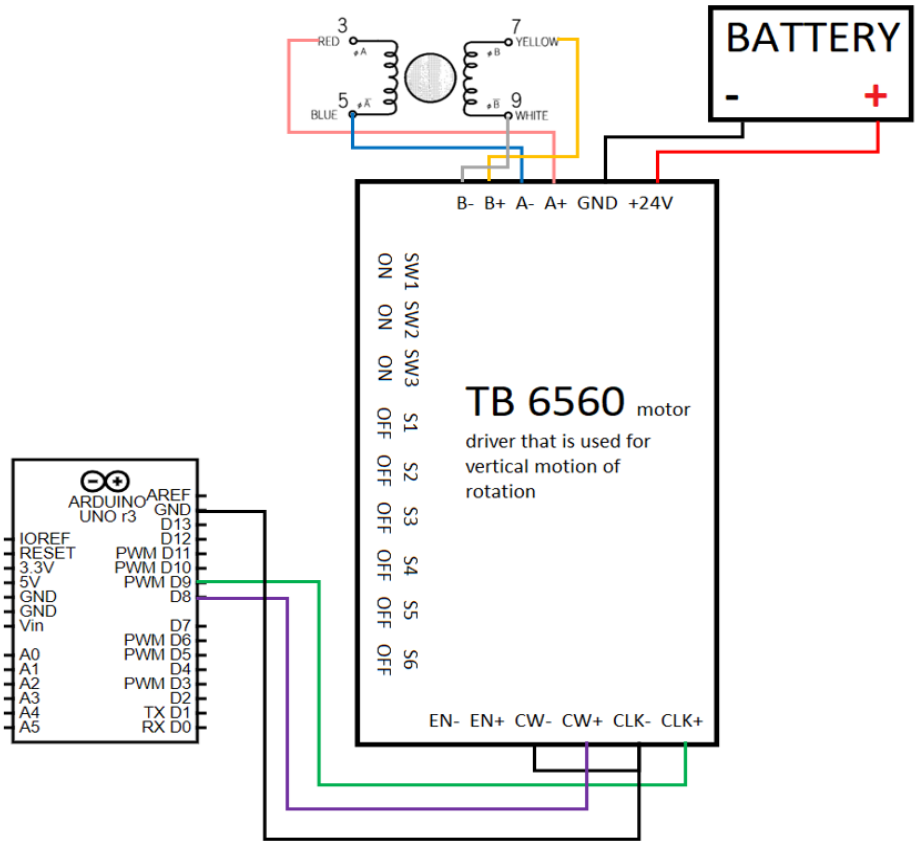

Figure 38: Schematic of the connections between Arduino, stepper motor and TB6560 motor driver for the control of vertical motion of rotation of the solar panel.

As shown in **Figure 38**, the connections between the motor driver that is used in controlling vertical motion of rotation of the panel, Arduino, Battery source and stepper motor is shown.

The stepper motor used for vertical motion of rotation of the panel is used in bi-polar settings so it has two coils. First coil has red and blue wires which are connected to B- and B+ pins whereas the second coil has yellow and white wires which are connected to A- and A+ pins of the TB6560 motor driver.

The correct pairs of the coils have been found simply by trial and error method. First, a random pair of wires from the stepper motor is chosen and their bare ends are

connected with each other. Later on the rotor of the stepper motor is tried to spin, if there is a feel of resistance formation that means the selected wires are the correct pairs.

CLK- and CLK+ pins of the TB6560 motor driver are used for the control of the pulses of the stepper motor and the rotation direction of the stepper motor is controlled by CW+ and CW- pins of the motor driver. EN- and EN+ are the enable pins of the driver.

In this project enable pins are left unconnected which means the pins are always LOW and the driver is always enabled. The CW- and CLK- pins are both negative therefore they are grounded together. [13]

Same connection procedure is applied for the control of horizontal motion of rotation of the panel and the schematic is shown below in **Figure 39.**

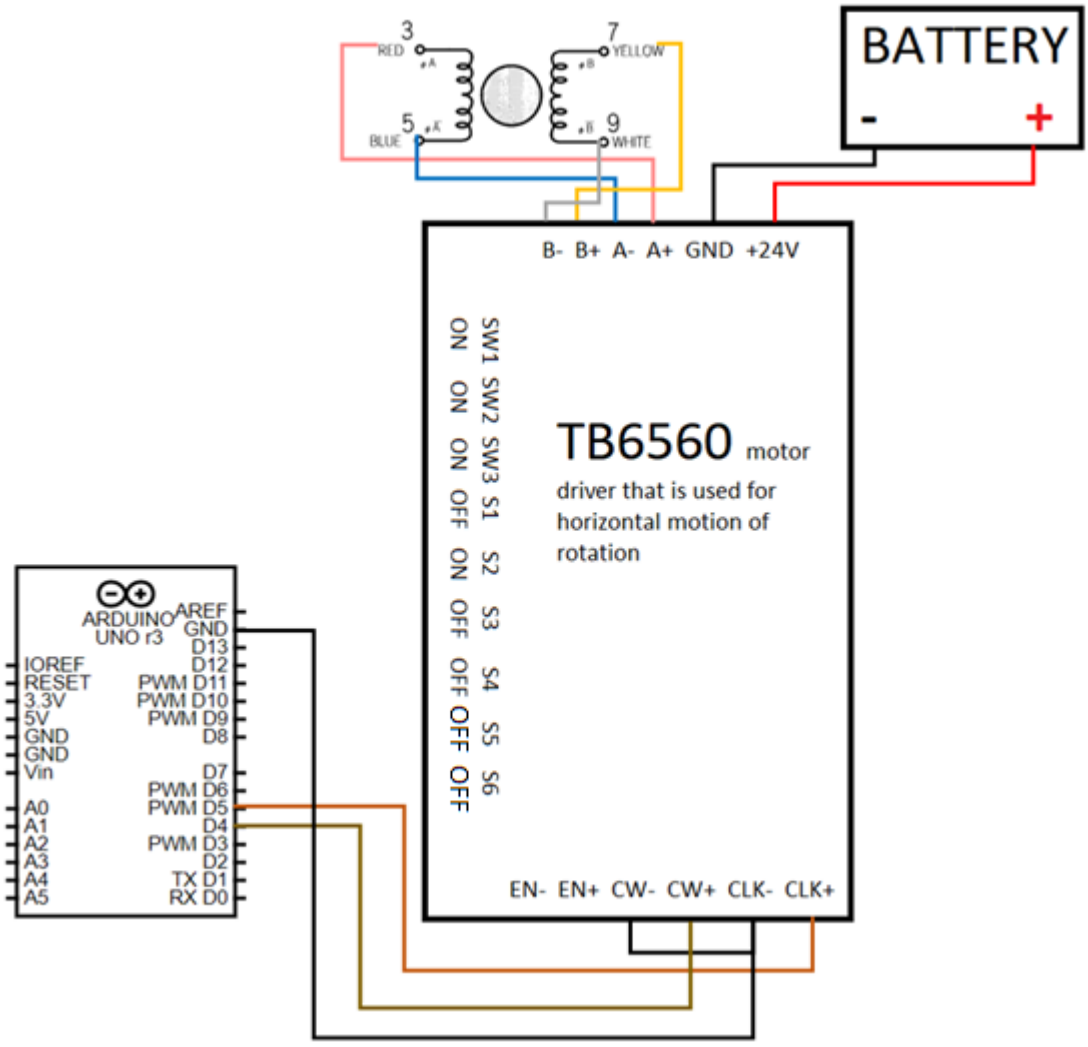

Figure 39: Schematic of the connections between Arduino, stepper motor and TB6560 motor driver for the control of horizontal motion of rotation of the solar panel.

The steps shown below are the logic behind the code that is uploaded to the Arduino in order to activate the solar tracking mechanism of the device;

Step 1: The " *Stepper.h* " library is included in the code.

Step 2: Steps per revolution is defined as 200.

Step 3: Maximum step count for the vertical motion stepper motor is defined as 1160.

Step 4: Maximum step count for the horizontal motion stepper motor is defined as 500.

Step 5: Step count for both horizontal and vertical motors have been defined.

Step 6: Steps per revolution for the vertical stepper motor is attained to digital pin D8 and D9 of the Arduino where D9 is the PWM pin.

Step 7: Steps per revolution for the horizontal stepper motor is attained to digital pin D4 and D5 of the Arduino where D5 is the PWM pin.

Step 8: In the *setup* part, the vertical motor and the horizontal motor speed is set to 70.

Step 9: In the *loop* part, a mathematical formula is written to calculate the difference between the sum of right side LDR`s (top right, bottom right) and the sum of left side LDR`s (top left, bottom left). The result of this formula shows the difference of the LDR values that are used for controlling the vertical motion.

Step 10: A mathematical formula is written to calculate the difference between the sum of left side LDR`s (top left, bottom left) and the sum of right side LDR`s (top right, bottom right). The result of this formula shows the difference of the LDR values that are used for controlling the horizontal motion.

Step 11: An " if " function is written to operate the horizontal stepper motor according to the mathematical formula that compares the horizontal motion LDR values.

Step 12: An " if " function is written to operate the vertical stepper motor according to the mathematical formula that compares the vertical motion LDR values.

3.2 Building Process of the DAST Concept

In this section, the building phase of the DAST concept is going to be explained. This section consists of two parts that explains the conversation process of the DAST system from a PLD (party lighting device) and also the assembly process of the concept where it will get its final appearance.

3.2.1 Conversion from PLD to DAST System

In this part, the modification of the PLD system into the DAST system is going to be explained. The main frame of this design has been originally used for party lighting systems shown in **Figure 40**. The original design consists of a system with dual axis rotation. The design has been modified and all the unnecessary parts have been removed. Then the solar panel and the LDR circuit has been attached to the design as shown in **Figure C.3**.

Figure 40: PLD (Party Lighting Device).[2]

Figure 41: The look of PLD after the removal of plastic covers.

All the plastic covers and unnecessary parts such as colorful lenses, the coils and electronic components (that are not going to be used for dual axis tracking purpose) have been removed from the device as shown in **Figure 41**.

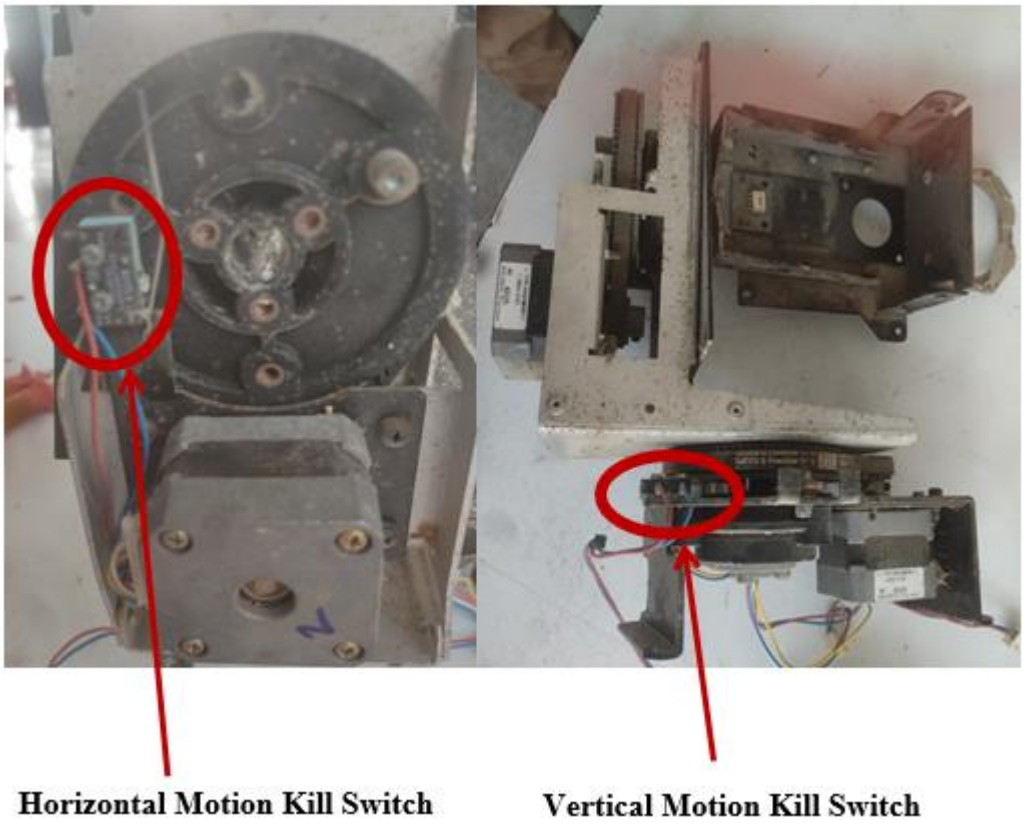

Figure 42: Kill switch mechanisms of the device to prevent over rotation.

As it can be seen from **Figure 42** the party lighting device has 2 kill switches (one switch for each motion) in order to prevent over rotation and damage the stepper motors.

The kill switches are not removed from the device as they can later be used for another purpose which is explained in **Future works** part.

After the removal process, the final look of the frame of the DAST is like shown in **Figure C.4**.

Next step is to install the electronic components and solar panel to this frame

according to the CAD design.

3.2.2 Assembly of DAST System

This part explains the steps that are followed to create the DAST concept. All the electronic components and tools that are required for this process are explained in this part.

In order to make a proper circuit and connect wires, soldering wire is going to be used with soldering iron which is shown in **Figure A.1**. In order to test the electrical compatibility and also make error testing, a multimeter is used (shown in **Figure A.2**).

Two KH42HM2B017 stepper motors (shown in **Figure B.4**) are used in the original design of the party lighting device (PLD). They have been kept the same, there is no need to change the stepper motors. They are quite powerful to rotate the panel that is going to be used.

However, two stepper motor drivers are going to be needed in order to control the stepper motors because the original controllers of the PLD are not suitable for our purpose thus two TB6560 stepper motor drivers (shown in **Figure B.3**) are going to be used to control the stepper motors.

Four LDR sensors are going to be used together with 10 kΩ resistors as shown in **Figure 43**. One resistor for each of the LDR`s. The idea here is to program the Arduino in such a way of getting a value from the LDR readings and by this way sending directions to stepper motors.

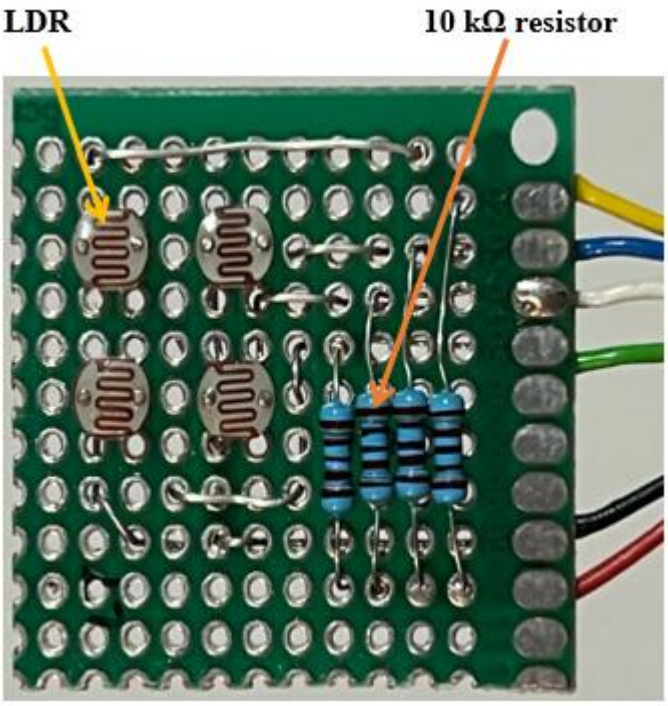

Figure 43: The placement of LDR sensors and resistors.

Before the installation of electrical components to the DAST system, all the electrical connections were made on the bread board with the help of jumper wires (shown in **Figure A.3**). An Arduino alternative device called FUNDUINO UNO (as shown in **Figure B.5**) is used for code generation and uploading in order to test the program and components working properly.

After the confirmation of the program and the correct connections, an 80 X 60 mm experimental pertinax board and also 2 mm diameter wire heat shrink is used to make a proper circuit as shown in **Figure A.4**.

A power supply shown in **Figure B.6**, that is capable of giving 24V, 12V and 5V is used during the testing operations. A 24V battery could also be used for the testing purposes but it is not used.

The reason for this is not to drop the capacitance of the battery (the testing period takes so much time) because the same battery is going to be used in the DAST system that is explained in the 3.1.2 CAD of the Structure part.

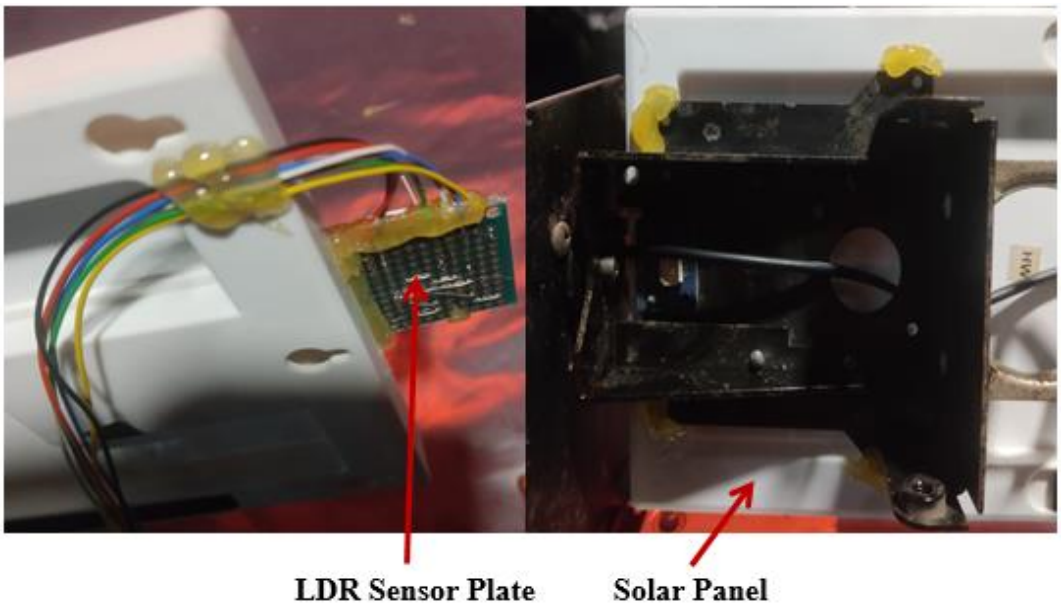

Figure 44: The mounting of the LDR Sensor Plate and Solar Panel is shown.

A 12V solar panel is glued to the Top Part of the structure from several different points and the LDR Sensor Plate is connected to the solar panel. The LDR and solar panel cables are then glued together in a more organized manner to the back side of the solar panel as it can be seen from **Figure 44**.

As shown with the red circle in **Figure 45**, all the cables are taken out through a hole inside the big pulley. The gluing operation is done by the hot melt adhesive glue gun shown in **Figure A.5.** The look of the DAST system after the installation of the solar PV panel can be seen in **Figure C.2.**

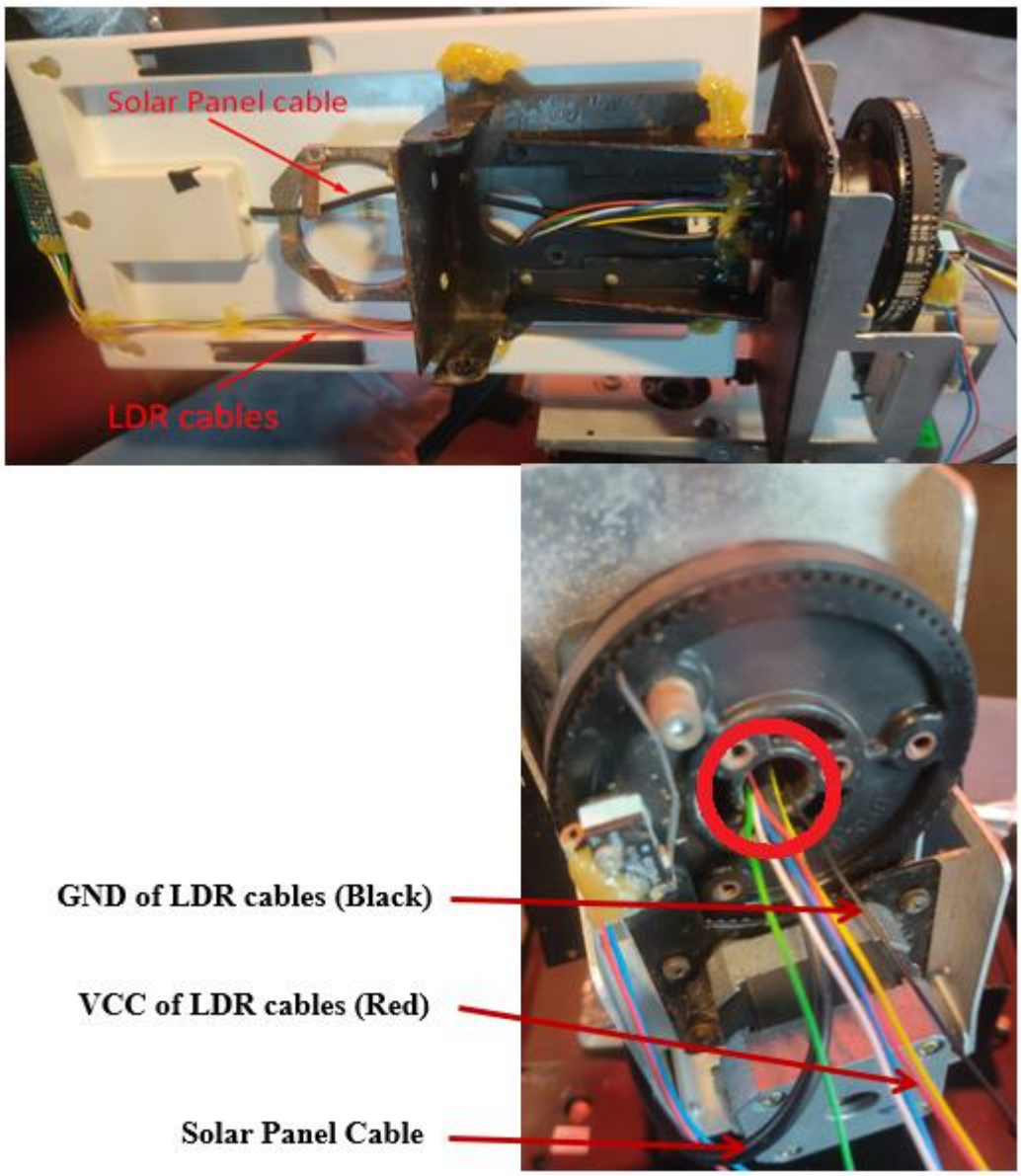

Figure 45: shows the orientation of LDR and Solar panel cables

A stepdown converter is used (shown in **Figure B.7**) to drop the voltage of the serial connected two 12V 20Ah Lead Acid Gel Battery (12V battery shown in **Figure B.8**) which makes 24V 20Ah of battery. In this design Arduino is preferred to work in 5V because all the voltage comparisons that have been defined in the code are according to 5V.

All the electronic components have been glued on top of transparent plexiglass plastic parts (as shown in **Figure A.6**) by using a hot melt adhesive gun. This is done because the electronic components are going to be placed on top of a sheet metal that is named “Component base “.

As metal is electrically conductive, the bottom of electrical components should be insulated before mounting them in order to prevent short circuit.

As the electronic components are operating they start to produce some heat and that can melt the plastic insulator base if it does not have a high temperature withstand capacity. Plexiglass is selected as an insulator base for the electrical components not only because of preventing short-circuit but also its ability to withstand temperatures of up to 80 °C. [16]

Chapter 4

DATA ANALYSIS, RESULTS AND CONCLUSION

This chapter presents and interprets the data analysis and results of the study conducted. The findings are in five parts, namely; Data Analysis and Results of ZAST System, Data Analysis and Results of DAST System, Data Analysis and Results of AAST System, the comparison of the results between those three systems and lastly the conclusion on the findings with the summary of the test results are discussed.

4.1 Data Analysis and Results of ZAST System

In this part, the data analysis and also the results of the ZAST system is going to be explained. This part shows the location and time of the test, the voltage values taken from the solar panel, the current and power values taken from the load is shown. All the steps of the test are explained.

The performance analysis of the ZAST System took place on 27.09.2023 and the starting time was at 14:23:32.125 pm whereas the finishing time was at 14:52:22.827 pm. Overall lap time was approximately 28 min. 50 sec. The path that has been followed is shown in **Figure 46** below.

Figure 46: shows the path that has been traced during the testing process.

The steps that are followed for the testing procedure is shown below;

Step-1: At exactly 14:23:32.125 pm, the testing procedure of the ZAST system has been started and the path shown in **Figure 46** is followed.

Step-2: The movement of the vehicle and the serial monitor of Arduino activated at the same time.

Step-3: The movement of the vehicle and the activation of the Arduino serial monitor is stopped at the same time at 14:52:22.827 pm. Overall lap time was approximately 28 min. 50 sec.

Step-4: All the data that was showing in the monitor has been recorded until the path that was set is finished.

As there was no delay given to Arduino code, the voltage readings on Arduino serial monitor for this test consist of 6017 lines. This is because of the time setup of Arduino which uses hr/min/sec/millisec concept so this concept is modified and summarized to the hr/min/sec concept.

After this time setup, the number of lines in the table dropped to 174 lines. In order to make the comparison between the systems more valid, the number of lines kept the same. The data is extracted as a Time vs Solar Panel voltage (V), Solar Panel voltage (mV), Load Current (mA), Load Power (W) table and all the readings with respect to time are shown in **Table 6.**

Table 6: Shows the data of the solar panel recorded during testing of the ZAST system.

Data Analysis of ZAST System

Reading no:	Time (hr/min/sec)	Solar Panel Voltage (V)	Solar Panel Voltage (mV)	Load Current (mA)	Load Power (W)
1	14:23:32	3.833	3833	73	0.279809
2	14:23:42	3.882	3882	171	0.663822
3	14:23:52	3.931	3931	122	0.479582
4	14:24:02	3.979	3979	122	0.485438
5	14:24:12	4.077	4077	73	0.297621
6	14:24:22	4.126	4126	269	1.109894
7	14:24:32	4.15	4150	24	0.0996
8	14:24:42	4.248	4248	24	0.101952
9	14:24:52	4.272	4272	24	0.102528
10	14:25:02	4.321	4321	73	0.315433
11	14:25:12	4.37	4370	24	0.10488
12	14:25:22	4.419	4419	24	0.106056
13	14:25:32	4.443	4443	122	0.542046
14	14:25:42	4.443	4443	73	0.324339
15	14:25:52	4.565	4565	24	0.10956
16	14:26:02	4.59	4590	24	0.11016
17	14:26:12	4.639	4639	73	0.338647
18	14:26:22	4.614	4614	24	0.110736
19	14:26:32	4.614	4614	24	0.110736
20	14:26:42	4.614	4614	24	0.110736
21	14:26:52	4.59	4590	171	0.78489

22	14:27:02	4.541	4541	24	0.108984
23	14:27:12	4.541	4541	73	0.331493
24	14:27:22	4.492	4492	24	0.107808
25	14:27:32	4.468	4468	24	0.107232
26	14:27:42	4.395	4395	24	0.10548
27	14:27:52	4.346	4346	24	0.104304
28	14:28:02	4.297	4297	24	0.103128
29	14:28:12	4.272	4272	73	0.311856
30	14:28:22	4.224	4224	73	0.308352
31	14:28:32	4.224	4224	171	0.722304
32	14:28:42	4.175	4175	24	0.1002
33	14:28:52	4.15	4150	73	0.30295
34	14:29:02	4.15	4150	122	0.5063
35	14:29:12	4.102	4102	122	0.500444
36	14:29:22	4.126	4126	171	0.705546
37	14:29:32	4.15	4150	73	0.30295
38	14:29:42	4.175	4175	122	0.50935
39	14:29:52	4.15	4150	73	0.30295
40	14:30:02	4.175	4175	73	0.304775
41	14:30:12	4.15	4150	122	0.5063
42	14:30:22	4.175	4175	24	0.1002
43	14:30:32	4.175	4175	22	0.09185
44	14:30:42	4.175	4175	73	0.304775
45	14:30:52	4.199	4199	24	0.100776
46	14:31:02	4.199	4199	24	0.100776
47	14:31:12	4.199	4199	171	0.718029
48	14:31:22	4.199	4199	171	0.718029
49	14:31:32	4.199	4199	171	0.718029
50	14:31:42	4.199	4199	122	0.512278
51	14:31:52	4.224	4224	73	0.308352
52	14:32:02	4.297	4297	24	0.103128
53	14:32:12	4.321	4321	24	0.103704
54	14:32:22	4.419	4419	24	0.106056
55	14:32:32	4.565	4565	24	0.10956

56	14:32:42	4.81	4810	24	0.11544
57	14:32:52	5.176	5176	24	0.124224
58	14:33:02	5.298	5298	122	0.646356
59	14:33:12	5.298	5298	171	0.905958
60	14:33:22	5.322	5322	122	0.649284
61	14:33:32	5.371	5371	122	0.655262
62	14:33:42	5.298	5298	122	0.646356
63	14:33:52	4.785	4785	73	0.349305
64	14:34:02	4.468	4468	24	0.107232
65	14:34:12	3.467	3467	24	0.083208
66	14:34:22	3.516	3516	22	0.077352
67	14:34:32	4.761	4761	24	0.114264
68	14:34:42	4.883	4883	73	0.356459
69	14:34:52	5.029	5029	73	0.367117
70	14:35:02	5.103	5103	73	0.372519
71	14:35:12	5.151	5151	73	0.376023
72	14:35:22	5.2	5200	24	0.1248
73	14:35:32	5.2	5200	171	0.8892
74	14:35:42	5.151	5151	171	0.880821
75	14:35:52	5.103	5103	24	0.122472
76	14:36:02	5.176	5176	122	0.631472
77	14:36:12	5.054	5054	73	0.368942
78	14:36:22	5.103	5103	24	0.122472
79	14:36:32	5.078	5078	24	0.121872
80	14:36:42	3.735	3735	122	0.45567
81	14:36:52	3.882	3882	73	0.283386
82	14:37:02	5.225	5225	73	0.381425
83	14:37:12	5.225	5225	122	0.63745
84	14:37:22	5.225	5225	73	0.381425
85	14:37:32	5.2	5200	73	0.3796
86	14:37:42	3.906	3906	24	0.093744
87	14:37:52	3.638	3638	171	0.622098
88	14:38:02	5.273	5273	73	0.384929
89	14:38:12	5.298	5298	24	0.127152

90	14:38:22	5.054	5054	73	0.368942
91	14:38:32	5.322	5322	122	0.649284
92	14:38:42	5.176	5176	24	0.124224
93	14:38:52	5.2	5200	122	0.6344
94	14:39:02	5.273	5273	122	0.643306
95	14:39:12	5.127	5127	73	0.374271
96	14:39:22	5.322	5322	122	0.649284
97	14:39:32	5.347	5347	171	0.914337
98	14:39:42	5.371	5371	122	0.655262
99	14:39:52	5.371	5371	269	1.444799
100	14:40:02	5.347	5347	122	0.652334
101	14:40:12	5.322	5322	73	0.388506
102	14:40:22	5.444	5444	122	0.664168
103	14:40:32	5.444	5444	24	0.130656
104	14:40:42	5.42	5420	24	0.13008
105	14:40:52	5.444	5444	73	0.397412
106	14:41:02	5.444	5444	24	0.130656
107	14:41:12	5.444	5444	122	0.664168
108	14:41:22	5.444	5444	22	0.119768
109	14:41:32	5.469	5469	171	0.935199
110	14:41:42	5.42	5420	122	0.66124
111	14:41:52	5.444	5444	24	0.130656
112	14:42:02	5.444	5444	171	0.930924
113	14:42:12	5.444	5444	73	0.397412
114	14:42:22	5.444	5444	73	0.397412
115	14:42:32	5.493	5493	73	0.400989
116	14:42:42	5.493	5493	73	0.400989
117	14:42:52	5.518	5518	171	0.943578
118	14:43:02	5.542	5542	122	0.676124
119	14:43:12	5.542	5542	73	0.404566
120	14:43:22	5.566	5566	269	1.497254
121	14:43:32	5.518	5518	122	0.673196
122	14:43:42	5.493	5493	73	0.400989
123	14:43:52	5.493	5493	171	0.939303

124	14:44:02	5.42	5420	171	0.92682
125	14:44:12	5.371	5371	73	0.392083
126	14:44:22	5.298	5298	171	0.905958
127	14:44:32	5.2	5200	24	0.1248
128	14:44:42	5.176	5176	24	0.124224
129	14:44:52	5.078	5078	171	0.868338
130	14:45:02	5.151	5151	73	0.376023
131	14:45:12	5.078	5078	24	0.121872
132	14:45:22	5.103	5103	73	0.372519
133	14:45:32	5.127	5127	171	0.876717
134	14:45:42	5.2	5200	22	0.1144
135	14:45:52	3.516	3516	122	0.428952
136	14:46:02	3.857	3857	122	0.470554
137	14:46:12	3.613	3613	73	0.263749
138	14:46:22	3.442	3442	171	0.588582
139	14:46:32	3.442	3442	171	0.588582
140	14:46:42	3.418	3418	171	0.584478
141	14:46:52	4.98	4980	122	0.60756
142	14:47:02	5.029	5029	24	0.120696
143	14:47:12	5.005	5005	24	0.12012
144	14:47:22	5.054	5054	171	0.864234
145	14:47:32	5.078	5078	73	0.370694
146	14:47:42	5.103	5103	171	0.872613
147	14:47:52	5.151	5151	73	0.376023
148	14:48:02	5.273	5273	73	0.384929
149	14:48:12	5.298	5298	171	0.905958
150	14:48:22	5.273	5273	24	0.126552
151	14:48:32	5.322	5322	73	0.388506
152	14:48:42	5.396	5396	24	0.129504
153	14:48:52	5.322	5322	122	0.649284
154	14:49:02	5.298	5298	24	0.127152
155	14:49:12	5.298	5298	24	0.127152
156	14:49:22	4.224	4224	122	0.515328
157	14:49:32	5.371	5371	24	0.128904

158	14:49:42	5.42	5420	122	0.66124
159	14:49:52	5.469	5469	24	0.131256
160	14:50:02	4.175	4175	73	0.304775
161	14:50:12	5.469	5469	73	0.399237
162	14:50:22	5.469	5469	171	0.935199
163	14:50:32	5.42	5420	73	0.39566
164	14:50:42	5.42	5420	24	0.13008
165	14:50:52	5.42	5420	24	0.13008
166	14:51:02	5.469	5469	73	0.399237
167	14:51:12	5.444	5444	122	0.664168
168	14:51:22	5.493	5493	122	0.670146
169	14:51:32	5.518	5518	171	0.943578
170	14:51:42	5.493	5493	24	0.131832
171	14:51:52	5.469	5469	24	0.131256
172	14:52:02	5.542	5542	24	0.133008
173	14:52:12	5.542	5542	24	0.133008
174	14:52:22	5.518	5518	24	0.132432

Step-5: Later on all the data is extracted from the serial monitor and transferred to an excel table shown in **Table 6** above.

The average panel voltage, load current and power values of the ZAST system is calculated from the excel table by using the AVERAGE command. The average panel voltage is 4.840977011 V which is approximately 4.84 V. The average load current is 84.2183908 mA which is approximately 84.23 mA. Finally the average load power is 0.47079755287 W which is approximately 0.47 W.

The test of the ZAST System is done by eliminating the AAST mode of the solar tracker which is simply done by plugging off the stepper motor connections of the

azimuth axis solar tracker.

Step-6: After finishing the excel table, in order to check the efficiency of the panel regarding time; Panel Voltage vs Time, Load Current vs Time and Load Power vs Time graph has been created on excel as shown in **Figure 47, Figure 48** and **Figure 49** below.

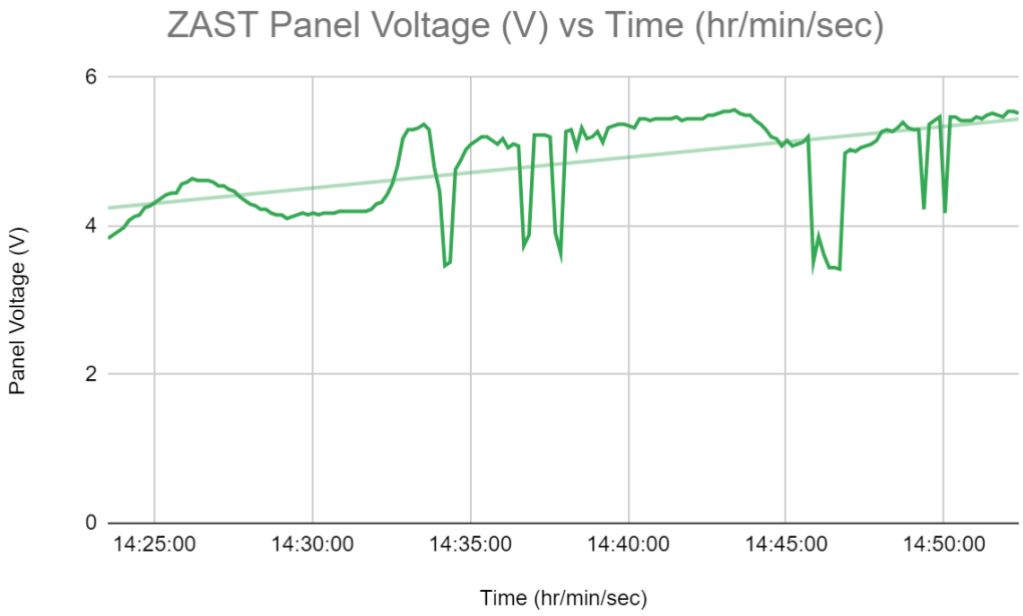

Figure 47: Panel Voltage Graph of ZAST system with respect to time.

The maximum voltage reading of the test shown in **Figure 47** happens to be 5.566 V and minimum voltage reading is 3.418 V. MAXIMUM and MINIMUM command of the excel is used to find out those answers. 5.566 V reading is recorded at 14:43:22 pm while 3.418 V reading is recorded at 15:25:51 pm. An increase in overall panel voltage can be seen from Figure 47.

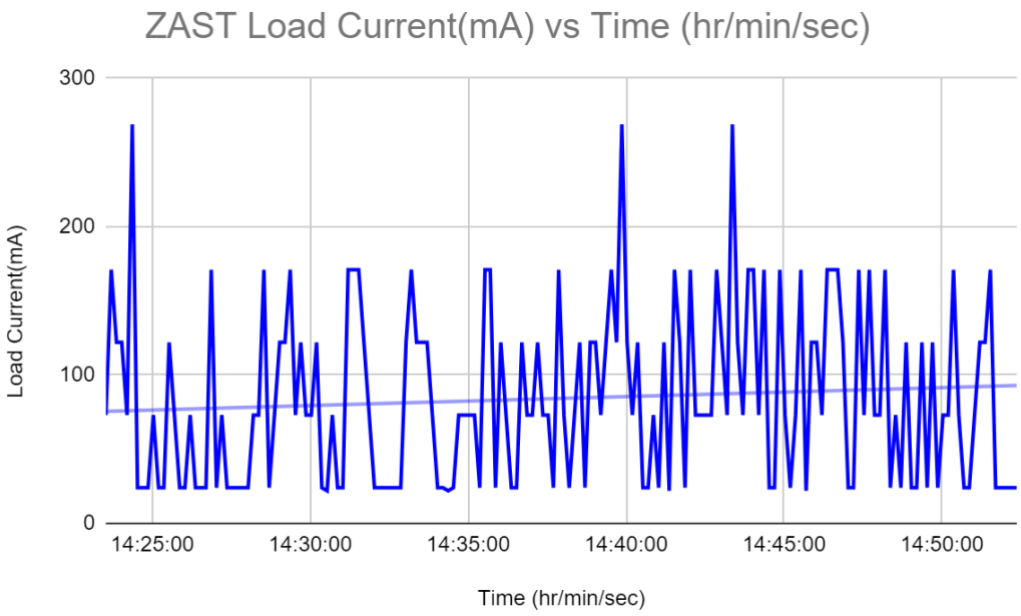

Figure 48: Load Current Graph of ZAST system with respect to time.

The maximum load current reading of the test shown in **Figure 48** happens to be 269 mA and minimum load current reading is 22 mA. MAXIMUM and MINIMUM command of the excel is used to find out those answers. 269 mA reading is recorded at 14:43:22 pm while 22 mA reading is recorded at 14:30:32 pm. An increase in overall load current can be seen from **Figure 48**.

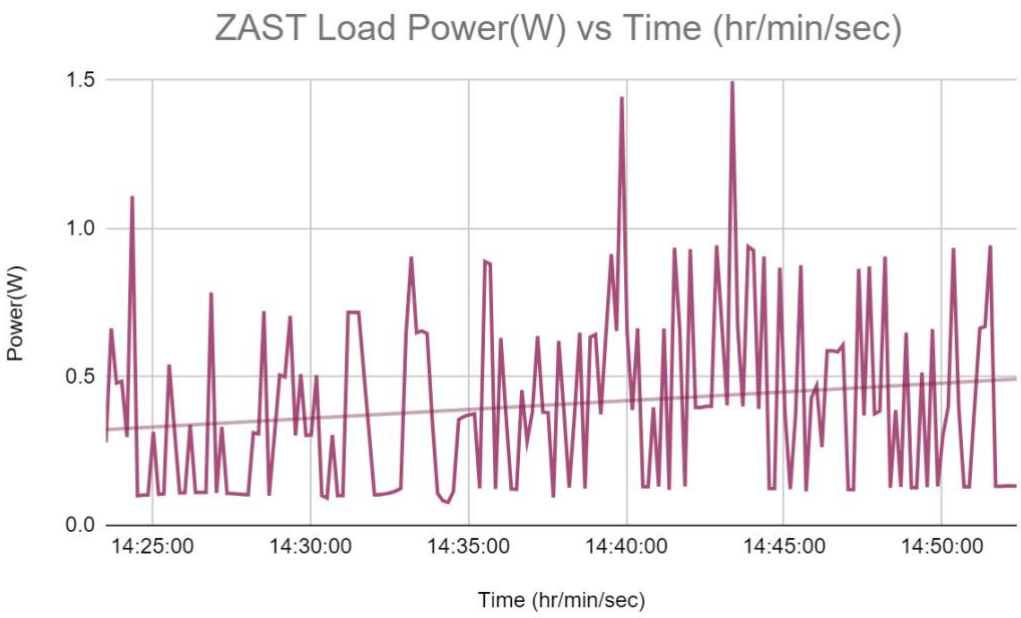

Figure 49: Load Power Graph of ZAST system with respect to time.

The maximum load power reading of the test shown in **Figure 49** happens to be 1.497254 W and minimum load power reading is 0.077352 W. MAXIMUM and MINIMUM command of the excel is used to find out those answers. 1.497254 W reading is recorded at 14:43:22 pm while 0.077352 W reading is recorded at 14:34:22 pm. An increase in overall load power can be seen from **Figure 49**.

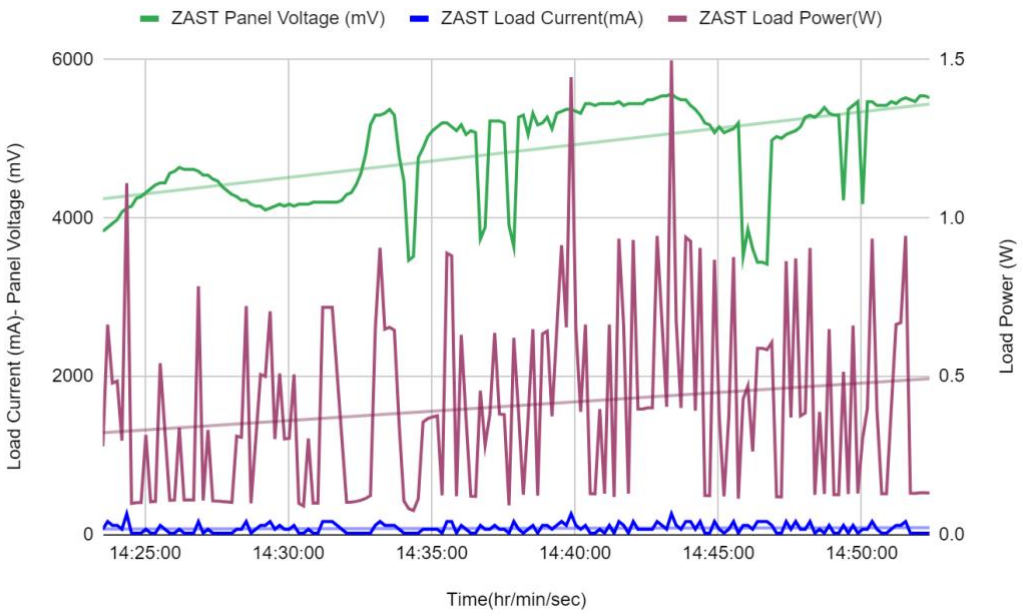

Figure 50: Load Current-Load Power-Panel Voltage Graph of ZAST system with respect to time.

As it can be seen from Figure 50, the maximum panel voltage of 5.566 V, the maximum load current of 269 mA and maximum load power of 1.497254 W are all recorded at the same time 14:43:22 pm. Also from **Figure 50** it can be seen that the load power, panel voltage and load current is increasing proportionally. At 14:43:22 pm the ZAST system reached its MPP (maximum power point) level.

4.2 Data Analysis and Results of DAST System

In this part, the data analysis and also the results of the DAST system is going to be explained.

This part shows the location and time of the test, the voltage values taken from the solar panel, the current and power values taken from the load is shown. All the steps of the test are explained.

The same path that is used for testing of the ZAST system shown in **Figure 43**, is used as well for the testing of the DAST system. The data analysis of the DAST System took place on 27.09.2023 at 15:10:09.081 pm immediately after the ZAST test whereas the finishing time was at 15:38:59.407 pm.

The steps that are followed for the testing procedure is shown below;

Step-1: At exactly 15:10:09.081 pm the testing procedure has been started.

Step-2: The movement of the vehicle and the serial monitor of Arduino activated at the same time.

Step-3: The movement of the vehicle and the activation of the Arduino serial monitor is stopped at the same time at 15:38:59.407 pm. Overall lap time was approximately 28 min. 50 sec.

Step-4: All the data that was showing in the monitor has been recorded until the path that was set is finished.

As there was no delay given to Arduino code, the voltage readings on Arduino serial monitor for this test consist of 5118 lines. This is because of the time setup of Arduino which uses hr/min/sec/millisec concept so this concept is modified and summarized to the hr/min/sec concept.

After this time setup, the number of lines in the table dropped to 174 lines. The data is extracted as a Time vs Solar Panel voltage (V), Solar Panel voltage (mV), Load Current (mA), Load Power (W) table and all the readings with respect to time are shown in Table 7.

Table 7: Shows the data of the solar panel recorded during testing of the DAST system.

Data Analysis of DAST System

Reading no:	Time (hr/min/sec)	Solar Panel Voltage (V)	Solar Panel Voltage (mV)	Load Current (mA)	Load Power (W)
1	15:10:09	5.444	5444	73	0.397412
2	15:10:19	5.493	5493	171	0.939303
3	15:10:29	5.518	5518	220	1.21396
4	15:10:39	5.542	5542	122	0.676124
5	15:10:49	5.64	5640	220	1.2408
6	15:10:59	5.688	5688	220	1.25136
7	15:11:09	5.64	5640	171	0.96444
8	15:11:19	5.664	5664	220	1.24608
9	15:11:29	5.664	5664	220	1.24608
10	15:11:39	5.688	5688	220	1.25136
11	15:11:49	5.713	5713	122	0.696986
12	15:11:59	5.713	5713	269	1.536797
13	15:12:09	5.713	5713	269	1.536797
14	15:12:19	5.713	5713	318	1.816734
15	15:12:29	5.688	5688	269	1.530072
16	15:12:39	5.713	5713	367	2.096671
17	15:12:49	5.762	5762	269	1.549978
18	15:12:59	5.713	5713	171	0.976923
19	15:13:09	5.737	5737	269	1.543253
20	15:13:19	5.737	5737	318	1.824366
21	15:13:29	5.737	5737	220	1.26214
22	15:13:39	5.737	5737	220	1.26214
23	15:13:49	5.713	5713	171	0.976923
24	15:13:59	5.762	5762	220	1.26764
25	15:14:09	5.762	5762	318	1.832316
26	15:14:19	5.713	5713	220	1.25686
27	15:14:29	5.762	5762	220	1.26764
28	15:14:39	5.786	5786	269	1.556434
29	15:14:49	5.762	5762	220	1.26764
30	15:14:59	5.713	5713	171	0.976923

31	15:15:09	5.713	5713	171	0.976923
32	15:15:19	5.737	5737	171	0.981027
33	15:15:29	5.737	5737	269	1.543253
34	15:15:39	5.713	5713	171	0.976923
35	15:15:49	5.688	5688	171	0.972648
36	15:15:59	5.664	5664	122	0.691008
37	15:16:09	5.664	5664	171	0.968544
38	15:16:19	5.664	5664	122	0.691008
39	15:16:29	5.664	5664	171	0.968544
40	15:16:39	5.664	5664	73	0.413472
41	15:16:49	5.664	5664	171	0.968544
42	15:16:59	5.664	5664	24	0.135936
43	15:17:09	5.664	5664	122	0.691008
44	15:17:19	5.615	5615	24	0.13476
45	15:17:29	5.64	5640	24	0.13536
46	15:17:39	5.64	5640	24	0.13536
47	15:17:49	5.591	5591	73	0.408143
48	15:17:59	5.615	5615	122	0.68503
49	15:18:09	5.664	5664	73	0.413472
50	15:18:19	5.64	5640	73	0.41172
51	15:18:29	5.688	5688	73	0.415224
52	15:18:39	5.713	5713	220	1.25686
53	15:18:49	5.762	5762	73	0.420626
54	15:18:59	5.737	5737	24	0.137688
55	15:19:09	5.688	5688	73	0.415224
56	15:19:19	5.566	5566	122	0.679052
57	15:19:29	4.614	4614	171	0.788994
58	15:19:39	3.124	3124	464	1.449536
59	15:19:49	3.052	3052	415	1.26658
60	15:19:59	3.076	3076	415	1.27654
61	15:20:09	3.784	3784	318	1.203312
62	15:20:19	3.979	3979	415	1.651285
63	15:20:29	4.077	4077	122	0.497394
64	15:20:39	4.224	4224	318	1.343232

65	15:20:49	4.297	4297	269	1.155893
66	15:20:59	4.468	4468	318	1.420824
67	15:21:09	4.565	4565	122	0.55693
68	15:21:19	4.565	4565	318	1.45167
69	15:21:29	4.614	4614	220	1.01508
70	15:21:39	4.712	4712	171	0.805752
71	15:21:49	4.785	4785	122	0.58377
72	15:21:59	4.565	4565	269	1.227985
73	15:22:09	4.883	4883	171	0.834993
74	15:22:19	4.761	4761	171	0.814131
75	15:22:29	4.761	4761	269	1.280709
76	15:22:39	4.907	4907	24	0.117768
77	15:22:49	4.883	4883	171	0.834993
78	15:22:59	5.176	5176	269	1.392344
79	15:23:09	5.054	5054	171	0.864234
80	15:23:19	5.298	5298	220	1.16556
81	15:23:29	5.225	5225	171	0.893475
82	15:23:39	5.371	5371	220	1.18162
83	15:23:49	5.298	5298	220	1.16556
84	15:23:59	5.444	5444	171	0.930924
85	15:24:09	5.493	5493	122	0.670146
86	15:24:19	5.42	5420	122	0.66124
87	15:24:29	5.42	5420	122	0.66124
88	15:24:39	5.566	5566	24	0.133584
89	15:24:49	5.591	5591	122	0.682102
90	15:24:59	5.64	5640	24	0.13536
91	15:25:09	5.615	5615	269	1.510435
92	15:25:19	5.64	5640	122	0.68808
93	15:25:29	5.615	5615	122	0.68503
94	15:25:39	5.664	5664	122	0.691008
95	15:25:49	5.664	5664	73	0.413472
96	15:25:59	5.664	5664	24	0.135936
97	15:26:09	5.615	5615	24	0.13476
98	15:26:19	5.591	5591	24	0.134184

99	15:26:29	5.566	5566	122	0.679052
100	15:26:39	5.493	5493	220	1.20846
101	15:26:49	5.42	5420	122	0.66124
102	15:26:59	5.42	5420	122	0.66124
103	15:27:09	5.42	5420	318	1.72356
104	15:27:19	5.444	5444	73	0.397412
105	15:27:29	5.469	5469	73	0.399237
106	15:27:39	5.469	5469	122	0.667218
107	15:27:49	5.518	5518	122	0.673196
108	15:27:59	5.518	5518	171	0.943578
109	15:28:09	5.518	5518	73	0.402814
110	15:28:19	5.518	5518	73	0.402814
111	15:28:29	5.444	5444	24	0.130656
112	15:28:39	5.444	5444	171	0.930924
113	15:28:49	5.42	5420	122	0.66124
114	15:28:59	5.469	5469	122	0.667218
115	15:29:09	5.444	5444	122	0.664168
116	15:29:19	5.42	5420	220	1.1924
117	15:29:29	5.396	5396	73	0.393908
118	15:29:39	5.371	5371	171	0.918441
119	15:29:49	5.347	5347	269	1.438343
120	15:29:59	5.273	5273	220	1.16006
121	15:30:09	5.225	5225	171	0.893475
122	15:30:19	5.151	5151	171	0.880821
123	15:30:29	5.103	5103	318	1.622754
124	15:30:39	5.005	5005	171	0.855855
125	15:30:49	4.956	4956	220	1.09032
126	15:30:59	4.932	4932	269	1.326708
127	15:31:09	4.81	4810	269	1.29389
128	15:31:19	4.81	4810	171	0.82251
129	15:31:29	4.736	4736	269	1.273984
130	15:31:39	4.785	4785	318	1.52163
131	15:31:49	4.688	4688	318	1.490784
132	15:31:59	3.076	3076	611	1.879436

133	15:32:09	3.149	3149	660	2.07834
134	15:32:19	2.979	2979	562	1.674198
135	15:32:29	3.003	3003	660	1.98198
136	15:32:39	4.614	4614	367	1.693338
137	15:32:49	4.639	4639	318	1.475202
138	15:32:59	4.761	4761	269	1.280709
139	15:33:09	4.761	4761	269	1.280709
140	15:33:19	4.81	4810	367	1.76527
141	15:33:29	4.883	4883	220	1.07426
142	15:33:39	4.932	4932	318	1.568376
143	15:33:49	5.005	5005	269	1.346345
144	15:33:59	5.005	5005	415	2.077075
145	15:34:09	5.054	5054	464	2.345056
146	15:34:19	5.005	5005	464	2.32232
147	15:34:29	5.054	5054	415	2.09741
148	15:34:39	4.956	4956	904	4.480224
149	15:34:49	5.005	5005	904	4.52452
150	15:34:59	5.103	5103	806	4.113018
151	15:35:09	5.151	5151	709	3.652059
152	15:35:19	5.078	5078	611	3.102658
153	15:35:29	4.98	4980	709	3.53082
154	15:35:39	4.883	4883	611	2.983513
155	15:35:49	4.785	4785	611	2.923635
156	15:35:59	4.688	4688	806	3.778528
157	15:36:09	4.712	4712	855	4.02876
158	15:36:19	4.688	4688	904	4.237952
159	15:36:29	4.565	4565	953	4.350445
160	15:36:39	4.468	4468	953	4.258004
161	15:36:49	4.517	4517	1149	5.190033
162	15:36:59	4.541	4541	855	3.882555
163	15:37:09	4.614	4614	1295	5.97513
164	15:37:19	4.614	4614	1295	5.97513
165	15:37:29	4.614	4614	904	4.171056
166	15:37:39	4.663	4663	1002	4.672326

167	15:37:49	4.688	4688	855	4.00824
168	15:37:59	4.712	4712	1002	4.721424
169	15:38:09	4.782	4782	1100	5.2602
170	15:38:19	4.761	4761	1100	5.2371
171	15:38:29	4.81	4810	953	4.58393
172	15:38:39	4.297	4297	1051	4.516147
173	15:38:49	2.905	2905	1197	3.477285
174	15:38:59	2.881	2881	1491	4.295571

Step-5: Later on all the data is extracted from the serial monitor and transferred to an excel table shown in **Table 7** above.

The average panel voltage, load current and power values of the DAST system is calculated from the excel table by using the AVERAGE command. The average panel voltage is 5.132425287 V which is approximately 5.13 V. The average load current is 320.1609195 mA which is approximately 320.16 mA. Finally the average load power is 1.525961902 W which is approximately 1.53 W.

Another reason for completing the data analysis of the DAST system right after the ZAST test, is not to lose so much time and be as much as in the same time zone so that in case of comparison it can be estimated that all of the tests have been done at the same circumstances.

Step-6: After finishing the excel table, in order to check the efficiency of the panel regarding time; Panel Voltage vs Time, Load Current vs Time and Load Power vs Time graph has been created on excel as shown in **Figure 51, Figure 52** and **Figure**

53 below.

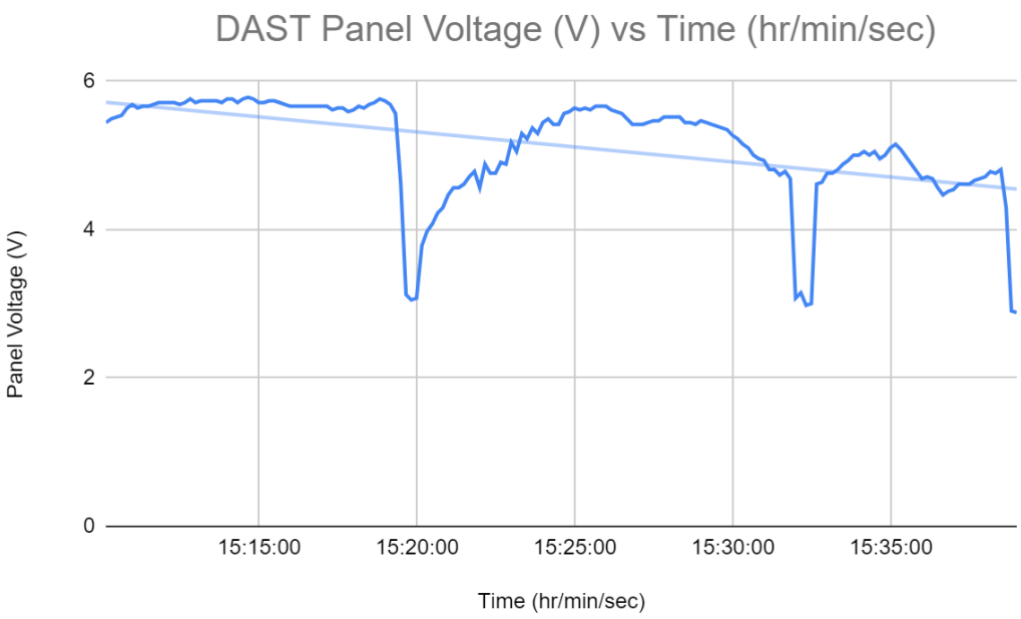

Figure 51: Panel Voltage Graph of DAST system with respect to time.

The maximum voltage reading of the test shown in **Figure 51** happens to be 5.786 V and minimum voltage reading is 2.881 V. MAXIMUM and MINIMUM command of the excel is used to find out those answers. 5.786 V reading is recorded at 15:14:39 pm while 2.881 V reading is recorded at 15:38:59 pm. A decrease in overall panel voltage can be seen from **Figure 51**.

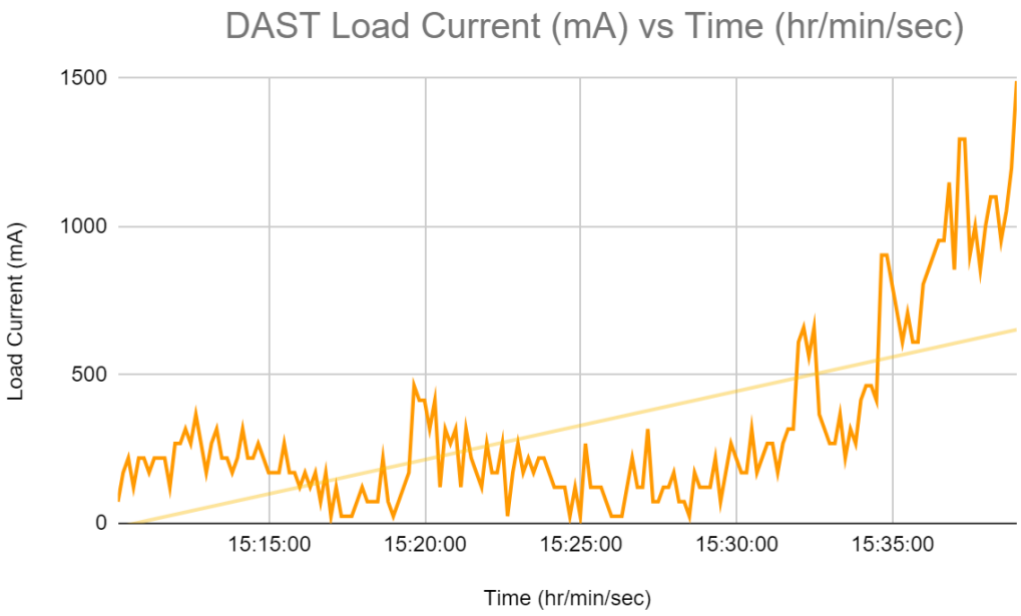

Figure 52: Load Current Graph of ZAST system with respect to time.

The maximum load current reading of the test shown in **Figure 52** happens to be 1491 mA and minimum load current reading is 24 mA. MAXIMUM and MINIMUM command of the excel is used to find out those answers. 1491 mA reading is recorded at 15:38:59 pm while 24 mA reading is recorded at 15:28:29 pm. An increase in overall load current can be seen from **Figure 52**.

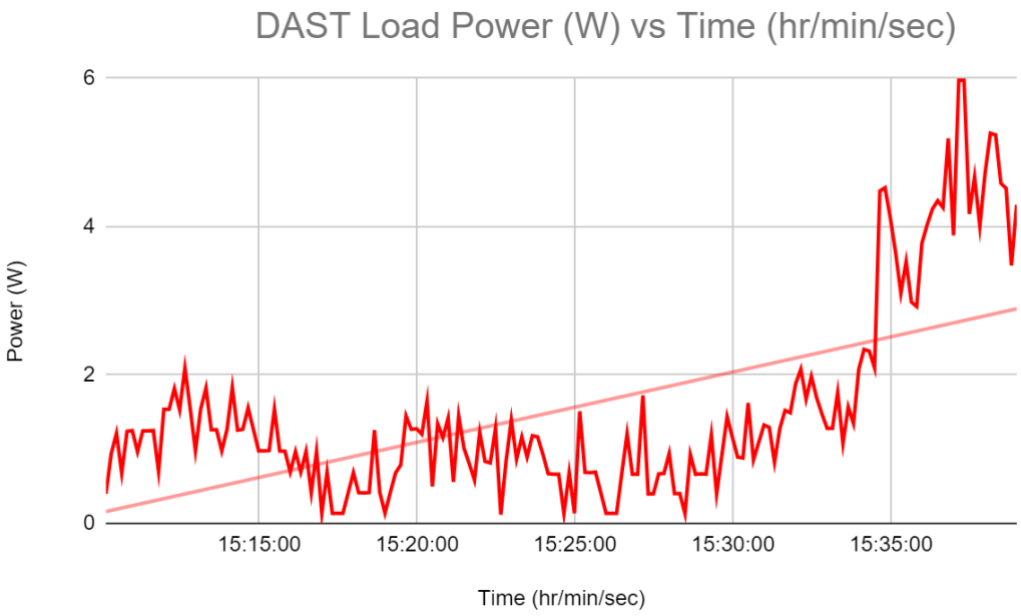

Figure 53: Load Power Graph of DAST system with respect to time.

The maximum load power reading of the test shown in **Figure 53** happens to be 5.97513 W and minimum load power reading is 0.117768 W. MAXIMUM and MINIMUM command of the excel is used to find out those answers. 5.97513 W reading is recorded at 15:37:09 pm while 0.117768 W reading is recorded at 15:22:39 pm. An increase in overall load power can be seen from **Figure 53**.

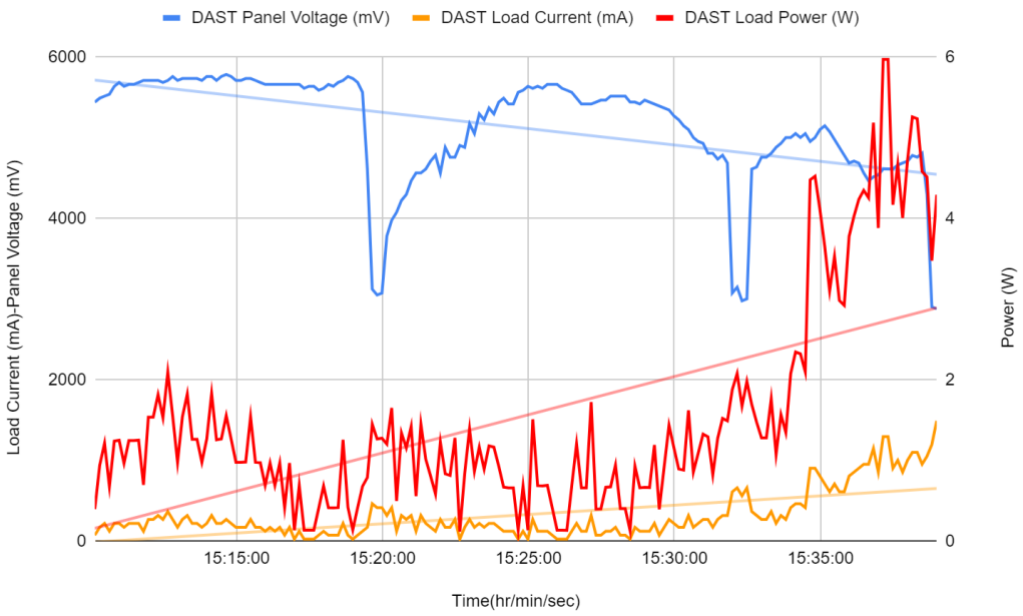

Figure 54: Load Current-Load Power-Panel Voltage Graph of DAST system with respect to time.

As it can be seen from **Figure 54**, the maximum panel voltage of 5.786 V is recorded at 15:14:39 pm, the maximum load current of 1491 mA is recorded at 15:38:59 pm and maximum load power of 5.97513 W is recorded at 15.37.09 pm. Also from **Figure 54** it can be seen that the load power and load current is increasing proportionally while panel voltage is decreasing. At 15.37.09 pm the ZAST system reached its MPP (maximum power point) level.

4.3 Data Analysis and Results of AAST System

In this part, the data analysis and also the results of the AAST system is going to be explained. This part shows the location and time of the test, the voltage values taken from the solar panel, the current and power values taken from the load is shown. All the steps of the test are explained.

The same path that was used for testing of DAST and ZAST systems shown in

Figure 43, has been used as well for the testing of the AAST system.

The data analysis of the AAST System took place on 27.09.2023 at 15:56:36.081 pm immediately after the DAST test whereas the finishing time was at 16:25:26.407 pm. Overall lap time was approximately 28 min. 50 sec.

The steps that are followed for the testing procedure is shown below;

Step-1: At exactly 15:56:36.081 pm, the testing procedure of the AAST system has been started and the same path is followed.

Step-2: The movement of the vehicle and the serial monitor of Arduino activated at the same time.

Step-3: The movement of the vehicle and the activation of the Arduino serial monitor is stopped at the same time at 16:25:26.407 pm.

Step-4: All the data that was showing in the monitor has been recorded until the path that was set is finished.

As there was no delay given to Arduino code, the voltage readings on Arduino serial monitor for this test consist of 5651 lines. This is because of the time setup of Arduino which uses hr/min/sec/millisec concept so this concept is modified and summarized to the hr/min/sec concept.

After this time setup, the number of lines in the table dropped to 174 lines also. In order to make the comparison between the systems more valid, the number of lines kept the same. The data is extracted as a Time vs Solar Panel voltage (V), Solar Panel voltage (mV), Load Current (mA), Load Power (W) table and all the readings with

respect to time are shown in **Table 8.**

Table 8: Shows the data of the solar panel recorded during testing of the AAST system.

Data Analysis of AAST System

Reading no:	Time (hr/min/sec)	Solar Panel Voltage (V)	Solar Panel Voltage (mV)	Load Current (mA)	Load Power (W)
1	15:56:36	5.42	5444	269	1.45798
2	15:56:46	5.444	5493	318	1.731192
3	15:56:56	5.469	5518	171	0.935199
4	15:57:06	5.518	5542	318	1.754724
5	15:57:16	5.518	5640	367	2.025106
6	15:57:26	5.542	5688	318	1.762356
7	15:57:36	5.566	5640	318	1.769988
8	15:57:46	5.566	5664	269	1.497254
9	15:57:56	5.591	5664	269	1.503979
10	15:58:06	5.591	5688	318	1.777938
11	15:58:16	5.615	5713	367	2.060705
12	15:58:26	5.64	5713	269	1.51716
13	15:58:36	5.664	5713	171	0.968544
14	15:58:46	5.664	5713	269	1.523616
15	15:58:56	5.688	5688	367	2.087496
16	15:59:06	5.737	5713	220	1.26214
17	15:59:16	5.713	5762	269	1.536797
18	15:59:26	5.737	5713	367	2.105479
19	15:59:36	5.762	5737	318	1.832316
20	15:59:46	5.713	5737	269	1.536797
21	15:59:56	5.737	5737	367	2.105479
22	16:00:06	5.737	5737	415	2.380855
23	16:00:16	5.737	5713	318	1.824366
24	16:00:26	5.737	5762	415	2.380855
25	16:00:36	5.737	5762	318	1.824366
26	16:00:46	5.737	5713	367	2.105479

27	16:00:56	5.762	5762	367	2.114654
28	16:01:06	5.762	5786	318	1.832316
29	16:01:16	5.762	5762	269	1.549978
30	16:01:26	5.762	5713	318	1.832316
31	16:01:36	5.762	5713	171	0.985302
32	16:01:46	5.737	5737	220	1.26214
33	16:01:56	5.762	5737	415	2.39123
34	16:02:06	5.737	5713	318	1.824366
35	16:02:16	5.762	5688	415	2.39123
36	16:02:26	5.786	5664	269	1.556434
37	16:02:36	5.762	5664	220	1.26764
38	16:02:46	5.762	5664	367	2.114654
39	16:02:56	5.762	5664	367	2.114654
40	16:03:06	5.737	5664	367	2.105479
41	16:03:16	5.786	5664	562	3.251732
42	16:03:26	5.762	5664	220	1.26764
43	16:03:36	5.737	5664	269	1.543253
44	16:03:46	5.762	5615	122	0.702964
45	16:03:56	5.737	5640	220	1.26214
46	16:04:06	5.786	5640	73	0.422378
47	16:04:16	5.762	5591	415	2.39123
48	16:04:26	5.762	5615	318	1.832316
49	16:04:36	5.737	5664	318	1.824366
50	16:04:46	5.762	5640	318	1.832316
51	16:04:56	5.737	5688	464	2.661968
52	16:05:06	5.737	5713	220	1.26214
53	16:05:16	5.713	5762	318	1.816734
54	16:05:26	5.713	5737	171	0.976923
55	16:05:36	5.688	5688	318	1.808784
56	16:05:46	5.713	5566	367	2.096671
57	16:05:56	5.737	4614	269	1.543253
58	16:06:06	5.737	3124	269	1.543253
59	16:06:16	5.688	3052	269	1.530072
60	16:06:26	5.542	3076	318	1.762356

61	16:06:36	5.127	3784	171	0.876717
62	16:06:46	4.102	3979	73	0.299446
63	16:06:56	3.32	4077	24	0.07968
64	16:07:06	3.174	4224	73	0.231702
65	16:07:16	3.125	4297	24	0.075
66	16:07:26	3.076	4468	24	0.073824
67	16:07:36	3.027	4565	24	0.072648
68	16:07:46	3.003	4565	122	0.366366
69	16:07:56	3.027	4614	122	0.369294
70	16:08:06	3.052	4712	24	0.073248
71	16:08:16	3.052	4785	24	0.073248
72	16:08:26	3.076	4565	24	0.073824
73	16:08:36	3.125	4883	122	0.38125
74	16:08:46	3.198	4761	171	0.546858
75	16:08:56	3.32	4761	24	0.07968
76	16:09:06	3.394	4907	73	0.247762
77	16:09:16	3.491	4883	73	0.254843
78	16:09:26	3.613	5176	24	0.086712
79	16:09:36	3.711	5054	24	0.089064
80	16:09:46	3.809	5298	122	0.464698
81	16:09:56	3.711	5225	24	0.089064
82	16:10:06	3.906	5371	122	0.476532
83	16:10:16	3.979	5298	24	0.095496
84	16:10:26	3.955	5444	24	0.09492
85	16:10:36	4.15	5493	24	0.0996
86	16:10:46	4.077	5420	73	0.297621
87	16:10:56	4.346	5420	73	0.317258
88	16:11:06	4.175	5566	24	0.1002
89	16:11:16	4.541	5591	220	0.99902
90	16:11:26	4.614	5640	73	0.336822
91	16:11:36	4.736	5615	171	0.809856
92	16:11:46	4.761	5640	122	0.580842
93	16:11:56	4.81	5615	24	0.11544
94	16:12:06	4.858	5664	73	0.354634

95	16:12:16	4.956	5664	122	0.604632
96	16:12:26	5.029	5664	220	1.10638
97	16:12:36	5.078	5615	171	0.868338
98	16:12:46	4.883	5591	122	0.595726
99	16:12:56	5.176	5566	318	1.645968
100	16:13:06	5.2	5493	220	1.144
101	16:13:16	5.176	5420	122	0.631472
102	16:13:26	5.273	5420	171	0.901683
103	16:13:36	5.127	5420	220	1.12794
104	16:13:46	5.371	5444	269	1.444799
105	16:13:56	5.444	5469	318	1.731192
106	16:14:06	5.42	5469	318	1.72356
107	16:14:16	5.469	5518	269	1.471161
108	16:14:26	5.469	5518	122	0.667218
109	16:14:36	4.834	5518	73	0.352882
110	16:14:46	5.493	5518	220	1.20846
111	16:14:56	5.493	5444	220	1.20846
112	16:15:06	5.518	5444	318	1.754724
113	16:15:16	5.542	5420	220	1.21924
114	16:15:26	5.591	5469	318	1.777938
115	16:15:36	5.615	5444	367	2.060705
116	16:15:46	5.615	5420	318	1.78557
117	16:15:56	5.64	5396	269	1.51716
118	16:16:06	5.64	5371	269	1.51716
119	16:16:16	5.688	5347	269	1.530072
120	16:16:26	5.688	5273	367	2.087496
121	16:16:36	5.713	5225	415	2.370895
122	16:16:46	5.664	5151	269	1.523616
123	16:16:56	5.737	5103	171	0.981027
124	16:17:06	5.737	5005	220	1.26214
125	16:17:16	5.762	4956	318	1.832316
126	16:17:26	5.737	4932	367	2.105479
127	16:17:36	5.762	4810	220	1.26764
128	16:17:46	5.737	4810	171	0.981027

129	16:17:56	5.737	4736	367	2.105479
130	16:18:06	5.713	4785	269	1.536797
131	16:18:16	5.737	4688	171	0.981027
132	16:18:26	5.713	3076	220	1.25686
133	16:18:36	5.737	3149	415	2.380855
134	16:18:46	5.737	2979	415	2.380855
135	16:18:56	5.762	3003	269	1.549978
136	16:19:06	5.737	4614	367	2.105479
137	16:19:16	5.737	4639	415	2.380855
138	16:19:26	5.737	4761	220	1.26214
139	16:19:36	5.737	4761	367	2.105479
140	16:19:46	5.688	4810	269	1.530072
141	16:19:56	5.688	4883	318	1.808784
142	16:20:06	5.664	4932	220	1.24608
143	16:20:16	5.64	5005	171	0.96444
144	16:20:26	5.64	5005	171	0.96444
145	16:20:36	5.615	5054	415	2.330225
146	16:20:46	5.615	5005	318	1.78557
147	16:20:56	5.615	5054	367	2.060705
148	16:21:06	5.615	4956	220	1.2353
149	16:21:16	5.615	5005	220	1.2353
150	16:21:26	3.223	5103	73	0.235279
151	16:21:36	3.467	5151	73	0.253091
152	16:21:46	3.296	5078	24	0.079104
153	16:21:56	3.247	4980	122	0.396134
154	16:22:06	3.296	4883	24	0.079104
155	16:22:16	3.369	4785	24	0.080856
156	16:22:26	5.615	4688	269	1.510435
157	16:22:36	5.591	4712	171	0.956061
158	16:22:46	5.591	4688	464	2.594224
159	16:22:56	5.591	4565	269	1.503979
160	16:23:06	5.542	4468	318	1.762356
161	16:23:16	5.566	4517	269	1.497254
162	16:23:26	5.542	4541	220	1.21924

163	16:23:36	5.615	4614	220	1.2353
164	16:23:46	3.296	4614	24	0.079104
165	16:23:56	3.296	4614	73	0.240608
166	16:24:06	5.566	4663	415	2.30989
167	16:24:16	3.247	4688	24	0.077928
168	16:24:26	5.591	4712	220	1.23002
169	16:24:36	5.591	4782	367	2.051897
170	16:24:46	5.542	4761	220	1.21924
171	16:24:56	5.029	4810	171	0.859959
172	16:25:06	3.174	4297	24	0.076176
173	16:25:16	3.149	2905	122	0.384178
174	16:25:26	3.125	2881	171	0.534375

Step-5: Later on all the data is extracted from the serial monitor and transferred to an excel table shown in **Table 8** above.

The average panel voltage, load current and power values of the AAST system is calculated from the excel table by using the AVERAGE command. The average panel voltage is 5.092810345 V which is approximately 5.1 V. The average load current is 227.5229885 mA which is approximately 227.52 mA. Finally the average load power is 1.248314971 W which is approximately 1.25 W.

As can be seen from **Table 8** shown above, the data analysis of the AAST System took place at 15:56:36.081 pm which is immediately after the DAST test. It is done by eliminating the ZAST mode of the solar tracker which is simply done by plugging off the stepper motor connections of the azimuth axis solar tracker.

Another reason for completing the data analysis of the AAST system right after the DAST test, is not to lose so much time and be as much as in the same time zone so

that in case of comparison it can be estimated that all of the tests have been done at the same circumstances.

The same steps that are followed in data analysis of DAST and ZAST systems have been followed in this section and a data analysis table is created on excel as shown in **Table 8**.

Step-6: After finishing the excel table, in order to check the efficiency of the panel regarding time; Panel Voltage vs Time, Load Current vs Time and Load Power vs Time graph has been created on excel as shown in **Figure 55, Figure 56** and **Figure 57** below.

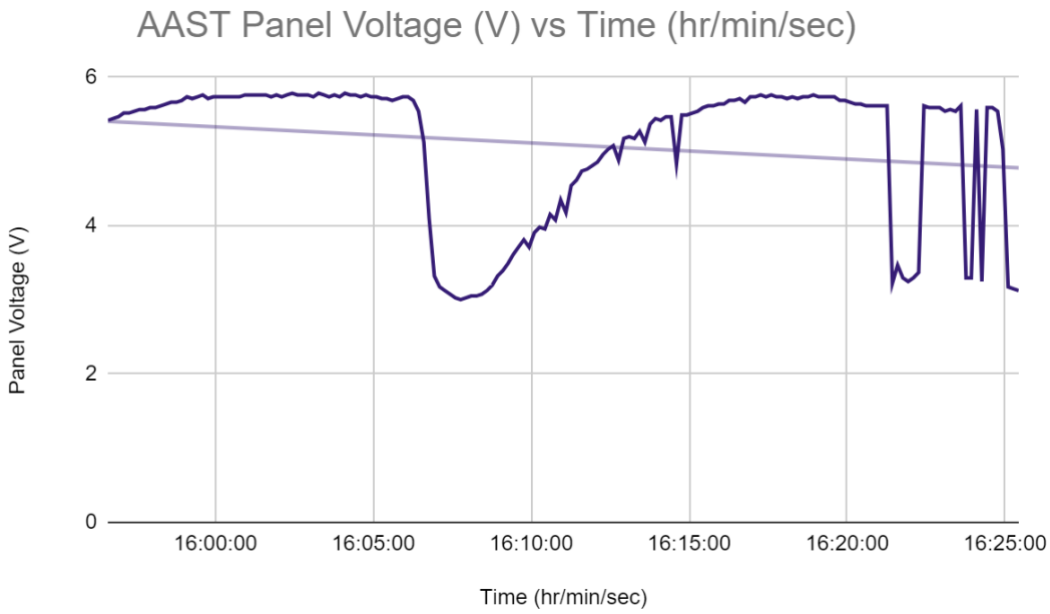

Figure 55: Panel Voltage Graph of AAST system with respect to time.

The maximum voltage reading of the test shown in **Figure 55** happens to be 5.786 V

and minimum voltage reading is 3.003 V. MAXIMUM and MINIMUM command of the excel is used to find out those answers. 5.786 V reading is recorded at 16:03:16 pm while 3.003 V reading is recorded at 16:07:46 pm. A decrease in overall panel voltage can be seen from **Figure 55**.

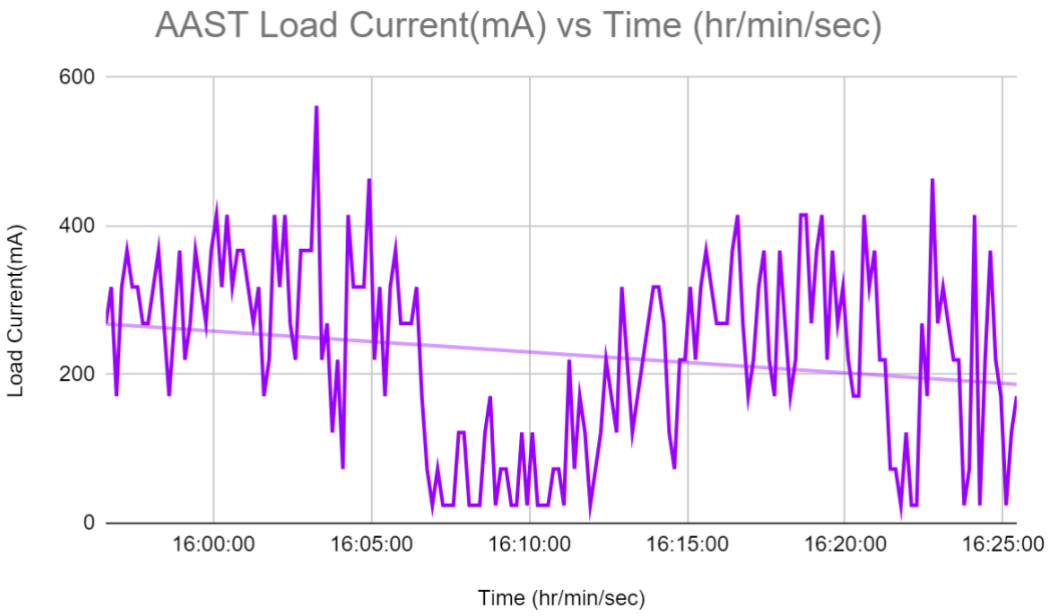

Figure 56: Load Current Graph of AAST system with respect to time.

The maximum load current reading of the test shown in **Figure 56** happens to be 562 mA and minimum load current reading is 24 mA. MAXIMUM and MINIMUM command of the excel is used to find out those answers. 562 mA reading is recorded at 16:03:16 pm while 24 mA reading is recorded at 16:25:06 pm. A decrease in overall load current can be seen from **Figure 56**.

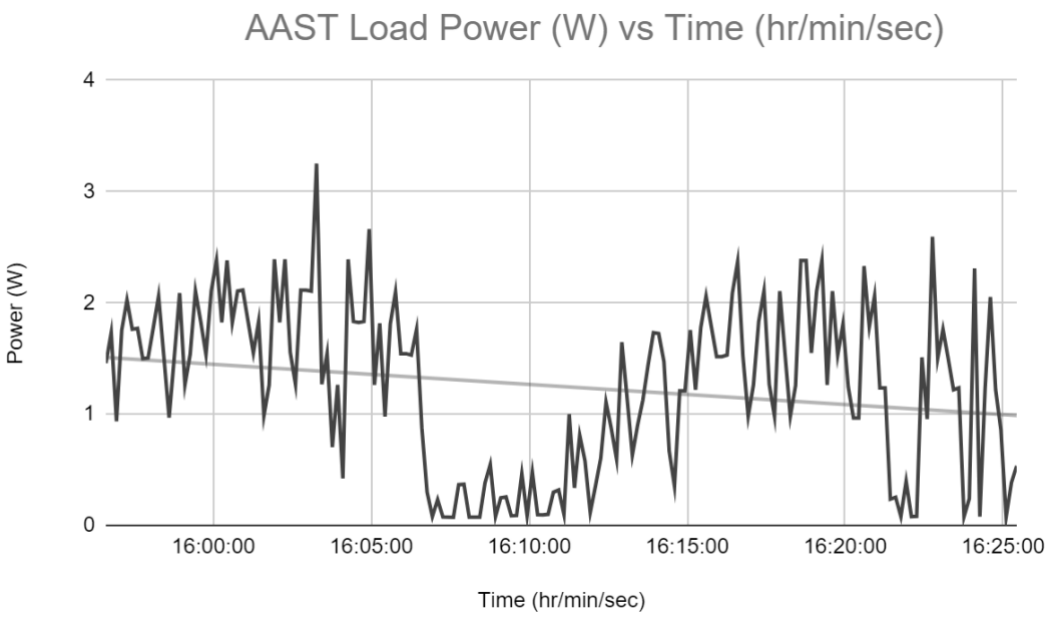

Figure 57: Load Power Graph of AAST system with respect to time.

The maximum load power reading of the test shown in **Figure 57** happens to be 3.251732 W and minimum load power reading is 0.072648 W. MAXIMUM and MINIMUM command of the excel is used to find out those answers. 3.251732 W reading is recorded at 16.03.16 pm while 0.072648 W reading is recorded at 16.07.36 pm. A decrease in overall load power can be seen from **Figure 57**.

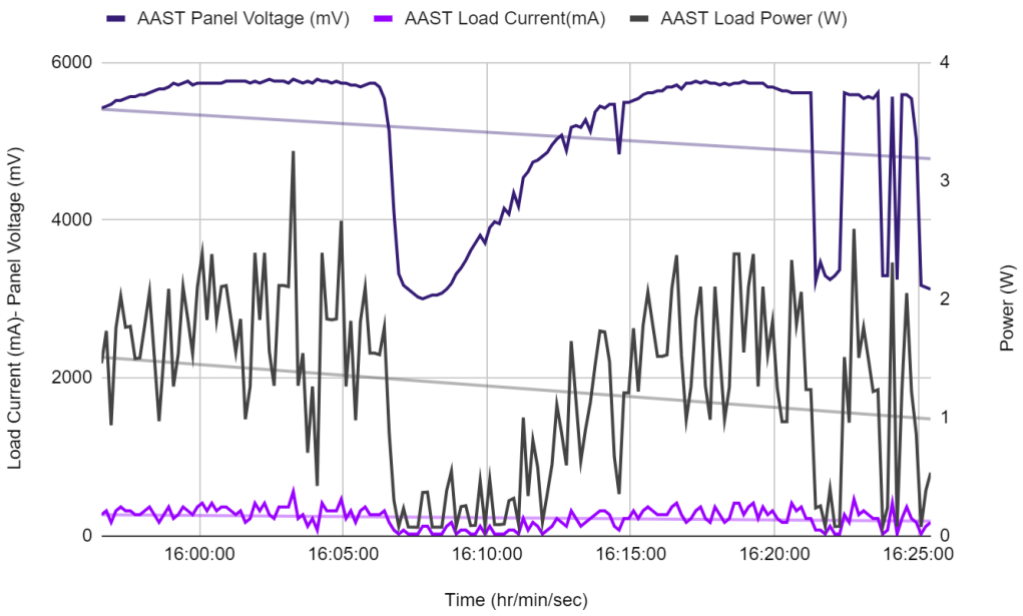

Figure 58: Load Current-Load Power-Panel Voltage Graph of AAST system with respect to time.

As it can be seen from **Figure 58**, the maximum panel voltage of 5.786 V, the maximum load current of 562 mA and maximum load power of 3.251732 W are all recorded at the same time 16:03:16 pm. Also from **Figure 58** it can be seen that panel voltage, load current and load power is decreasing proportionally. At 16:03:16 pm the AAST system reached its MPP (maximum power point) level.

4.4 Comparison of DAST, ZAST and AAST Systems

In this part the efficiency comparison between the DAST, ZAST and AAST Systems are going to be explained.

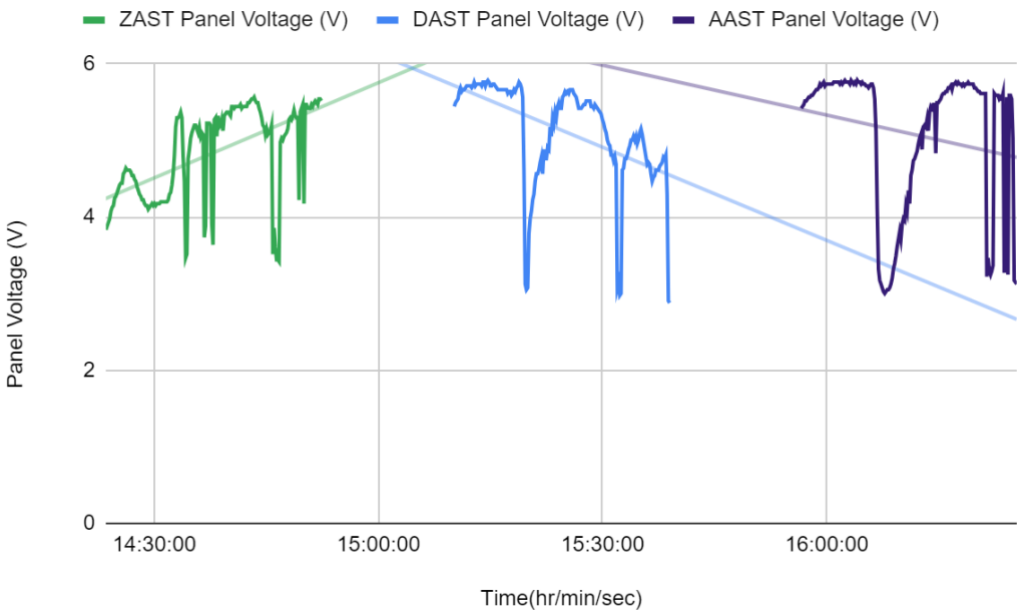

Figure 59: Panel Voltage Graph comparison between DAST, ZAST and AAST systems with respect to time.

As it can be seen from **Figure 59**, all the panel voltage data is combined into the same graph for better understanding. It is visible that each graph has a pale straight line passing through each other. Those lines represent the average voltage reading of different systems.

By looking at the average voltage reading line of the DAST and AAST system, it can be observed that the average voltage of the system is decreasing towards the end of the test. This is because of the weather conditions. It was sunny at the beginning of the test and became cloudy towards the end of the test, that's why the average voltage reading decreases directly.

For the average voltage readings of the ZAST system, it can be observed that the average voltage reading is increasing towards the end of the test. This is because of the weather conditions. It was cloudy at the beginning of the test and became sunny

towards the end of the tests, that's why the average voltage reading increases directly.

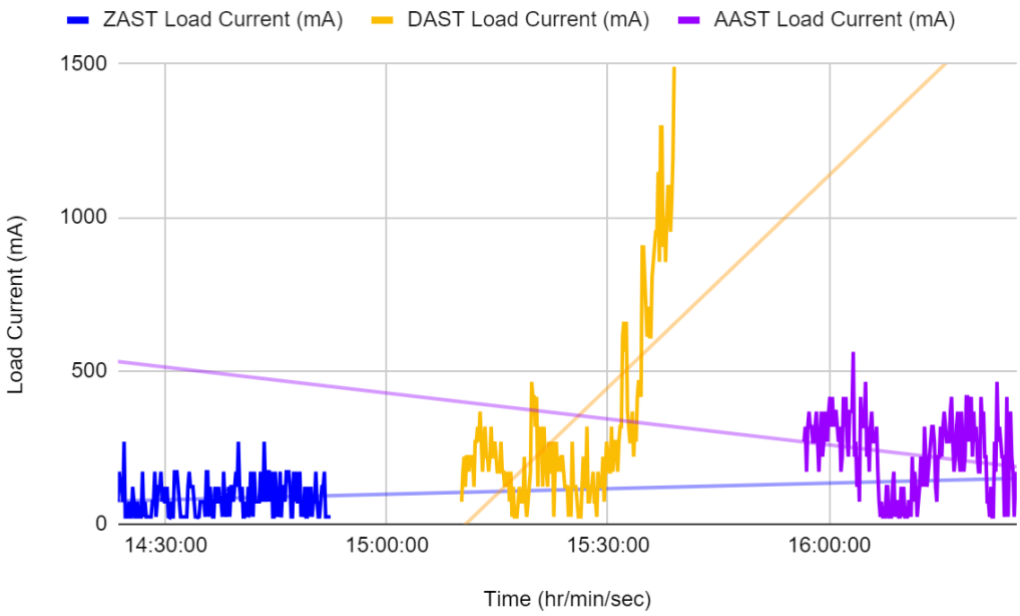

Figure 60: Load Current Graph comparison between DAST, ZAST and AAST systems with respect to time.

As it can be seen from **Figure 60**, all the load current data is combined into the same graph for better understanding. It is visible that each graph has a pale straight line passing through each other. Those lines represent the average load current reading of different systems.

By looking at the average load current reading line of the DAST and ZAST system, it can be observed that the average load current of the system is increasing towards the end of the test. For the average load current reading of the AAST system, it can be observed that the average load current reading is decreasing towards the end of the test.

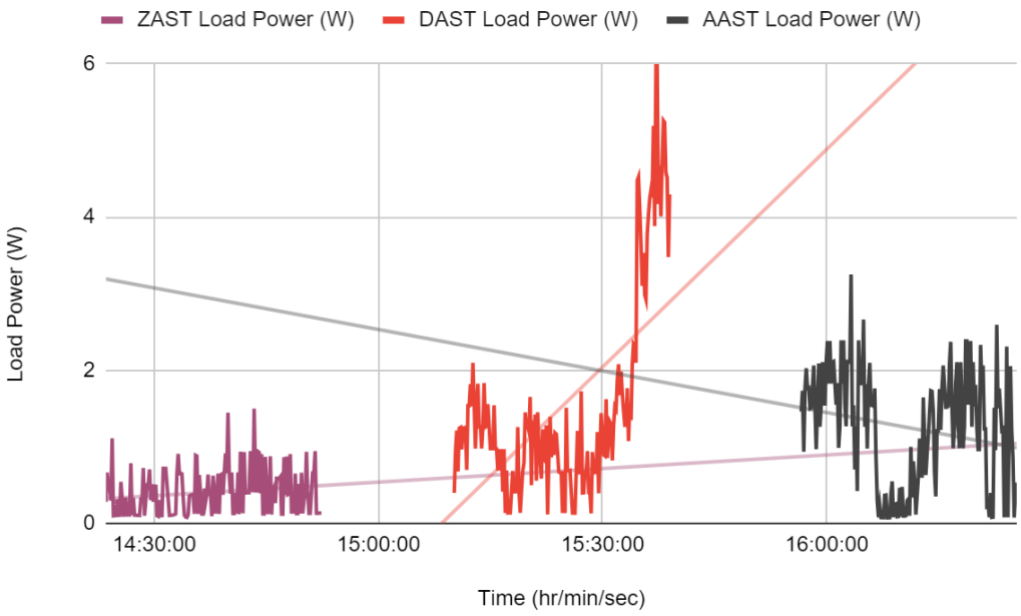

Figure 61: Load Power Graph comparison between DAST, ZAST and AAST systems with respect to time.

As it can be seen from **Figure 61**, all the load power data is combined into the same graph for better understanding. It is visible that each graph has a pale straight line passing through each other. Those lines represent the average load power reading of different systems.

By looking at the average load power reading line of the DAST and ZAST system, it can be observed that the average load power of the system is increasing towards the end of the test. For the average load power reading of the AAST system, it can be observed that the average load power reading is decreasing towards the end of the test.

From the load current and load power versus time graphs shown in **Figure C.3** and **Figure C.4** it can be seen that there is a correlation between current and power. The power produced by the panel is directly proportional to the current produced by the

panel.

Table 9: Shows the readings according to different system selections

Readings		System Used		
		DAST	ZAST	AAST
Panel Voltage Readings (V)	Average Voltage	5.13	4.84	5.09
	Maximum Voltage	5.79	5.57	5.79
	Minimum Voltage	2.88	3.42	3.00
Load Current Readings (mA)	Average Load Current	320.16	84.23	227.52
	Maximum Load Current	1491	269	562
	Minimum Load Current	24	22	24
Load Power Readings (W)	Average Load Power	1.53	0.47	1.25
	Maximum Load Power	5.98	1.50	3.25
	Minimum Load Power	0.12	0.08	0.07
Charge Produced (mAh)	Average Charge	666.23	175.28	473.45
Energy harvested (Wh)	Average Energy	3.18	0.98	2.60

According to the data shown in **Table 9**, the DAST system setting caused the solar panel to produce an average voltage of 5.13 V, average load current of 320.16 mA,

average load power of 1.53 W and a maximum voltage production of 5.79 V, maximum load current of 1491 mA, maximum load power of 5.98 W followed by a minimum voltage reading of 2.88 V, minimum load current of 24 mA, minimum load power of 0.12 W.

However in the ZAST setting, the same panel could give only 4.84 V as an average voltage, average load current of 84.23 mA, average load power of 0.47 W and 5.57 V of maximum voltage, maximum load current of 269 mA, maximum load power of 1.50 W reading with a minimum voltage reading of 3.42 V, minimum load current of 22 mA, minimum load power of 0.08 W.

AAST system setting on the other hand, caused the same solar panel to produce an average voltage of 5.09 V, average load current of 227.52 mA, average load power of 1.25 W with a maximum voltage production of 5.79 V, maximum load current of 562 mA, maximum load power of 3.25 W followed by a minimum voltage production of 3.00 V, minimum load current of 24 mA, minimum load power of 0.07 W.

The highest panel voltage comes from the DAST system as it has the highest average voltage reading of 5.13 V. Second highest yield comes from the AAST system with a 5.09 V voltage average and the least panel voltage is the ZAST system with a voltage average of 4.84 V.

The highest load current comes from the DAST system as it has the highest average load current reading of 320.16 mA. Second highest yield comes from the AAST

system with a 227.52 mA load current average and the least load current is the ZAST system with an average of 84.23 mA.

The highest load power comes from the DAST system as it has the highest average load power reading of 1.53 W. Second highest yield comes from the AAST system with a 1.25 W load power average and the least load power is the ZAST system with an average of 0.47 W.

Table 10: Shows the highest readings with different system modes

Ranking		**Reading**	**Mode used**
Panel Voltage	1st highest	5.79 V	DAST
	1st highest	5.79 V	AAST
	2nd highest	5.57 V	ZAST
Load Current	1st highest	1491 mA	DAST
	2nd highest	562 mA	AAST
	3rd highest	269 mA	ZAST
Load Power	1st highest	5.98 W	DAST
	2nd highest	3.25 W	AAST
	3rd highest	1.50 W	ZAST

The highest voltage comes from the DAST and AAST systems settings with 5.79 V reading and the second highest reading comes from the ZAST system setting which

is 5.57 V. The highest load current comes from the DAST systems settings with 1491 mA reading and the second highest reading comes from the AAST system setting which is 562 mA and finally the third highest load current reading comes from the ZAST system settings which is 269 mA.

The highest load power comes from the DAST systems settings with 5.98 W reading and the second highest reading comes from the AAST system setting which is 3.25 W and finally the third highest load current reading comes from the ZAST system settings which is 1.50 W.

In order to make an efficiency comparison between the DAST, ZAST and AAST systems, the average value of charge produced by the systems are calculated in mAh type. After the calculation of charge produced by the systems, the energy harvested is calculated in Wh type for all of the systems.

The complete duration of the DAST system test is 28 min. 50 sec. which is 0.48 hours (as shown below in **Equation 4.1**).

28 min. 50 sec = (28 x 60) + 50 1 hr = 60 x 60

=1730 sec. = 3600 sec.

3600 sec 1 hr

1730 sec ? hr

(1730 x 1) / 3600 = **0.48 hr** (4.1)

In the DAST system, average load current of 320.16 mA is produced in 0.48 hr so the average value of charge produced by the DAST system is **666.23 mAh** as shown below in **Equation 4.2.**

320.16 mA 0.48 hr

? mA 1 hr

(320.16 x 1) / 0.48 = **666.23 mAh** (4.2)

The average load power produced in the DAST system is 1.53 W in 0.48 hr so the average value of energy produced by the DAST system is **3.18 Wh** as shown below in **Equation 4.3.**

1.53 W 0.48 hr

? W 1 hr

(1.53 x 1) / 0.48 = **3.18 Wh** (4.3)

The complete duration of the ZAST system test is 28 min. 50 sec. which is 0.48 hours (as shown below in **Equation 4.1**). In the ZAST system, average load current of 84.236 mA is produced in 0.48 hr so the average value of charge produced by the

ZAST system is **175.28 mAh** as shown below in **Equation 4.4.**

84.23 mA 0.48 hr

? mA 1 hr

(84.23 x 1) / 0.48 = **175.28 mAh** (4.4)

The average load power produced in the ZAST system is 0.47 W in 0.48 hr so the average value of energy produced by the ZAST system is **0.98 Wh** as shown below in **Equation 4.5.**

0.47 W 0.48 hr

? W 1 hr

(0.47 x 1) / 0.48 = **0.98 Wh** (4.5)

The complete duration of the AAST system test is 28 min. 50 sec. which is 0.48 hours (as shown below in **Equation 4.1**). In the AAST system, average load current of 227.52 mA is produced in 0.48 hr so the average value of charge produced by the AAST system is **473.45 mAh** as shown below in **Equation 4.6.**

227.52 mA 0.48 hr

? mA 1 hr

(227.52 x 1) / 0.48 = **473.45 mAh** (4.6)

The average load power produced in the AAST system is 1.25 W in 0.48 hr so the average value of energy produced by the AAST system is **2.60 Wh** as shown below in **Equation 4.7.**

1.25 W 0.48 hr

? W 1 hr

(1.25 x 1) / 0.48 = **2.60 Wh** (4.7)

4.5 Summary and Conclusion

The factors that are kept constant (as much as possible) during the data collection of this experiment are weather conditions, the track that is followed, the speed of the vehicle and the time zone.

A selected path has been followed by a vehicle with Zenithal Axis Solar Tracker mode activated first. Then the data has been collected.

In order not to get affected by the change in weather conditions and the position change of the sun, the duration of the track is kept short. So after approximately 28 min.50 sec. of track time, the mode of Solar Tracker is changed to Dual Axis Solar Tracker mode and the same track has been followed by the same vehicle with approximately the same speed. After completing the track, data of the Dual Axis Solar Tracker mode is saved.

Again after approximately 28 min. 50 sec. of track time the mode of Solar Tracker changed into Azimuth mode and the same track has been followed by the same

vehicle with approximately the same speed. After completing the track at approximately 28 min. 50 sec., the data of the AAST (Azimuth Axis Solar Tracker) mode is saved.

According to the Data analysis in this work, Dual-Axis Solar Tracking (DAST) System produced more charge then the rest of the systems with an estimated average charge rate of 666.23 maH and harvested the most energy average of 3.18 Wh.

Azimuth-Axis Solar Tracking (AAST) System produced the second most charge with an estimated average charge rate of 473.5 maH and harvested the second most energy average of 2.60 Wh.

Finally, Zenithal-Axis Solar Tracking (ZAST) System produced the least charge with an estimated average charge rate of 175.28 maH and harvested the least energy average of 0.98 Wh.

As a result, the DAST system produced 192.78 mAh more charge and also 0.58 Wh more energy than the AAST system, whereas the AAST system produced 298.17 mAh more charge and also 1.62 Wh more energy than the ZAST system.

Due to the ability of charge and energy production capacity of DAST systems, the need for panel size also decreases drastically which makes those systems economically much more desirable.

Chapter 5

IMPROVEMENTS

In this chapter, possible improvements that can be done to increase the reliability of the test results is discussed. The recommendations and future scope of this study is presented.

5.1 Recommendations

In this section, the effect of climate changes and the effect of speed of stepper motors on the test results is discussed. Suggestions to improve the test results are also presented.

5.1.1 Effect of Climate Change

Dual Axis Solar Trackers can give different data and show different power output because of the change of the seasons.

Long-term experiments need to be performed to test the effect of seasons on the power output of the Dual Axis Solar Tracker.

5.1.2 Effect of Stepper Motor Speed

The speed of stepper motors can affect the power output of the PV panel of the Dual Axis Solar Tracker.

DAST is not mounted on a stationary point, it is placed on a sea vehicle. Thus the stepper motor speed can be slower to trace the sunlight which will result in a delay

on the horizontal and vertical rotation of the panel. As the panel delays to follow the sunlight, the power output of the panel would be lesser than it should be.

In order to overcome this problem the speed of the stepper motors can be increased from the code. However this may not be enough so in that case bigger stepper motors can be implemented.

Another solution to speed up the rotation of the panel is to decrease the diameter of the big pulley that is connected to the stepper motor. That means using a smaller diameter big pulley will decrease the torque applied to turn the solar panel but it will increase the rotation speed.

5.2 Future Works

In this part, improvements need to be done in future for getting better results are going to be explained. The need for a kill switch mechanism, LDR sensor protection cap and solar charge controller is discussed in this part.

5.2.1 Kill Switch Operation

A Kill Switch mechanism can be added to the DAST concept in order to eliminate the need for an adjustment for a specific starting position. The mechanism should be added for both horizontal motion and vertical motion.

The PLD device originally has two kill switches. As shown in **Figure 62**, there is a small protrusion attached to the big pulley which is used for triggering the horizontal kill switch. The horizontal kill switch is triggered when the sheet metal part shown in **Figure 62** starts to push the trigger of the kill switch.

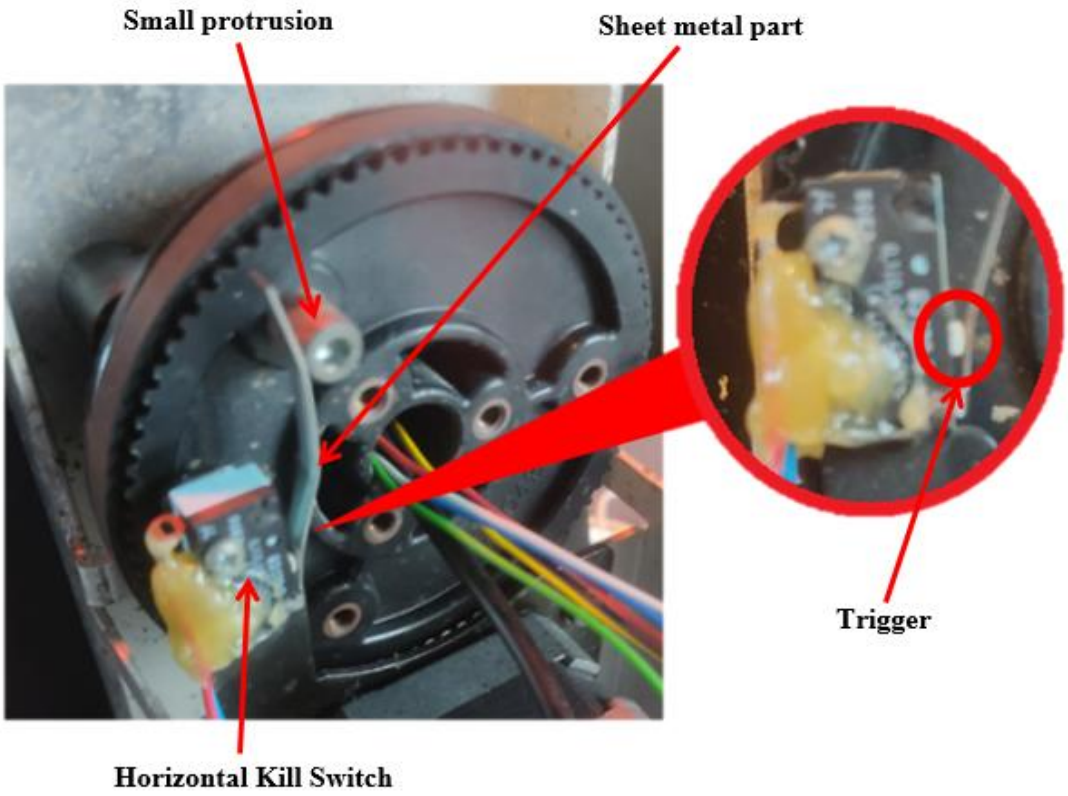

Figure 62: Horizontal kill switch mechanism.

There are two kill switches in the original PLD mechanism and both work with the same principle as explained before.

The horizontal and vertical kill switches shown in **Figure 63** (KS-H and KS-V) can be connected to digital pins of Arduino.

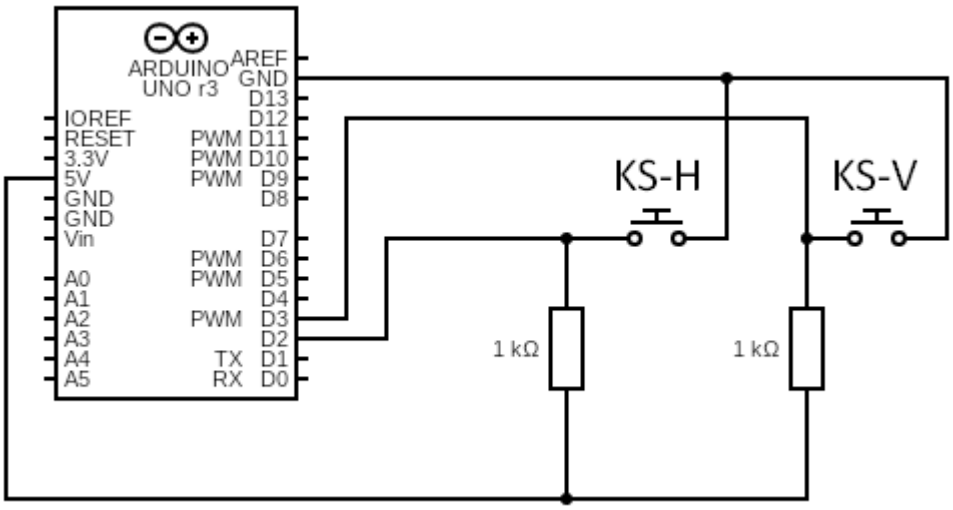

Figure 63: Shows the possible schematic connection of the kill switches with Arduino.

The steps shown below are the logic behind the code that can be uploaded to the Arduino in order to use kill switches as an activation button to make the Arduino find its correct starting position in order to prevent the solar tracker mechanism from over rotating or less rotating while operating; [1] [6]

Step 1: A kill switch can be defined inside the code for horizontal rotation as an integer.

Step 2: A kill switch can be defined inside the code for vertical rotation as an integer.

Step 3: Horizontal rotation kill switch can be defined inside the code as an input.

Step 4: Vertical rotation kill switch can be defined inside the code as an input.

Step 5: Horizontal rotation kill switch can be attained to one of the Digital pins of Arduino (for example D3) for reading the switch to understand whether it is activated or not.

Step 6: Vertical rotation kill switch can be attained to one of the Digital pins of Arduino (for example D3) for reading the switch to understand whether it is activated or not.

Step 7: An "if " function can be defined inside the code for the activation conditions of horizontal and vertical switches.

Step 8: A function can be defined after the activation of the kill switches for determining the starting position of the stepper motors.

5.2.2 LDR Sensor Protection Cap

A LDR Sensor protection cap can be added to the DAST concept in order to prevent the LDR`s and the 10 kΩ resistors from any impact coming from outside.

The protection cap should be transparent and it should have a permeable structure for the sunlight. The material of the cap should not be affected by sunlight and shouldn't reflect the rays of sunlight.

The protection cap should be capable of protecting the LDRs from humidity or precipitation as well so the IP rate of the protection cap should be 65- 67. The IEC 605029 is an international standard that establishes the IP rating system, which is utilized to categorize and describe the degree of ingress protection of electrical devices from water and solids. Through the allocation of a rating, the IP system guarantees consistent levels of protection for products that may encounter different environmental factors.

As it can be seen from **Figure 64** in the ingress protection marking, the first number indicates the solid protection level whereas the second number stands for water protection level. [52]

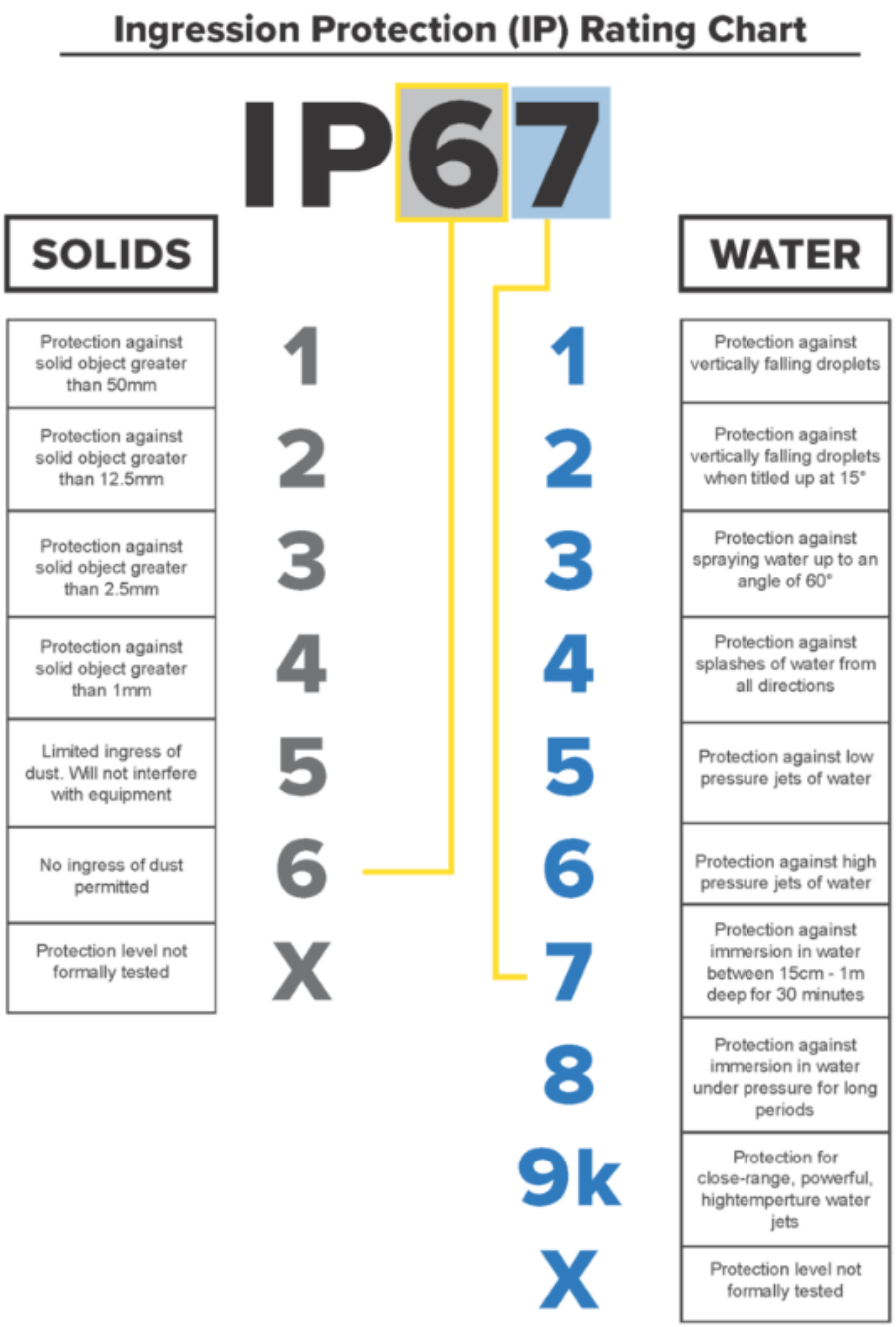

Figure 64: Ingress Protection table[52]

5.2.3 Solar Charge Controller

As the DAST is designed to be a standalone system, a solar charge controller shown in **Figure B.9** can be used to charge the battery while the DAST is operating.

The solar charge controller should be selected very carefully because it must handle the voltage and current outputs of the solar panel.

REFERENCES

[1] *Measure DC Voltage and Current with an Arduino*. (2021, January 23). DroneBot Workshop. https://dronebotworkshop.com/dc-volt-current/

[2] | *Lights* | *Video Tech* | *Dunedin*. (n.d.). | Lights | Video Tech | Dunedin. https://www.videotech.co.nz/shop/Lights/Lights+-+LED+Party+Light%3Fsku=01480.html

[3] *GrabCAD Making Additive Manufacturing at Scale Possible*. (n.d.). GrabCAD Making Additive Manufacturing at Scale Possible. https://grabcad.com/

[4] *AllSpark 120W Flexible Solar Panel - Bare panel*. (n.d.). Offroad Living. https://offroadliving.com.au/products/120w-allspark-flexible-solar-panel

[5] *4pcs 25V Voltage Sensor Module 3-Terminal Sensor Board Voltage Detector Module for Many Projects: Amazon.com: Industrial & Scientific*. (2022, February 1). 4pcs 25V Voltage Sensor Module 3-Terminal Sensor Board Voltage Detector Module for Many Projects: Amazon.com: Industrial & Scientific. https://www.amazon.com/Voltage-Sensor-3-Terminal-Detector-Arduino/dp/B07F8RFMD4

[6] *Voltage sensor (analog) with ESP32*. (2022, February 1). Arduino Forum. https://forum.arduino.cc/t/voltage-sensor-analog-with-esp32/953852/3

[7] H., & hectorhhg », M. A. (n.d.). *Stepper Motor + Arduino + Solar Tracker (EV)*. Instructables. https://www.instructables.com/Stepper-Motor-Arduino-Solar-Tracker-EV/

[8] Luijten, H., & H. (2015, November 4). *Arduino - Playing with a light sensitive resistor (LDR)*. Tweaking4All.com. https://www.tweaking4all.com/hardware/arduino/arduino-light-sensitive-resistor/

[9] *Circuit Diagram - A Circuit Diagram Maker*. (n.d.). Circuit Diagram - a Circuit Diagram Maker. https://www.circuit-diagram.org/

[10] *Arduino Search*. (n.d.). Arduino Search. https://search.arduino.cc/search?tab=&q=aref+pin

[11] *Thermistors and LDRs - Electric circuits – WJEC - GCSE Physics (Single Science) Revision - WJEC - BBC Bitesize*. (n.d.). BBC Bitesize. https://www.bbc.co.uk/bitesize/guides/zqxb4qt/revision/8

[12] *Pull-up Resistor vs Pull-down - Differences, Arduino Guide - Latest Open Tech From Seeed*. (2020, February 21). Latest Open Tech From Seeed. https://www.seeedstudio.com/blog/2020/02/21/pull-up-resistor-vs-pull-down-differences-arduino-guide/

[13] *How to use TB6560 Stepper Motor Driver with Arduino. – MYTECTUTOR*. (n.d.). How to Use TB6560 Stepper Motor Driver With Arduino. – MYTECTUTOR. https://mytectutor.com/how-to-use-tb6560-stepper-motor-driver-with-arduino/

[14] *TB6560 3A Stepper Motor Driver*. (n.d.). TB6560 3A Stepper Motor Driver - ElectroPeak. https://electropeak.com/tb6560-3a-stepper-motor-driver

[15] *Cast Colorless Methacrylate Transparent Acrylic Sheet 3mm - Buy Colorless Acrylic Sheet,Methacrylate Acrylic Sheet,Cast Acrylic Sheet Product on Alibaba.com*. (n.d.). Cast Colorless Methacrylate Transparent Acrylic Sheet 3mm - Buy Colorless Acrylic Sheet,Methacrylate Acrylic Sheet,Cast Acrylic Sheet Product on Alibaba.com. https://www.alibaba.com/product-detail/Cast-colorless-methacrylate-transparent-acrylic-sheet_1600200714928.html

[16] GmbH, R. (n.d.). *Temperature behavior*. PLEXIGLAS® | EN. https://www.plexiglas.de/en/temperature-behavior

[17] G. (n.d.). *Funduino UNO Rev3 (Arduino Uno Compatible)*. grobotronics.com. https://grobotronics.com/funduino-uno-rev3-arduino-uno-compatible.html?sl=en

[18] *Japan Servo Co. Ltd - Stepper Motor - 1.8 Deg/Step - DIY CNC KH42HM2B045 | eBay*. (n.d.). Japan Servo Co. Ltd - Stepper Motor - 1.8

Deg/Step - DIY CNC KH42HM2B045 | eBay. https://www.ebay.co.uk/itm/223468794713

[19] *4110-40, 200mm Jumper Wire Breadboard Jumper Wire in Black, Blue, Brown, Green, Grey, Orange, Purple, Red, White, Yellow | RS*. (n.d.). 4110-40, 200mm Jumper Wire Breadboard Jumper Wire in Black, Blue, Brown, Green, Grey, Orange, Purple, Red, White, Yellow | RS. https://ie.rs-online.com/web/p/breadboard-jumper-wires/2048241

[20] Magazine, S. (n.d.). *A Brief History of Solar Panels*. Smithsonian Magazine. https://www.smithsonianmag.com/sponsored/brief-history-solar-panels-180972006/

[21] *This Month in Physics History*. (n.d.). This Month in Physics History. http://www.aps.org/publications/apsnews/200904/physicshistory.cfm

[22] *Photovoltaic effect - Energy Education*. (n.d.). Photovoltaic Effect - Energy Education. https://energyeducation.ca/encyclopedia/Photovoltaic_effect

[23] *Photovoltaic Effect - an overview | ScienceDirect Topics*. (n.d.). Photovoltaic Effect - an Overview | ScienceDirect Topics. https://doi.org/10.1016/B978-0-08-100574-3.00018-7

[24] *Silicon Solar Cell: Types, Uses, Advantages & Disadvantages*. (2022, July 14). Solar Square Blog. https://www.solarsquare.in/blog/silicon-solar-cell/

[25] *PN Junction - Definition, Formation, Application, VI Characteristics and FAQs*. (2020, June 12). BYJUS. https://byjus.com/physics/p-n-junction/

[26] Storr, W. (2013, August 13). *PN Junction Theory for Semiconductor Diodes*. Basic Electronics Tutorials. https://www.electronics-tutorials.ws/diode/diode_2.html

[27] *https://www.worldscientific.com/doi/pdf/10.1142/9781786344496_0001?cookieSet=1*. (n.d.). https://www.worldscientific.com/doi/pdf/10.1142/9781786344496_0001?cookieSet=1

[28] *Dual Axis Solar Tracking System Basics: Everything You Need To Know*. (2022, August 31). Solar Square Blog. https://www.solarsquare.in/blog/dual-axis-solar-tracking-system/

[29] *Dual-Axis Tracking - an overview | ScienceDirect Topics*. (n.d.). Dual-Axis Tracking - an Overview | ScienceDirect Topics. https://doi.org/10.1016/B978-0-12-824555-2.00027-7

[30] Solar, T. S. (2019, October 16). *History of Photovoltaics (PV)*. True South Solar. https://truesouthsolar.net/history-of-photovoltaic-energy/

[31] *Edmond Becquerel: The Man Behind Solar Panels - Solenergy Systems Inc.* (2016, June 16). Solenergy Systems Inc. https://solenergy.com.ph/solar-panel-philippines-edmond-becquerel/

[32] *Charles Fritts | scientist*. (n.d.). Encyclopedia Britannica. https://www.britannica.com/biography/Charles-Fritts

[33] *The 19th Century Solar Engines of Augustin Mouchot, Abel Pifre, and John Ericsson — Land Art Generator*. (2012, February 29). Land Art Generator. https://landartgenerator.org/blagi/archives/2004

[34] *SOLAR NAVIGATOR CATAMARAN SCALE MODEL SPACE FRAME CONSTRUCTION*. (n.d.). SOLAR NAVIGATOR CATAMARAN SCALE MODEL SPACE FRAME CONSTRUCTION. http://www.solarnavigator.net/catamaran_model_space_frame.htm

[35] *PLANETSOLAR PLANET SOLAR BOAT TURANOR CIRCUMNAVIGATION*. (n.d.). PLANETSOLAR PLANET SOLAR BOAT TURANOR CIRCUMNAVIGATION. http://www.solarnavigator.net/planet_solar.htm

[36] *World's largest all-solar-powered boat shines in NYC*. (n.d.). World's Largest All-solar-powered Boat Shines in NYC. https://phys.org/news/2013-06-world-largest-all-solar-powered-boat-nyc.html

[37] *TRANSATLANTIC SUN 21 FIRST SOLAR POWERED ATLANTIC CROSSING ATTEMPT OCTOBER 2006*. (n.d.). TRANSATLANTIC SUN 21 FIRST SOLAR POWERED ATLANTIC CROSSING ATTEMPT OCTOBER 2006. http://www.solarnavigator.net/transatlantic_21.htm

[38] *Solarimpact - Solar-Powered Yacht with Swath Platform*. (2020, January 31). yachtemoceans.com. https://yachtemoceans.com/solarimpact-solar-yacht/

[39] *The boat – Fondation PlanetSolar*. (n.d.). The Boat – Fondation PlanetSolar. https://www.planetsolar.swiss/en/world-premiere/boat/

[40] *VOYAGER SOLAR POWERED AUTONOMOUS ROBOTIC BOATS UNMANNED*. (n.d.). VOYAGER SOLAR POWERED AUTONOMOUS ROBOTIC BOATS UNMANNED. https://www.bluebird-electric.net/artificial_intelligence_autonomous_robotics/Solar_Voyager_Autonomous_Robot_Boat_Unmanned.htm

[41] *Energy Observer*. (2023, April 14). Energy Observer. https://www.energy-observer.org/

[42] *CEA designs the energy system for Energy Observer: cutting-edge technology for an innovative project*. (n.d.). CEA/English Portal. https://www.cea.fr/english/Pages/News/CEA-designs-the-energy-system-for-Energy-Observer--cutting-edge-technology-for-an-innovative-project-.aspx

[43] Munna, M. S., Islam Bhuyan, M. A., Rahman, K. M., & Hoque, M. A. (2020, January 1). *Figure 1 from Design, implementation and performance analysis of a dual-axis autonomous solar tracker | Semantic Scholar*. Figure 1 From Design, Implementation and Performance Analysis of a Dual-axis Autonomous Solar Tracker | Semantic Scholar. https://www.semanticscholar.org/paper/Design%2C-implementation-and-performance-analysis-of-Munna-Bhuyan/d143c1d713073ec0ada345f7b28ebdc7428b7c71/figure/0

[44] *What is solar panel energy efficiency? | Enel X*. (n.d.). Enel X. https://corporate.enelx.com/en/question-and-answers/are-solar-panels-energy-efficient#:~:text=How%20efficient%20are%20solar%20panels,as%20much%20as%20nearly%2023%25.

[45] *What are Solar Cells? (Including Types, Efficiency and Developments)*. (n.d.). What Are Solar Cells? (Including Types, Efficiency and Developments) - TWI. https://www.twi-global.com/technical-knowledge/faqs/what-are-solar-cells.aspx

[46] *Solar Photovoltaic Cell Basics*. (n.d.). Energy.gov. https://www.energy.gov/eere/solar/solar-photovoltaic-cell-basics

[47] *Comprehensive review of environmental factors influencing the performance of photovoltaic panels: Concern over emissions at various phases throughout the lifecycle*. (2023, March 23). Comprehensive Review of Environmental

Factors Influencing the Performance of Photovoltaic Panels: Concern Over Emissions at Various Phases Throughout the Lifecycle - ScienceDirect. https://doi.org/10.1016/j.envpol.2023.121474

[48] (2013). *Application Note, The Spectral Mismatch Factor*. https://www.newport.com/medias/sys_master/images/images/h54/hdd/8797270605854/Spectral-Mismatch-App-Note-51.pdf

[49] A. (2020, January 21). *The Performance and Production of a Solar Panel [Guide]*. DualSun. https://dualsun.com/en/blog/solar-technology/performance-production-solar-panel/

[50] *AllEarth Solar Tracker | Vermont Solar Panels | AllEarth Renewables*. (n.d.). AllEarth Renewables. https://www.allearthrenewables.com/solar-products/solar-tracker/

[51] *What's the Difference Between Marine Solar Panels and Those For RVs and Cabins?* (n.d.). Renogy United States. https://www.renogy.com/blog/marine-solar-panels

[52] Hall, P. (2021, August 3). *IP Ratings Explained - Diamond HMI*. Diamond HMI. https://www.diamondhmi.co.uk/ip-ratings-explained/

[53] *KH42 series 800 type, 2- Phase Hybrid Stepping Motor 1.8°*, (n.d) https://docs.rs-online.com/5f76/0900766b80112640.pdf

[54] *Japan Servo | Electronic Components Distributor*. (n.d.). Japan Servo | Electronic Components Distributor. https://www.ibselectronics.biz/Manufacturer.asp?Name=Japan%20Servo

[55] *Invento 5PCS Photoresistor LDR CDS 5mm Light-Dependent Resistor Sensor GL5516 DIY : Amazon.in: Industrial & Scientific*. (2022, May 24). Invento 5PCS Photoresistor LDR CDS 5mm Light-Dependent Resistor Sensor GL5516 DIY : Amazon.in: Industrial & Scientific. https://www.amazon.in/Invento-Photoresistor-Light-Dependent-Resistor-Arduino/dp/B072R6M32Q

[56] *Hasan, K., Yousuf, S. B., Tushar, M. S. H. K., Das, B. K., Das, P., & Islam, Md. S. (2021). Effects of different environmental and operational factors on the PV performance: A comprehensive review. Energy Science & Engineering, 10(2), 656–675. https://doi.org/10.1002/ese3.1043*

[57] *Rahman, M. M., Hasanuzzaman, M., & Rahim, N. A. (2015). Effects of various parameters on PV-module power and efficiency. Energy Conversion and Management, 103, 348–358. https://doi.org/10.1016/j.enconman.2015.06.067*

APPENDICES

Appendix A: Tools and Equipment

This appendix is for showing the tools and equipment that are used to construct the DAST concept used in this study.

Figure A.1: 60W Soldering iron.

Figure A.2: TT T-ECHNI-C MY64 multimeter.

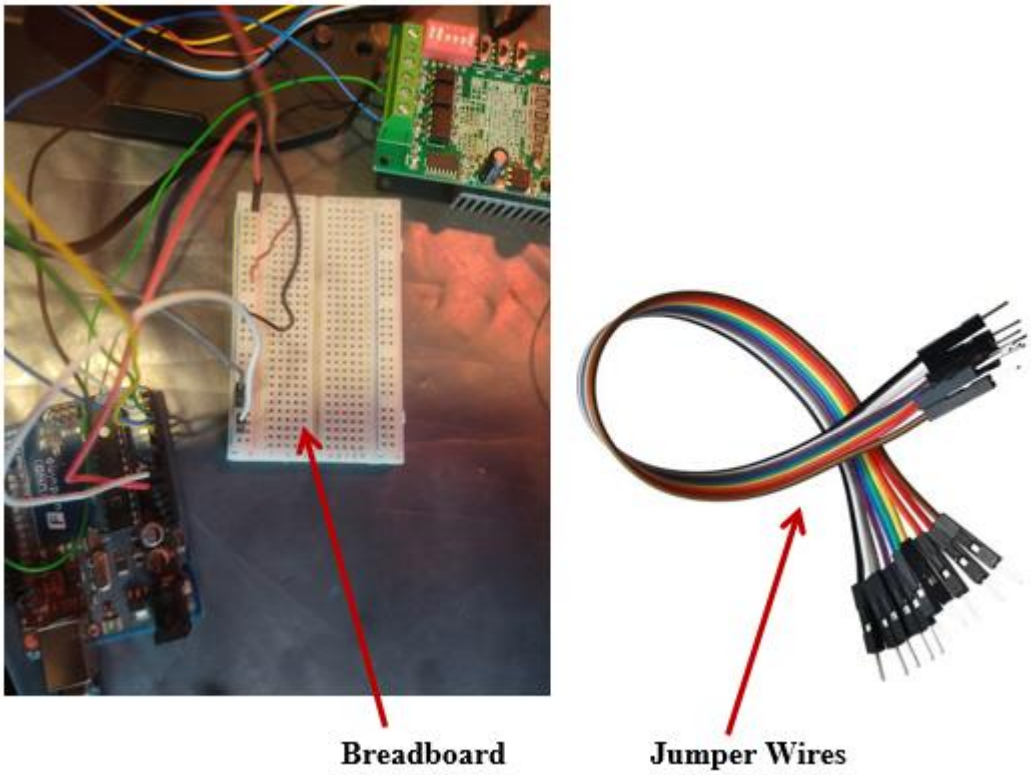

Figure A.3: Breadboard and Jumper wires.[19]

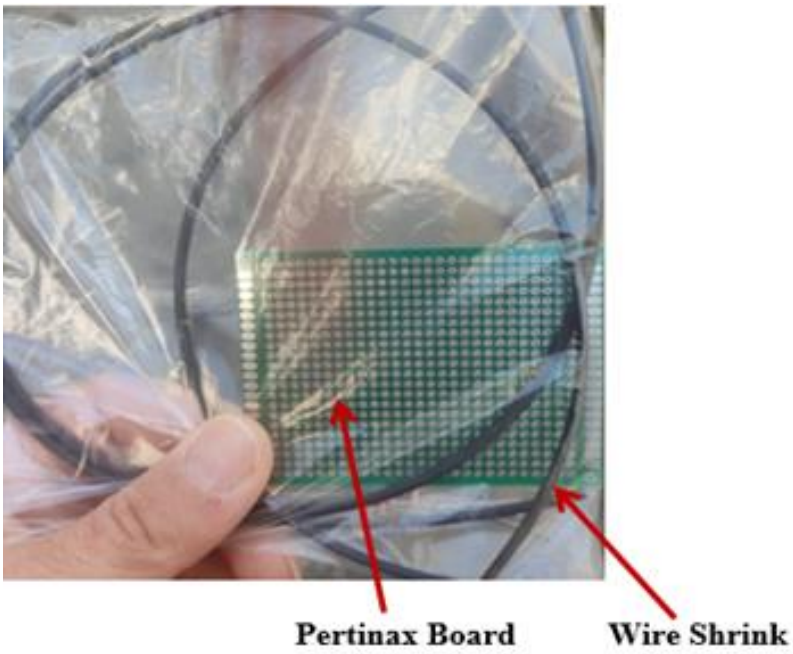

Figure A.4: 80 X 60 mm experimental pertinax board and 2 mm Ø wire heat shrink.

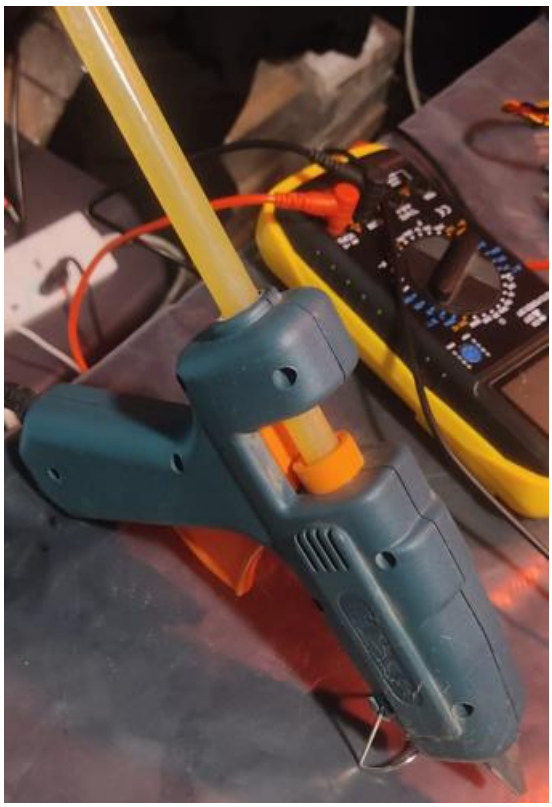

Figure A.5: Hot melt adhesive gun.

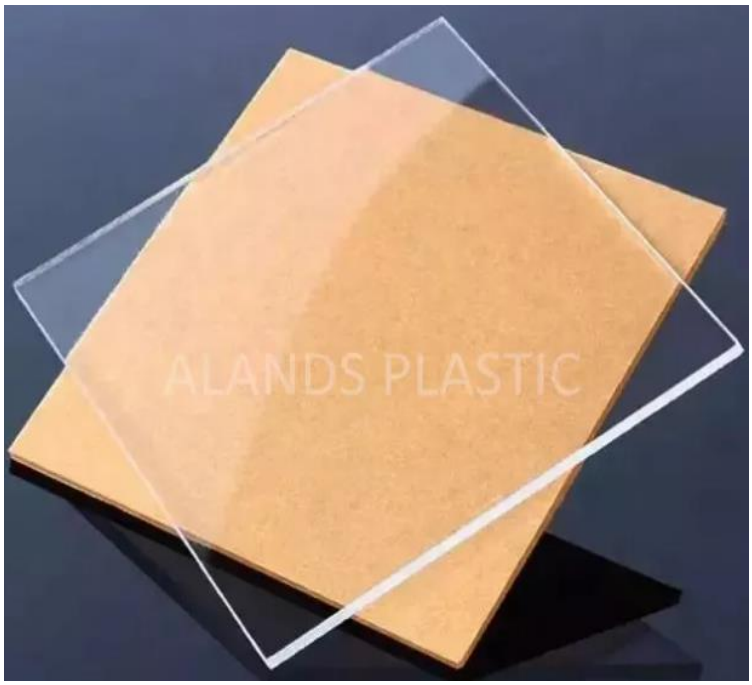

Figure A.6: Transparent plexi-glass (Acrylic).[15]

Appendix B: Electrical Components

This appendix is for showing the electrical components that are used to construct the DAST concept used in this study.

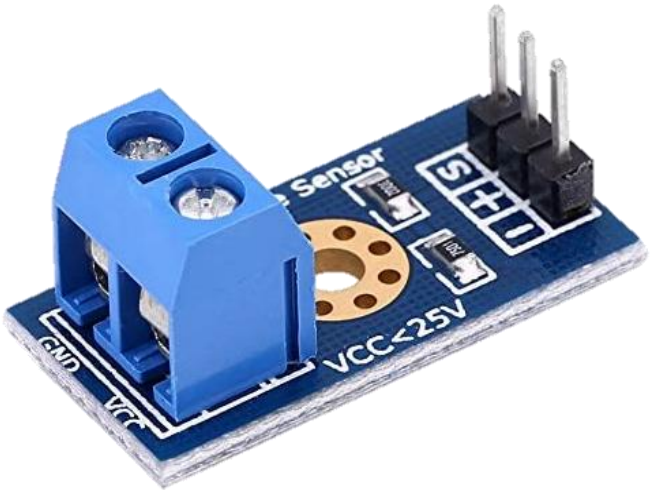

Figure B.1: Arduino VCC Voltage sensor [5]

Figure B.2: LDR (Light Dependent Resistor). [55]

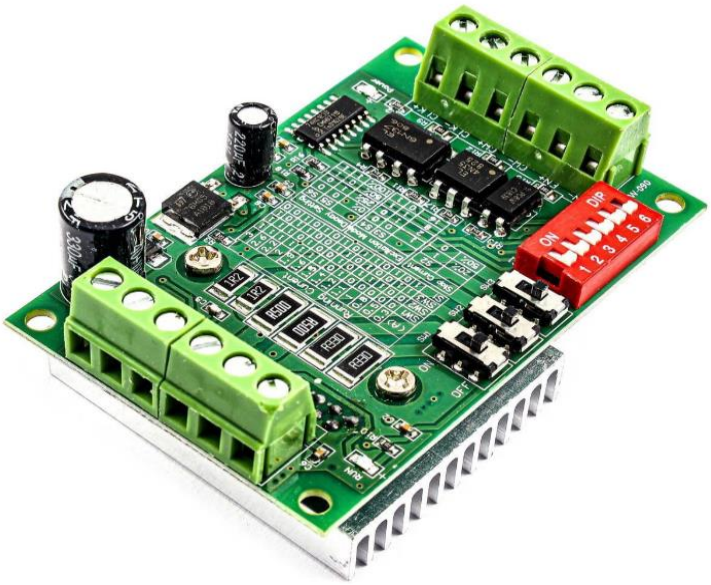

Figure B.3: TB-6560 stepper motor driver. [14]

Figure B.4: KH42HM2B017 stepper motor [18]

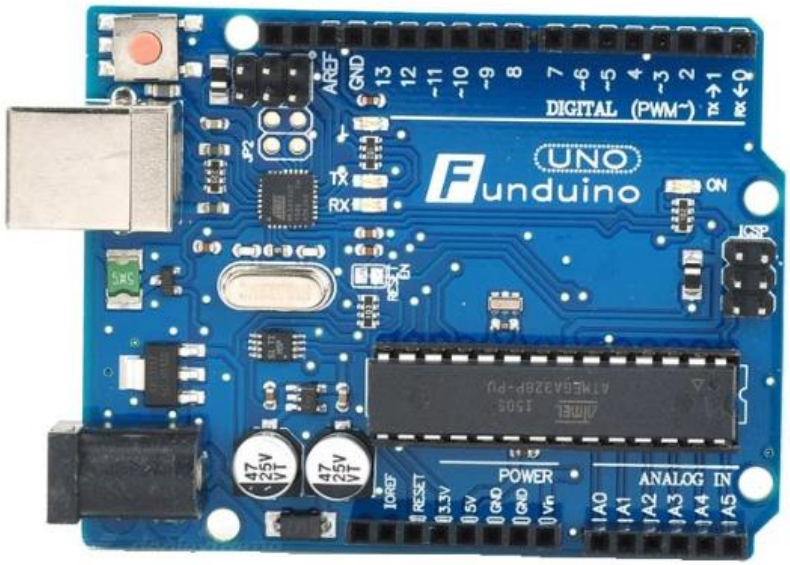

Figure B.5: Funduino UNO. [17]

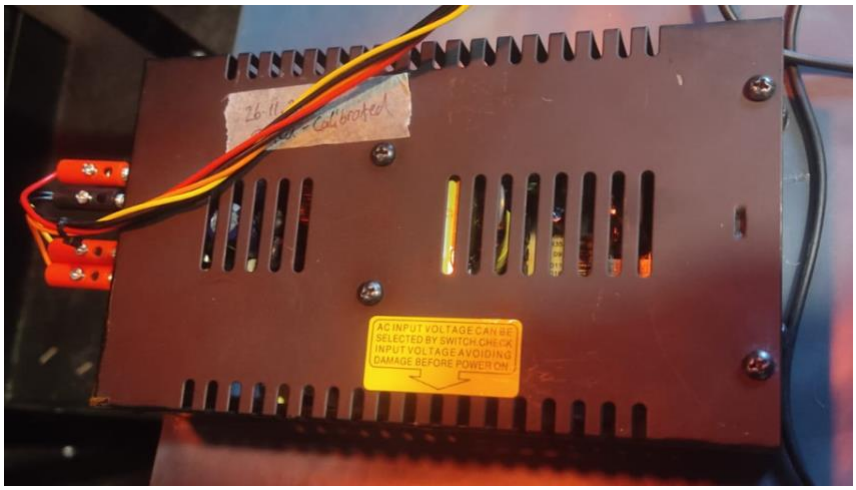

Figure B.6: Power Supply that is capable of giving 5V, 12V and 24V.

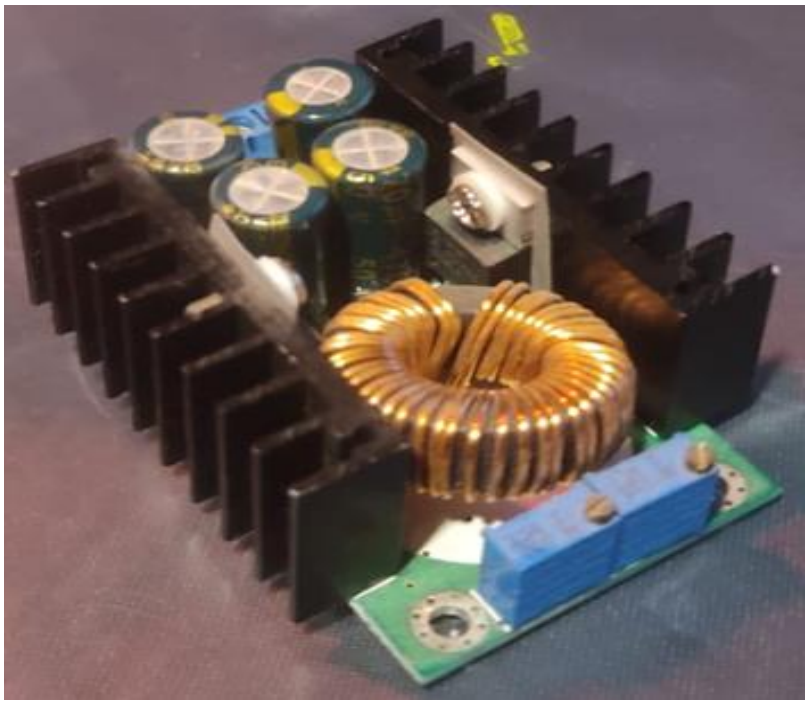

Figure B.7: Stepdown converter.

Figure B.8: 6-DZF-20, 12V 20Ah lead acid gel battery.

Figure B.9: Mexxsun CM20D solar charge controller.

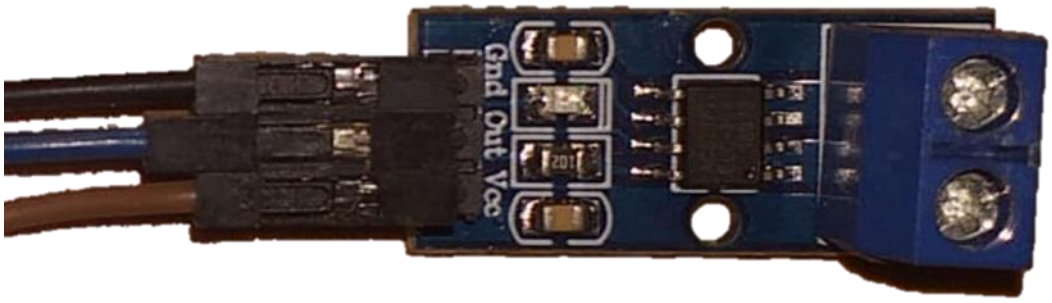

Figure B.10: ACS712 Hall- effect Sensor

Appendix C: Details of DAST concept preparation

This appendix is for showing some details of the process of DAST concept preparation that is used in this study.

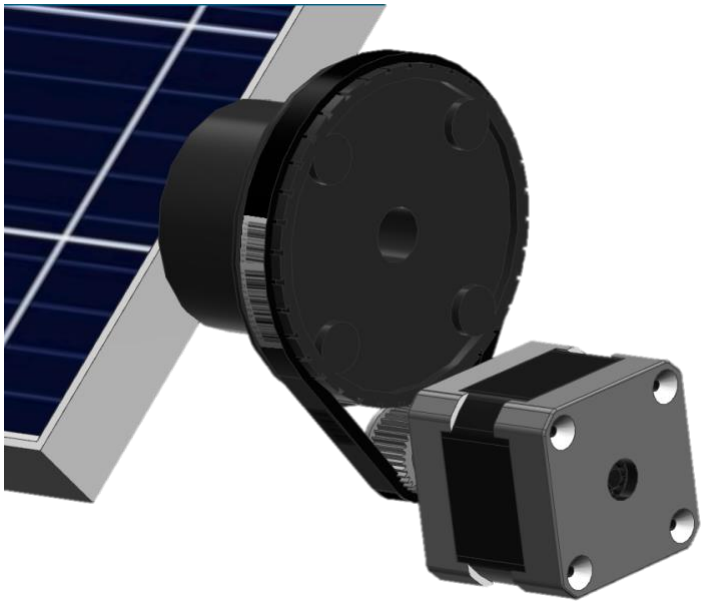

Figure C.1: Belted connection of stepper motor and big pulley of the horizontal rotation mechanism.

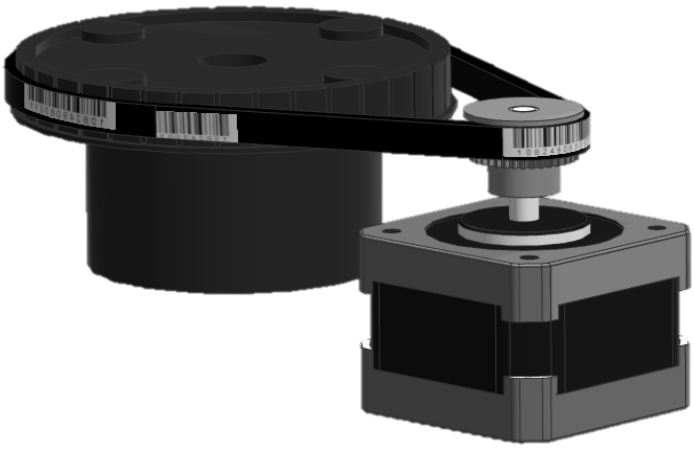

Figure C.2: Belted connection of stepper motor and big pulley of the vertical rotation. mechanism.

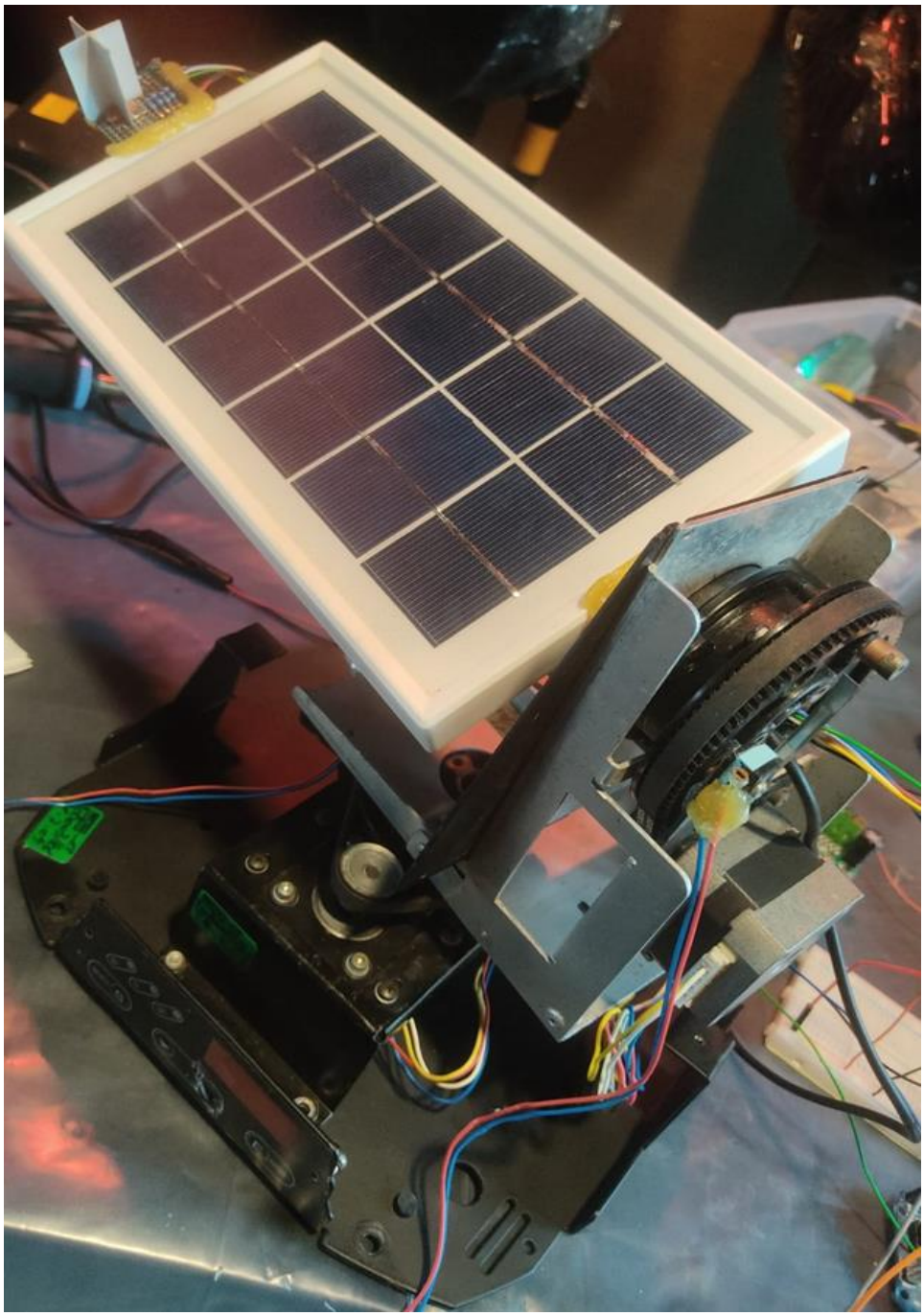

Figure C.3: The look of the DAST system after the installation of a solar PV panel.

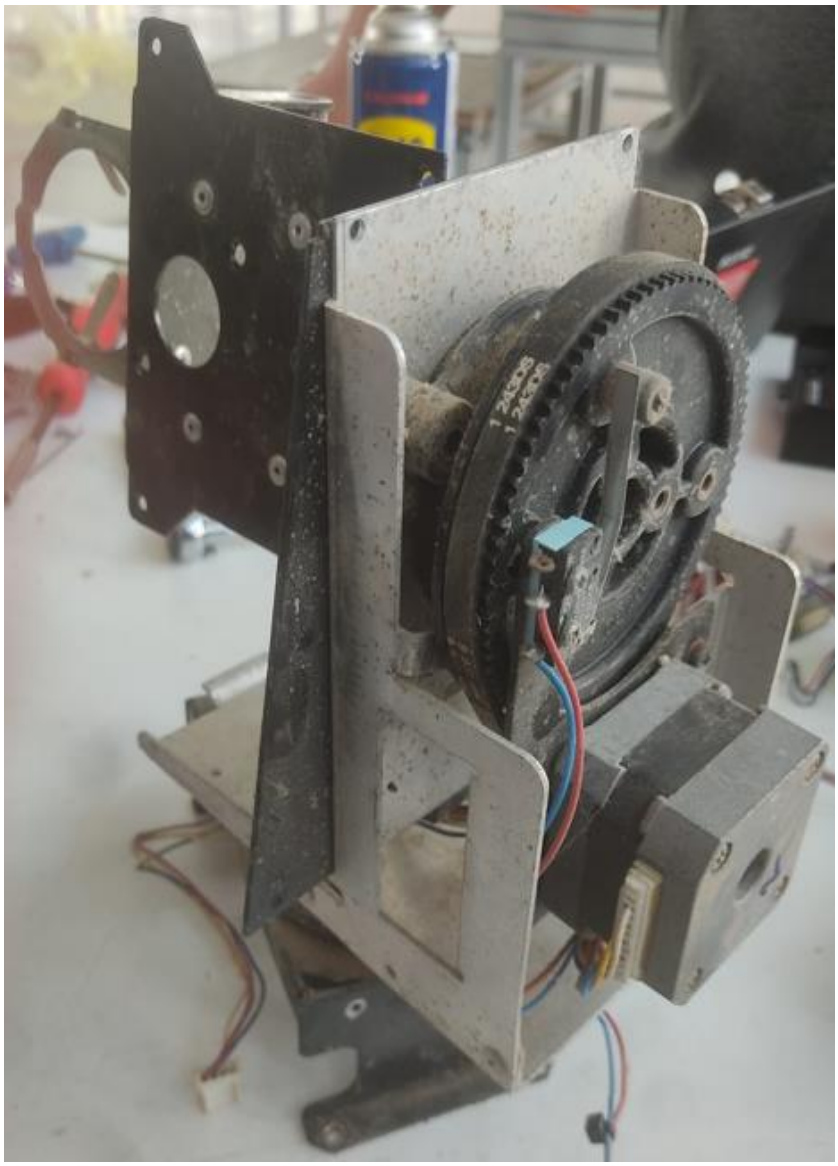

Figure C.4: Final look of the party lighting device after component removal